Design of Reducing Agent for Sintering of High-Performance Alloyed PM Steels Based on Different Carbon Grades Analysis

by

Aimn Hadhud

Diploma work No. 95/2012

at Department of Materials and Manufacturing Technology
CHALMERS UNIVSERITY OF TECHNOLOGY
Gothenburg, Sweden, 2012

Diploma work in the master program in Advanced Materials Engineering 95/2012

Preformed at: **Department of Materials and Manufacturing Technology**
Chalmers University of Technology
SE-41296 Gothenburg

Examiner and Supervisor: **Eduard Hryha, Ph.D.**
Department of Material and Manufacturing Technology
Chalmers University of Technology
SE-41296 Gothenburg

Design of Reducing Agent for Sintering of High-Performance Alloyed PM Steels Based on Different Carbon Grades Analysis

Aimn Hadhud

Diploma work No. 95/2012
Department of Materials and Manufacturing Technology
Chalmers University of Technology
SE-41296 Gothenburg
Sweden
Telephone +46(0)31-772-1000

CHALMERS Reproservice
Gothenburg, Sweden 2012

Abstract

Carbon activity in terms of carbon dissolution and reducing ability plays a major role in final performance of structural PM components. Graphite is the most common carbon source for structural PM components and due to the carbon effect on powder compressibility has to be admixed to the metal powder. The role of admixed graphite besides hardening the material by its diffusion into the pure or pre-alloyed iron particles is the reduction of the surface oxides to provide metal-metal contact between adjacent particles and thus allowing the neck formation to take place.

According to the latest experimental data, the carbon starts to be active at high temperature (>900ºC), after which graphite rapidly dissolves in the metallic matrix. This means that there is a lack of reducing agent at low temperature (700-900˚C) as well as in high temperature range (> 1100˚C) when there is no any carbon source left in the pores for reduction of the most stable surface oxides. The aim of this work is to evaluate the carbon activity of different carbon sources in order to design carbon source activity of which can cover required temperature range. This can be obtained by mixing of different carbon sources that are active at different temperatures as well as by modification of the existing grades.

Astaloy CrM (Höganäs AB, Sweden) was mixed with different carbon sources of various properties, namely PG25, PG10, F25, F10, KS4 and ENSACO 250 (TIMCAL SA, Switzerland). The mixes were then compacted to the density of ~7 g/cc. Interrupted sintering of compacts was performed in the range of temperatures from 700 until 1120˚C and sintering for 30 min at 1120˚C. Metallographic and fractographic analysis were the main methods to evaluate the carbon activity in this study. The investigation shows that the carbon starts to be active at ~ 900˚C in the case of KS4, F10 and PG10 and they are comparable in terms of the carbon dissolution and reducing ability, while PG25 and F25 are the less active, whereas ENSACO 250 is inactive at this temperature. However, the only carbon source that completely dissolves during heating to 1120 ºC throughout the compacts was ENSACO 250. After sufficient time was given, KS4, F10, PG10 and F25 were completely dissolved while some amount of PG25 remained un-dissolve at this temperature even after sintering for 30 min.

Key worlds: graphite, carbon black, sintered steels, surface oxide, oxide reduction.

TABLE OF CONTENT

Acknowledgement

I would like to start by thanking my examiner and supervisor Ass. Prof. Eduard Hryha, PhD for extending their unconditional support and guidance all along my thesis work. A special thanks to PM group at department of Materials and Manufacturing Technology for giving me invaluable information regard my thesis. I wish to thank Höganäs AB, Sweden and TIMCAL SA, Switzerland for providing the materials to my thesis work. Finally, i would like to thank my family, teachers and friends who have been a constant source of encouragement.

1. Introduction

The residual porosity and the strength of inter-particle bonding between the powder particles are the main factors that influence the final mechanical properties of the sintered parts [1, 2]. **Fig. 1a** shows the inter-particle connection or so called neck and residual porosity in the sintered part. As is shown by the figure, the cross-section of the powder neck is considerably increasing during sintering. Therefore improvement of the neck development during the heating stage will have a direct influence on mechanical properties. **Fig. 1b** shows also the broken inter-particle neck. There are different shape and size of oxides that are entrapped inside the neck. These oxides act as barrier for mass transport during diffusion which in turn influence the neck formation development and final strength.

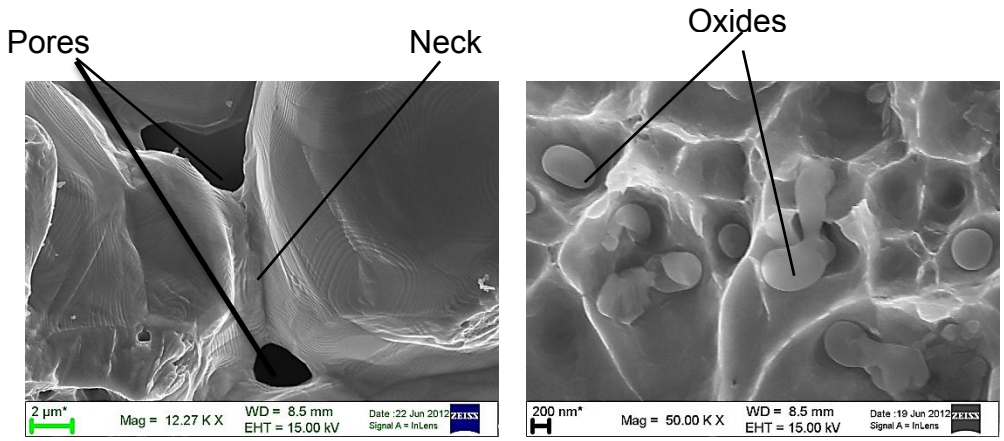

(a) (b)

Fig. 1: SEM images of sintered part showing (a) residual porosity and neck, (b) neck area with the presence of oxide inclusions

High-performance PM steels particularly pre-alloyed with Cr and Mn, are covered by thin iron oxide layer with the presence of small particulates that are rich in stable oxides. The composition of these particulates primarily depends on alloying element content. During the compaction process these oxides are entrapped inside the contact areas between particles, which consider as the potential area for neck formation. Therefore removal of these oxides is essential to assure metal-metal contact and thus allowing neck formation to take place. The main reducing agents during sintering process are the gas atmosphere and admixed graphite (most common carbon source) in powder mixture. The influence of gas reducing agent such as H_2 is limited by its permeability inside the compact [3].

However, when temperature is high enough, e.g. about 900˚C, carbothermal reduction starts. As soon as the iron oxide between inter-particle contacts is partially or completely reduced the necks start to form. However increase in temperature is followed by intensive neck formation. If the iron oxide is not fully reduced at this stage the residual iron oxides will be entrapped inside the neck formed and their reduction will be restricted at this stage. This results in transformation of the iron oxides into more stable oxides during heating stage [4]. Therefore removal of these iron oxides at early stage before intensive neck formation starts is one of the ways to minimize these oxides enclosure inside the neck. The temperatures at which carbothermal reduction starts depend strongly on the carbon source properties. The aim of this study is to define which carbon source has the ability to react with the surface iron oxide layer at lowest possible temperature and thus minimize the amount of entrapped

oxides inside the neck. The main disadvantage of such carbon source is that it will dissolve fast in the matrix which means that at high temperature there will be no any carbon source left in the pores for reduction of the most stable surface oxides. Therefore definition of carbon source that will be more stable at high temperature is another aim of this study. Based on that approach, mixing of different carbon sources could result in a new generation of carbon source that can cover required temperature ranges.

2. Theoretical Background

2.1. Introduction to PM

Powder metallurgy is the modern technology for metal-forming that offer a diversity of geometries and close dimensional tolerance. Large scale production such as automotive industry attracts to this technology due to its high profitability and process performance. Production utilizes two main manufacturing steps: compaction and sintering. This gives high productivity at low energy consumption and high material utilization. Unlike conventional steel process, the starting material in PM technology is lose metal powder, which is compacted to its defined shape. This compact is then heat treated (sintering) at a temperature around 2/3 of the melting point of alloy in order to strengthen powder compact. The main strengthening mechanism in sintered part with respect to alloying elements is through inter-particle bonding that takes place during sintering stage through diffusion process between the adjacent particles. However, a certain degree of residual porosity is inherent the sintered parts, which in turn reduce the mechanical properties for the same part produced by conventional methods. Nevertheless, the sintered part largely satisfies the requirement of mechanical properties for different application while keeping close dimensional stability and profitability of the final product. These are the main advantages over most existing metal forming techniques [1, 5].

2.2. The PM processing route of sintered components

Fig. 2.1 illustrates the PM processing route of PM component. The conventional route starts from powder production by water-atomization. The powder then is mixed with graphite (the main carbon source), lubricant and additives. A compact of defined shape is formed by densification of the powder mixture by uniaxial pressing. The compact is then sintered in reducing gas atmospheres in order to produce a finished or semi-finished sintered part. Alternative exists in each processing stage, see **Fig. 2.1**. The powder properties, the requirements on mechanical properties of sintered part and the investment costs set the demand on these alternatives. In this work the conventional route is of the primary interest [2, 5].

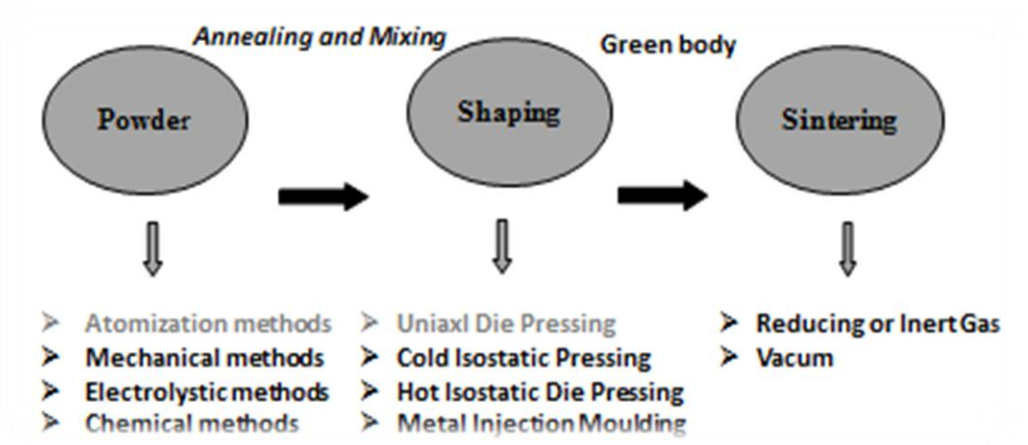

Fig. 2.1: Chart of processing route of PM component.

2.3. Classification of powder properties

The further processing and the final performance obtained in sintered part are largely influenced by the powder properties which can be described by its:

- Shape (irregular, spherical, etc.)
- Size and size distribution
- Structure (dendritic or cellular)
- Surface (chemistry and topography)

Therefore tailoring these properties for the further processing stages is one of the key parameters to improve the final mechanical properties in sintered part. The important needs for powder properties to be fulfilled can be summarized in

- Homogeneous microstructure to provide good final properties and processing of powder
- Clean surface in term of oxides to provide good sintering
- Suitable shape for a certain shaping technique
- Appropriate size for enhancing sintering and tailoring for certain shaping

It must be emphasized that the choice of the powder properties is normally based on compromise since many factors, mainly restricted by production methods, are indirect opposition to each other [6].

2.4. Alloying elements and alloying methods for PM steel

PM steel is alloyed with different elements. Traditionally, Ni, Mo, and Cu are the most used alloying elements in the case of structural sintered components [7]. The main advantage of using these elements in PM steels is their role in strengthening together with low stability of their respective oxides that can be reduced at sintering conditions that are easily achieved in industry. However, in recent ten years the cost of these elements has significantly increased [8]. Therefore demand on cheaper and more effective alloying elements increase. Cr and Mn are attracting much attention not only because they are cheaper, but also yield higher hardenability and better response to bulk and surface hardening treatment [9]. The main concern regarding these elements is their high affinity to oxygen which leads to the formation of thermodynamically stable oxides which are difficult to reduce in normal sintering condition. Furthermore, the risk of formation of more stable oxides during sintering is high if the sintering conditions are not adjusted properly [3, 9, 10]. Carbon is special case, due to its influence on powder compressibility it is added in form of admixed graphite.

There are three major ways to introduce these alloying elements to the PM steel [5, 7].

Admixing: The alloying elements are added to iron based powder in the form of elemental powder. In this way the base iron powder is unalloyed when the mix is pressed. This results in high compressibility of the mixture. The disadvantages of this material are heterogeneous microstructure due to slow diffusion of alloying elements, powder segregation and impossibility to use elements with high-sensitivity to oxygen.

Diffusion bonding: In this method the elemental powders are diffusion bonded to iron based powder during annealing process before pressing the powder. Thus the segregation effect is minimized. However, the compressibility is slightly reduced and sintered parts have inhomogeneous microstructure that is still better than admixed material

Pre-alloying: Both mentioned above methods do not provide a homogeneous distribution of alloying elements in the sintered part. Pre-alloying overcomes this disadvantage. Here the alloying elements, except carbon, are added to the iron melt prior to atomization. However due to the solid solution strengthening, the compressibility is reduced.

2.5. Pre-alloyed steel powder and fabrication method

Pre-alloyed PM steels powder is mainly fabricated by atomization process. In this process, a liquid metal stream is disintegrated into small droplets that solidify rapidly before they come into contact with each other or with a solid surface. This is done by applying high pressure water or gas. The shape, structure and the surface properties of the powders are largely influenced by atomization media and availability of oxygen during process, whereas the size of the powders is controlled by nozzle geometry, atomization pressure media, melting temperature, etc. [2].

Pre-alloyed powder produced by water-atomization is characterized by homogeneous distribution of alloying elements, irregular shape due to high cooling rate (low surface tension) and heterogeneous oxide layer covering the powder particles due to the presence of water vapour during process. The amount and composition of these oxides are strongly depended on particle size and alloying elements. Annealing under gaseous reducing atmosphere is therefore vital in order to minimize these oxides, particularly iron oxide. The main advantages of water atomization are low cost process and irregular shape that provides the necessary mechanical interlocking of the particles that suitable for die-pressing technique [2, 11].

Nitrogen, helium and argon are the most used in gas–atomization method. The presence of oxidising gases (water vapour, oxygen, etc.) is therefore avoided, which results in high purity powder surface obtained. Nevertheless, spherical shape of the powder particles does not allow its use in die-pressing. Hot isostatic pressing and metal injection moulding are the most used shaping methods for pre-alloyed PM steels powder produced by gas –atomization [1, 2].

2.5.1 Surface oxides in pre-alloyed PM steel powder

As it has been mentioned, the pre-alloyed PM steel powder produced by water-atomization is covered by an inhomogeneous oxides layer. These oxides act as obstacles that hinder the diffusion between the contact particles. Therefore, reduction of these oxides is crucial during the heating stage. Recent investigation [11] on Cr-alloyed powder and Mn –alloyed powder shows the presence of two types of surface oxide: homogeneous thin iron oxide layer (6 nm), covering all powder surface, and spherically shaped particulates (200 nm) that are rich in strong oxide forming elements. The composition of the particulate oxides is strongly dependent on powder composition and manufacturing. **Fig. 2.2** shows high resolution SEM image of Astaloy CrM powder where distribution of the particulate oxides on the powder surface can be seen. The main concern regarding these oxides is their stability which set the

demands on sintering condition (temperature and atmospheres composition). In general, more stable oxides require higher sintering temperatures and more strict sintering conditions [1, 2, 4, 14].

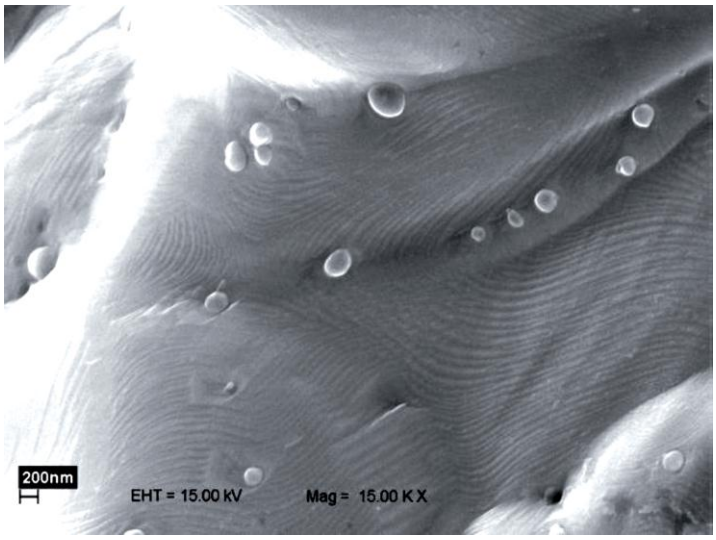

Fig. 2.2: High-resolution SEM image of 3%Cr-0.5%Mo pre-alloyed steel powder particle showing the presence of small surface oxide particulate feature [11].

2.6. Mixing and shaping.

Pre-alloyed PM steels are mixed with graphite, lubricant and additives. A homogeneous mixture is therefore required to avoid agglomeration. Due to the importance of graphite distribution on the powder surface, a special binder can be added to glue the graphite to the powder surface, i.e. Star mix process (Höganäs AB, Sweden). In this way the graphite efficiency in term of oxide reduction and homogeneous dissolution during the sintering is enhanced [7]. **Fig. 2.3** shows the appearance of admixed graphite inside the pores. When the temperature is high enough, the carbon activity of graphite starts and reduces the surface oxides to allow not only the neck formation, but also the carbon dissolution to take place.

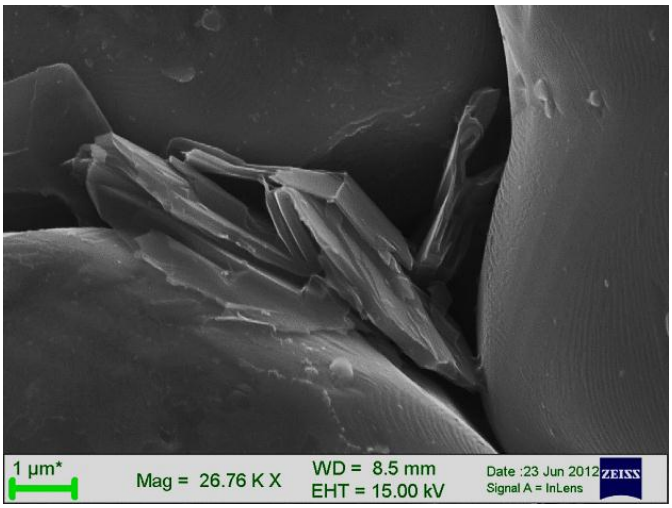

Fig. 2.3: SEM image shows the typical appearance of graphite powder in the pores.

After the powder mixture fill the die cavity, it is compacted to its defined shape between two or more uniaxially moving upper and lower punches [7]. During the compaction the powder particles are mechanically deformed and interlocked, see **Fig. 2.4**, leading to formation of solid interface at the point or planar particles contact. These contact play a vital role in the sintering stage, hence act as potential areas for nucleation and growth of inter-particle neck [12]. The major concern of influence of surface oxides of powder in this stage is related to the entrapped surface oxide inside the contact area. During heating stage the iron oxides will be (completely or partially) reduced first. This will allow the inter-particle necking to take place, while the residual oxide entrapped inside the neck formed, will be isolated from processing atmosphere. This in turn leads to a negative impact on neck development during the heating stage of sintering.

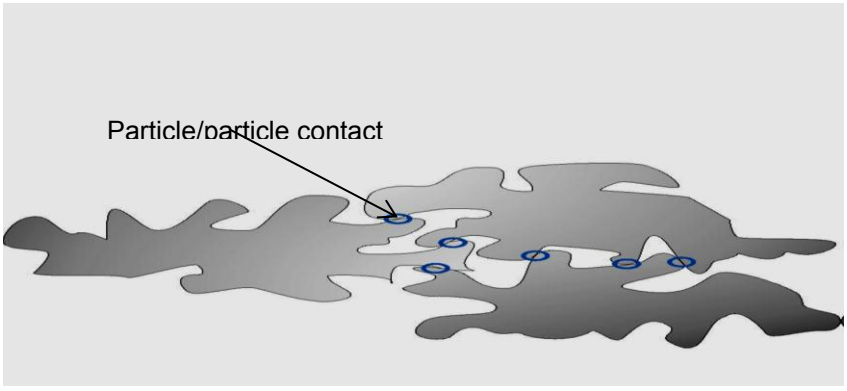

Fig. 2.4: Schema of interlocking mechanisms between powder particles and powder particle/particle contacts in compacted material.

2.7. Thermodynamic stability of oxides

Thermodynamic calculations, based on standard free energy changes, enable to determine the relative stability of metal oxides, and thus the requirements for sintering conditions at a given temperature and the pressure balance between oxidizing/reducing gases, $p(O_2)$, $p(CO_2)/p(CO)$ and $p(H_2O)/p(H_2)$ [10]. The variation of the standard free energy change with absolute temperature for a number of metal oxides is summarized in an Ellingham-Richardson diagram in [13]. The less stable oxides which are easily reduced occur at the top of the diagram, i.e. FeO and NiO, and more stable oxides at the bottom: SiO_2, MnO and Cr_2O_3.

Dissociation of oxides occurs according to reaction (1), where M denotes metal and M_xO_y metal oxide:

$$\mathbf{2/y\ M_xO_y \longleftrightarrow 2x/y\ M + O_2} \qquad \mathbf{(1)}$$

The standard Gibbs free energy change is then equal to:

$$\Delta G^\circ = 2x/y\ G^\circ (M) + G^\circ (O_2) - 2/y\ G^\circ (M_xO_y) \qquad (2)$$

$$\text{Hence } \Delta G^\circ = -\ RT \ln K \qquad (3)$$

Where R is the gas constant (R=8.314 J/mol K) and T is the temperature in Kelvin, K is the equilibrium constant and for reaction (1) is given by

$$K = [a^{2x/y} (M) * a (O_2)] / [a^{2/y} (M_xO_y)] \qquad (4)$$

Where (a) are the activities of the substance that take place in the reaction. The activity of pure metal and its oxides is unity whereas for ideal gases the activity equal to the partial pressures. Hence equation (4) becomes:

$K = p(O_2)$ (5)

From (3) and (5)

$$\mathbf{p(O_2) = \exp(-\Delta G^o / RT)} \quad (6)$$

Equation (6) provides the possibility to determine the oxygen partial pressures at given temperature to shift the reaction (1) forward (reduction) or backward (oxidation). Eingham-Richardson diagram also has scales for $p(CO_2)/p(CO)$ and $p(H_2O)/p(H_2)$.

2.8. Solid state sintering

Sintering provides thermal energy required to realize inter particle bonding between the powder particles and hence improve the strength of the compact. The driving force is the minimizing of total surface energy, realized by decrease in free surface. This is achieved at higher temperature at which the solid state diffusion is high enough to allow the atoms movement. The main mass transport mechanisms for the bonding of metal particles are: surface diffusion, evaporation and condensation, volume diffusion, grain boundary diffusion and viscous or plastic flow. Sintering stage can be divided into three stages: the initial stage of sintering, which is characterized by formation and growth of inter particle necks. Intermediate stage is characterized by intensive growth of necks leading to volume shrinkage and grain growth. This result in the reduction of open porosities and isolated pore appear instead. The last stage is the cooling stage where by controlled cooling desired microstructure is obtained [1, 2].

2.9. Sintering processes

During converting a green body to the sintered part compact undergoes three stages. **Fig. 2.5** shows schematic of a continuous mesh belt sintering furnace with the different stages: heating, sintering and cooling [14].

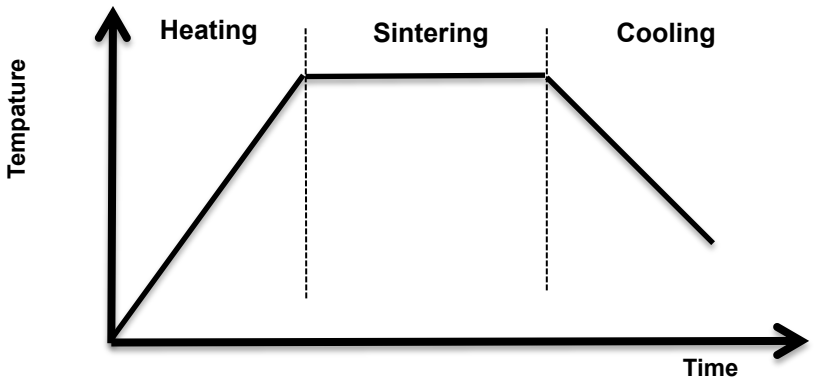

Fig. 2.5: Schematic of different stages in continuous mesh belt sintering furnace.

2.9.1. Heating stage

The compact entering the sintering furnace contains organic lubricant or binder. Most of the lubricants and binders melt below 150ºC and evaporate/decompose between 300ºC to 500ºC. The vapour species which are usually a mixture of methane CH_4, carbon dioxide CO_2, carbon monoxide CO, water vapour and other combustion products are purged out from the furnace by gas atmospheres. This process could be performed separately or in continuous sintering furnace during sintering process. The main factors that determine an efficient removal of delubrication products are mainly the temperature profile (dwelling temperature and heating rate), green density and atmosphere composition [2, 14**].** After the de-lubrication, surface oxides are reduced to allow inter-particle necks and carbon dissolution to take place. Gas atmosphere and admixed graphite are main reducing agents in PM steel. The most common used gaseous reducing agent is H_2 and due to high cost and explosion risk of pure H_2 it is usually mixed with N_2. The efficiency of the reduction of the surface iron oxide layer on the powder particles by H_2 largely depends on its permeability into the compact and thus the green density. Increasing temperature on the other hand reduce the open porosity through development of the necks. In general the reduction by H_2 is limited at high temperatures. However as the temperature progress and graphite becomes active, carbothermal reduction starts that is evident by formation of CO and CO_2 in atmosphere. Therefore monitoring the atmosphere composition $p(H_2O)/p(H_2)$ and $p(CO_2)/p(CO)$ is fundamental in sintering process to avoid the oxidation and decarburization. Increase in temperature increases the carbon activity and thus reduction rate until the carbon eventually dissolves in the matrix. One of the ways to indicate reduction of surface oxide is by fractographic analysis. **Fig. 2.6** shows SEM images for sample heated up to 1120˚C in N_2/10%H_2 atmosphere. As the figure shows, the inter-particle connections starts close to 900˚C and finishes when heated to final sintering temperature of 1120˚C while there are no inter-particle connections at 700˚C. This indicates that reduction of surface oxide taken place above 700˚C [1, 3, 4, 8, 14].

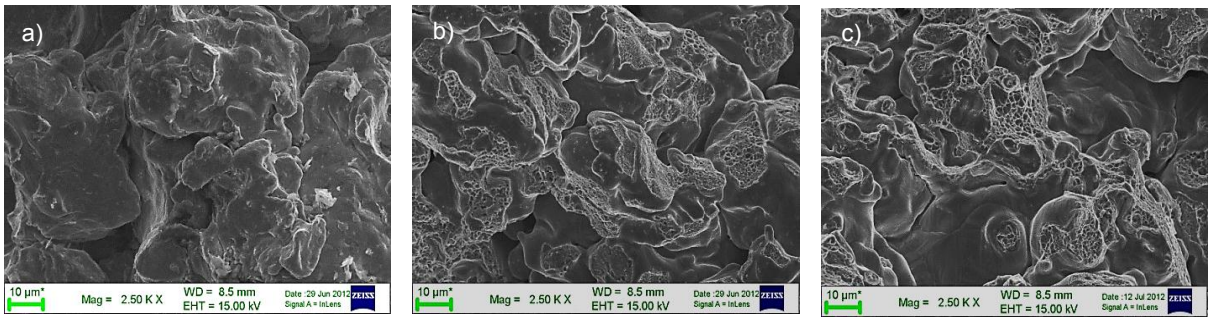

Fig. 2.6: SEM fractographs of the specimen heated to; (a) 700˚C, (b)900˚C and (C) 1120˚C in N_2/10%H_2.

2.9.2.1. Reduction reactions

As it has been mentioned, H_2 and admixed graphite are the main reducing agents in PM steel. The reduction by H_2 occurs through the reaction.

- **$2/y\ M_xO_y(s) + 2H_2\ (g) \longleftrightarrow 2x/y\ M(s) + 2H_2O\ (g)$ (7)**

The reaction takes place at low temperature between 300˚C and 500˚C and particularly close to the component surface.

Fig. 2.7 shows the influence of the sintering condition on efficiency of surface oxide reduction by H_2. Much better controlled atmosphere conditions during sintering in dilatometer result in efficient surface iron oxide layer reduction, evident by better developed inter-particle necks and extended area of carbon dissolution (bainitic microstructure). The main role of H_2 at high temperature is avoiding the oxidation by keeping $p(H_2O)$ /$p(H_2)$ ratio low and reduction of the oxide that might form at surface of the sample during the heating stage [3, 4, 8, 10].

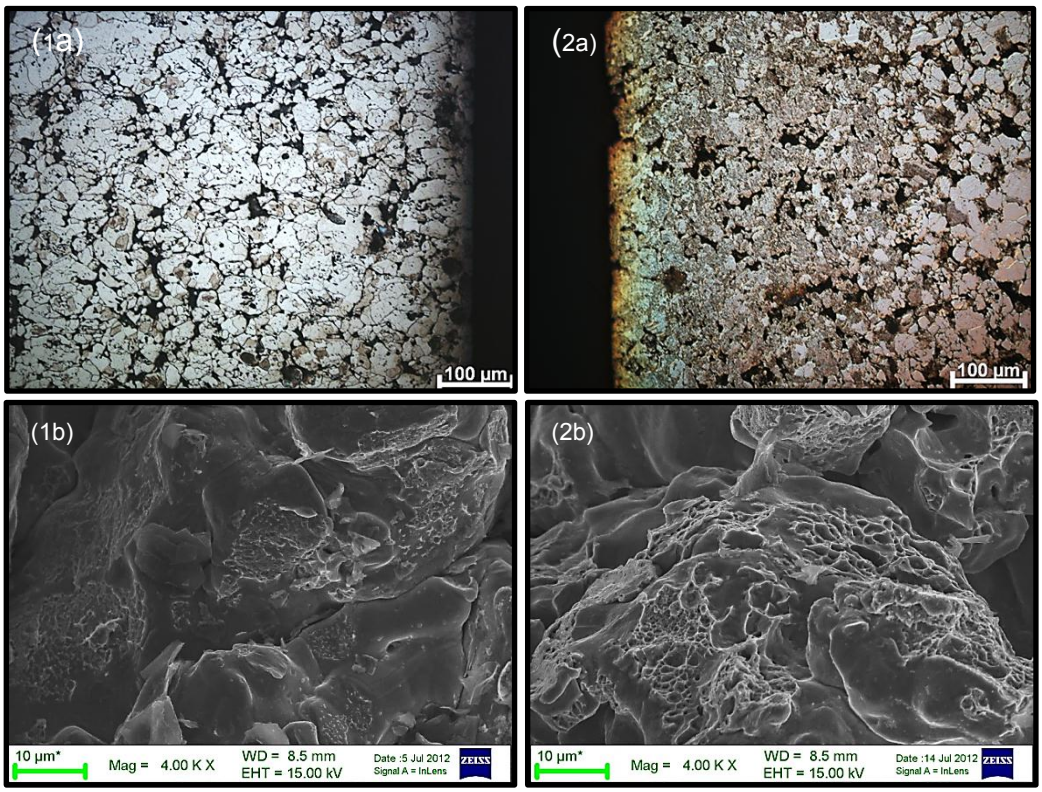

Fig. 2.7: Optical and SEM micrographs taken close to the edge of the samples heated up to 900ºC at different sintering condition showing the influence of reduction of iron oxide layer on powder particle by H_2, 1 (a,b) the sample heated in tube furnace in N_2/10%H_2 atmosphere, 2 (a,b) the sample heated in dilatometer NETZCH DIL 402C in Ar/10%H_2 atmosphere.

The reduction by carbon start in accordance with Eq. (8) through direct-carbothermal reduction when temperature is high enough (≥900ºC) to activate the graphite. However as soon as CO is formed, indirect carbothermal reduction Eq. (9) becomes the main reduction mechanism. With increasing temperature the carbon activity increases and regeneration of CO is ensured according to the reaction with remaining graphite (eq.10) [8, 9, 10].

- **$(2/y)\ M_xO_y(s) + 2C(s) \longleftrightarrow (2x/y)\ M(s) + 2CO(g)$ (8)**
- **$(2/y)\ M_xO_y(s) + 2CO(g) \longleftrightarrow (2x/y)\ M(s) + 2CO_2(g)$ (9)**

- $C(s) + CO_2(g) \longleftrightarrow 2CO(g)$ (10)

2.9.2. Sintering stage

At this stage the part is held at constant temperature (isothermal holding) for sufficient time in order to insure efficient neck formation and homogeneous carbon dissolution [1, 3]

2.9.3. Cooling stage

The desired microstructure is obtained by controlled cooling according to CCT diagram of the respective PM steel. However, another important aspect during cooling is keeping the oxygen potential low in order to prevent decarburisation and oxidation of the components. Normally dry nitrogen is used for cooling [14].

2.10. Crystal structure of graphite.

Graphite has a hexagonal structure. Graphene layers are stacked in the sequence ABABAB. Each carbon atom within aromatic layer (basal plane) is linked through covalent bond, whereas the bonding between layers is linked by van der Waals bonds which are very weak and can easily be broken. In general graphite structure can be described by its crystallite size (Lc), degree of ordering (La) and inter-layer spacing (d) **Fig. 2.8** [16].

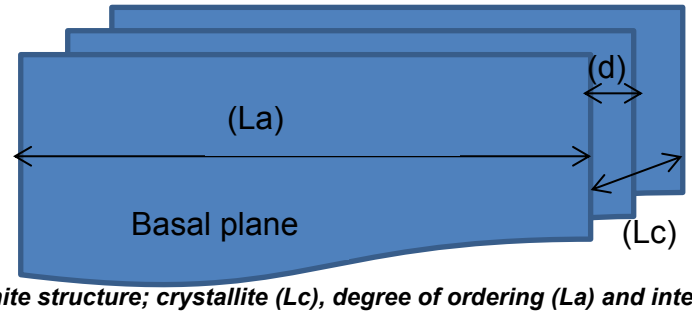

Fig. 2.8: Graphite structure; crystallite (Lc), degree of ordering (La) and inter-layer spacing (d).

2.10.1. Influence of graphite properties on carbon activity

Nowadays there are different grades of graphite on the market. Selection of the grade for the process is primarily based on their properties (morphology, particle size, crystallites orientation and ash content). In general the temperature at which carbothermal reduction (Eq. (8) and Eq. (9)) start indicates the reduction of residual surface oxides.

Particles morphology

Activity of carbon atoms in graphite is higher from the side of the basal planes than from the top of the basal plane. Theretofore more flaky powder particles show to be more active than the coarse ones. **Fig. 2.9** shows different grade of graphite, (a) natural graphite with flaky shape and synthetic graphite

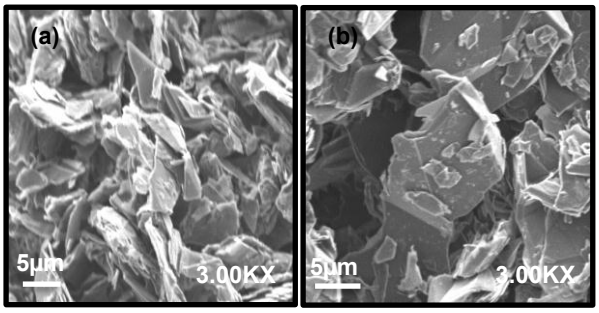

Fig. 2.9: "Flaky" (a) and more coarse (b) types of graphite.

with coarse shape [17, 18, 19].

Size

The activity of carbon in graphite is enhanced by increasing the specific surface area, which in turn leads to higher disorder structure on atomic scale. However, small particle sizes present additional concern as they tend to agglomerate [17, 18, 19].

Ash content

The influence of the ash on the carbon activity is depending on the composition of the ash and the physical distribution of the ash particles in the graphite. If ash exists in form of discrete lumps or particles, its influence on carbon activity is low. However the major concern regarding the influence of ash on carbon activity comes from infused ash in graphite which acts as a physical barrier for carbon activity [19].

3. Material and Experimental Setup

3.1. Material

Water atomized steel powder pre-alloyed with Cr and Mo known as Astaloy CrM, provided by Höganäs AB, Sweden, was used as the base powder in this study. In Table 1 the nominal composition of the powder material is given. To provide the required carbon content in the sintered part, a number of carbon sources, provided by TIMCAL SA, Switzerland, were utilized, namely: synthetic graphite powders (F25, F10 and KS4), natural graphite powders (PG25 and PG10) and carbon black powder (ENSACO 250). The characteristics of these powders are summarized in Table 2.

Table 1.Nominal chemical composition (in wt. %) of Astaloy CrM under investigation

	Cr	Mo	Mn	Si	C	O	Fe
Wt(%)	3	0.5	<0.1	<0.03	<0.01	<0.2	Bal

Table 2: Characteristics of graphite and carbon black powders

Graphite type	Type	Ash (%)	Moisture	Density Scott (g/cc)	BBT (m2/g)	Crystallinity	Particle size distribution(laser Malvern) (µm)		
							D10	D50	D90
PG25	Natural	3.6	0.1	0.08			4.0	10.0	22.0
PG10	Natural	3.5	0.1	0.06			2.5	5.5	11.5
F25	Synthetic	0.06	0.1	0.11		150	4.2	11.2	24.6
F10	Synthetic	0.6	0.1	0.09		80	2.6	6.3	12.6
KS4	Synthetic	0.07	0.1	0.07	26.0	60	1.2	2.4	4.7
ENSACO	Carbon black	0.01	0.2		66.1				

3.2. Experimental evaluation of the existing carbon source

Three basic carbon sources were evaluated during this study. All five standard graphite grades were analysed in as-received state (particle size, morphology) utilizing digital scanning electron microscope (DSEM).

3.3 Experimental evaluation of the reducing ability of different carbon sources

a) Specimens preparation: Astaloy CrM was mixed with 0.6 wt.% Kenolube as lubricant and 0.5 wt.% graphite or carbon black. The mixture was then uniaxially compacted at 600MPa into un-notched

Charpy test bars with the following dimensions: 10x10x55 mm (ISO 5754) and green density of ~ 7.0 g/cm^3 at Höganäs AB, Sweden.

b) Delubrication: the specimens were delubricated at 450˚C with a constant heating rate of 10˚C/min for 30 min in pure N_2 (flow~10 L/min) flowing atmosphere in Entech laboratory tube furnace. The specimens were rabidly cooled using pure N_2 with high flow rate.

c) The interrupted sintering trials: were carried out in two different furnaces. The first experiment was performed in an Entech laboratory tube furnace with a tube diameter of 43 mm. The specimens admixed with different grades of graphite (PG25, PG10, F25, F10 and KS4) were sampled together after heating to 700˚C, 900˚C and 1120˚C and after sintering at 1120˚C for 30 min. Heating rate of 10˚C/min was applied. Dry N_2/10%H_2 atmosphere with the flow of ~ 10 l/min was used as the sintering atmosphere. Before each sintering experiment the furnace was purged with pure N_2. The specimens were rapidly cooled using pure N_2 with high flow rate.

The second set of experiment was performed for all specimens at 900˚C in dilatometer Netzch DIL 402C. Specimens admixed with carbon black were all processed in dilatometer (700˚C, 900˚C and 1120˚C as well as sintered at 1120˚C for 30 min). Every specimen was processed individually with a constant heating rate of 10˚C/min in Ar/10%H_2 atmospheres with the flow of ~ 200 ml/min. The specimens were rabidly cooled using pure Ar with high flow rate.

d) Analysis of interrupted sintered specimens

1. Metallographic evaluation (microstructure, carbon dissolution): The samples are grinded, polished and etched with 2% nital for samples sampled at 700˚C and 900˚C and 2% nital+ 2% picral for samples sampled at 1120˚C and sintered at 1120˚C for 30min.

2. Fracture surface was studied on the fractured samples after impact-test using high resolution scanning electron microscope (LEO Gemini 1550) combined with Energy dispersive X-ray analysis (EDX, INCA Energy). Development of inter-particle necks, oxides composition, distribution and morphology were the main focus of fractographic analysis.

3. Chemical analysis (carbon and oxygen content): were performed utilizing LECO instrument in Höganäs AB, Sweden, in order to evaluate the changes in C-and O content during process.

4. Results

4.1 Analysis of the graphite powders (DSEM)

The following figure shows DSEM images for different grades. The graphite powder in general exhibit a flaky shape with differences in size and thickness as shown in **Fig. 4.1.1.**

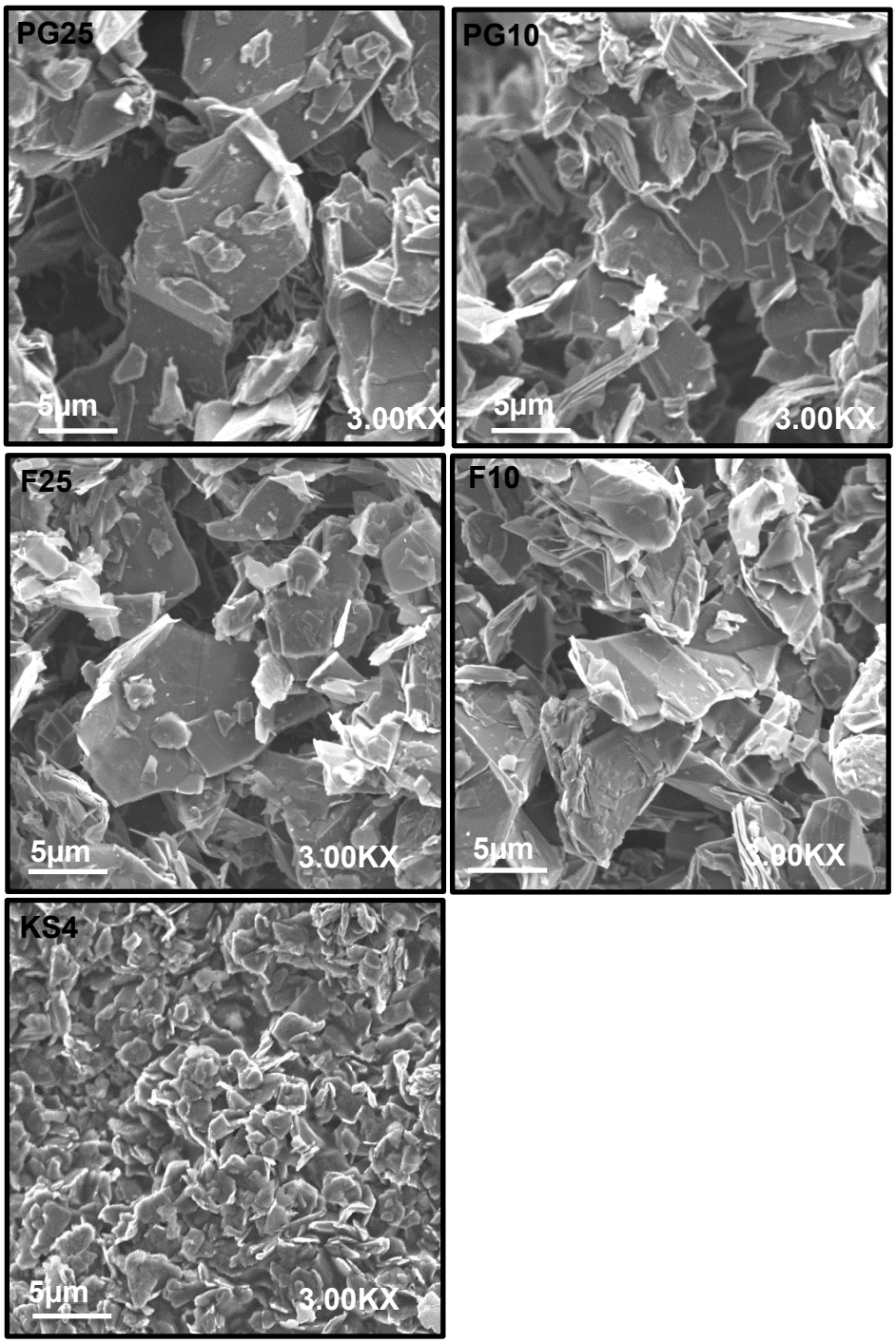

Fig.4.1.1: DSEM images of different graphite grades.

PG 25 has a flaky shape with the largest thickness among all grades whereas F25 has more bulky structure. PG10 and F10 are comparable in both size and thickness but they differ in shape, F10 more coarse whereas PG10 more flaky. KS4 with flaky shape can easily be distinguished from the other graphite grades. It has the smallest powder particle size and unlike the other graphite grades it has a better homogenous size distribution of graphite powder particles. **Fig. 4.1.2** shows SEM image for ENSACO 250 (carbon black). The image was taken from a compacted specimen. As seen in the Fig. 4.1.2 the carbon black (ENSACO 250) exhibits a spherically shaped particles sizing up to 0.2 μm and presented in large agglomerates.

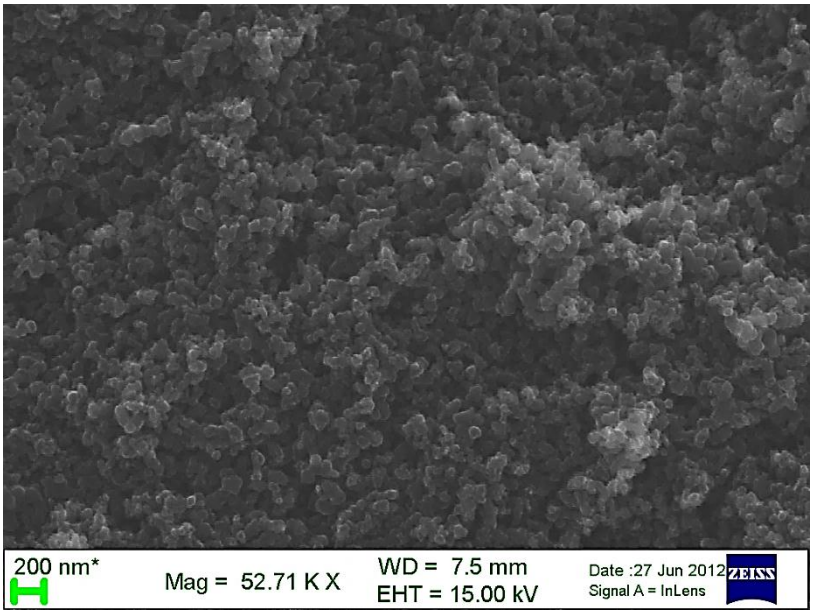

Fig.4.1.2: SEM image of ENSACO 250 (carbon black).

4.2 Metallography

Interrupted sintering at 700˚C(N_2/10%H_2)

Microstructure analyses of heated up to 700˚C for 1 min specimens are presented in Figs. 4.2.1 and 4.2.2. The images were taken from both the centre and edge of specimens. For all samples there was no indication of carbon dissolution in terms of perlite formation, see **Figs. 4.2.1** and **4.2.2.** Furthermore the individual particles and surface oxide can be easily distinguished at this stage.

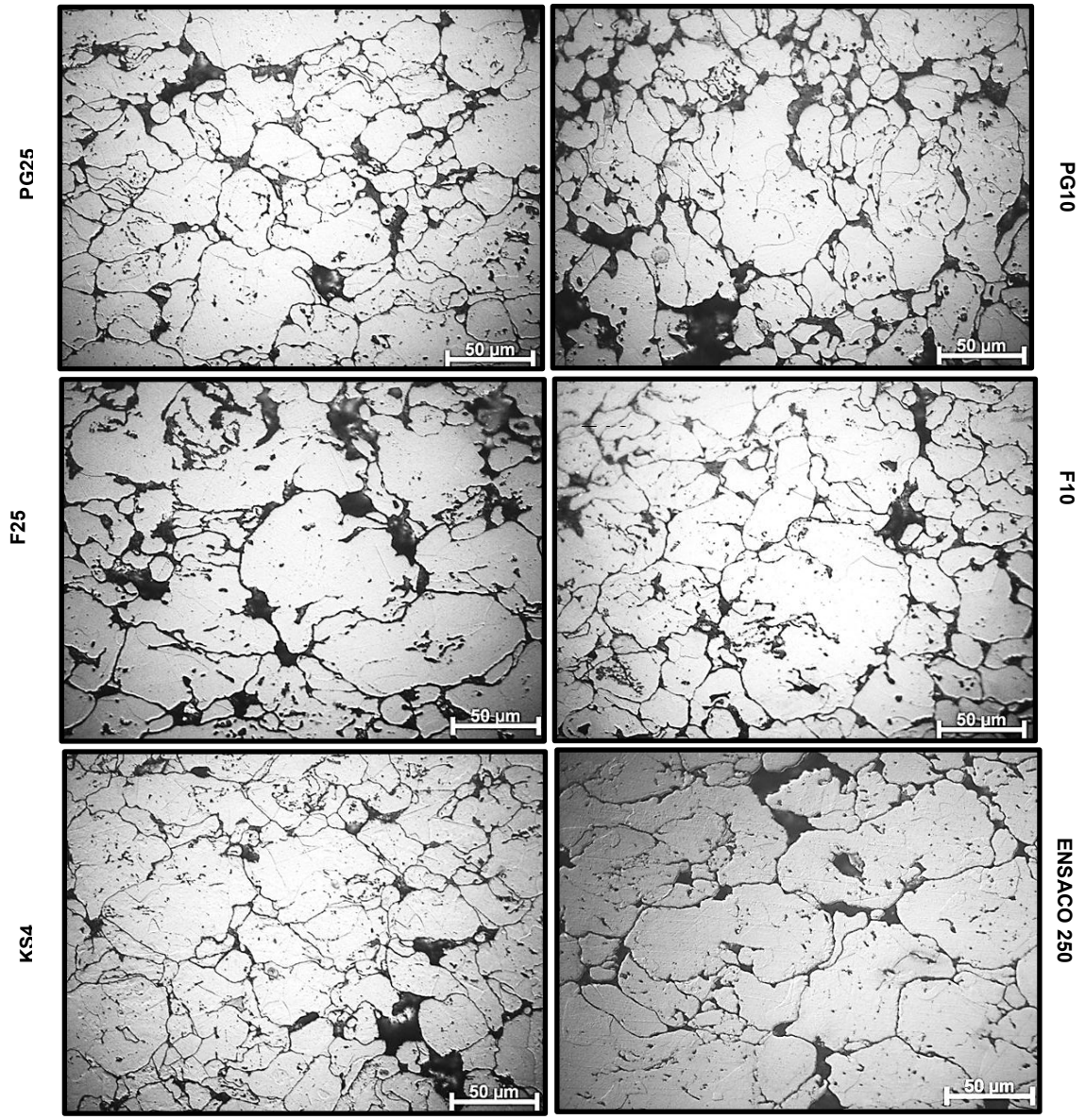

Fig.4.2.1: Microstructure of specimens heated to 700˚C in N_2/10%H_2, except ENSACO 250 in Ar/10%H_2-DIL (centre of the specimens).

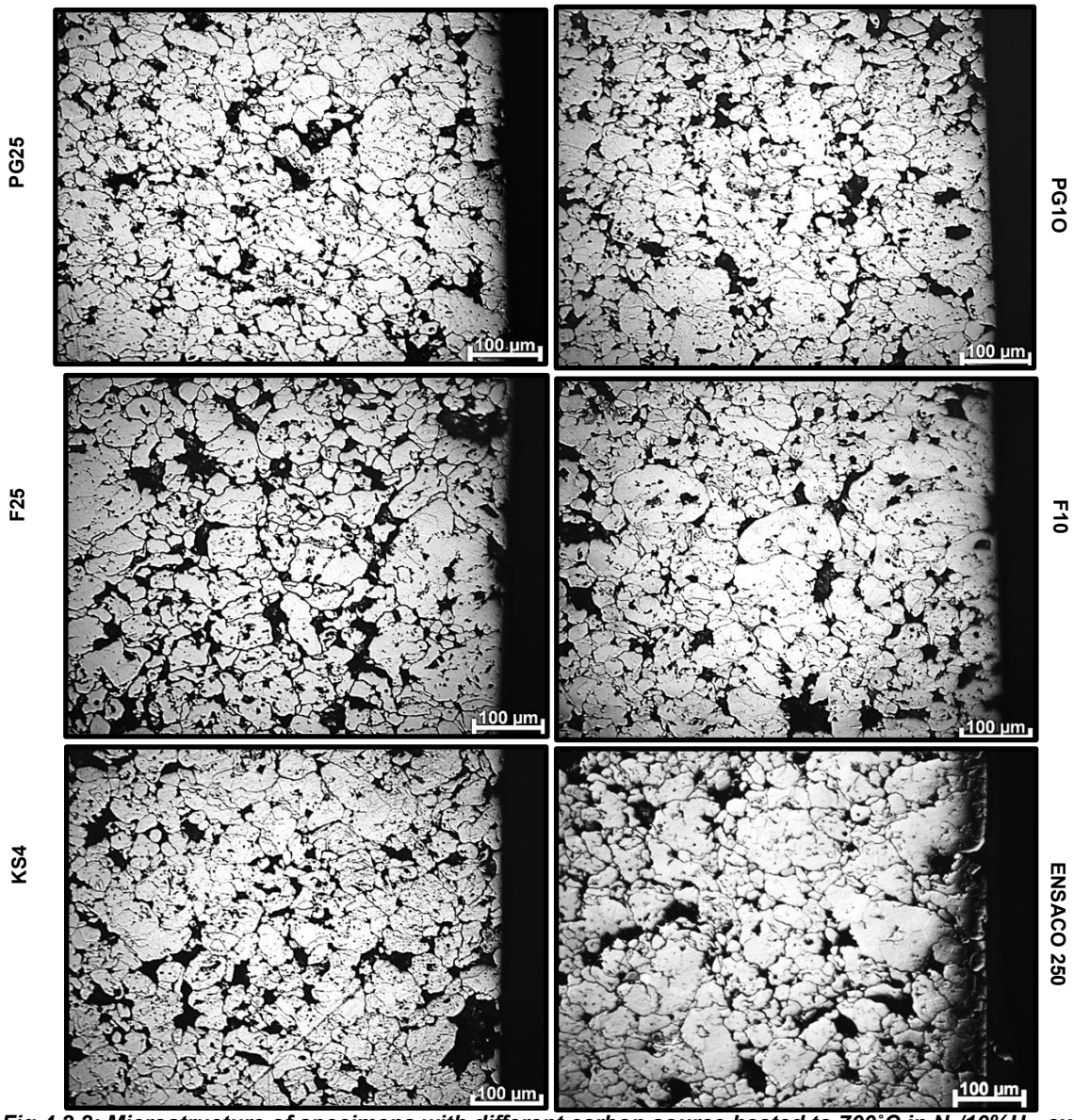

Fig.4.2.2: Microstructure of specimens with different carbon source heated to 700˚C in N_2/10%H_2, except ENSACO 250 in Ar/10%H_2-DIL (edge of the specimens).

Interrupted sintering at 900˚C (N_2/10%H_2)

At this temperature, pearlitic microstructure is registered for samples admixed with PG10, F10 and KS4, indicating that carbon dissolution has started, whereas PG25 and F25 are still inactive at this temperature, see **Fig. 4.2.3**. The amount of pearlite that is formed close to the edge of specimens is slightly higher than that at the centre of the specimens in all three cases, see **Fig. 4.2.4.** The difference in amount of pearlite formation between PG10, F10 and KS4 is hard to distinguish at both the centre and edge of samples at this stage.

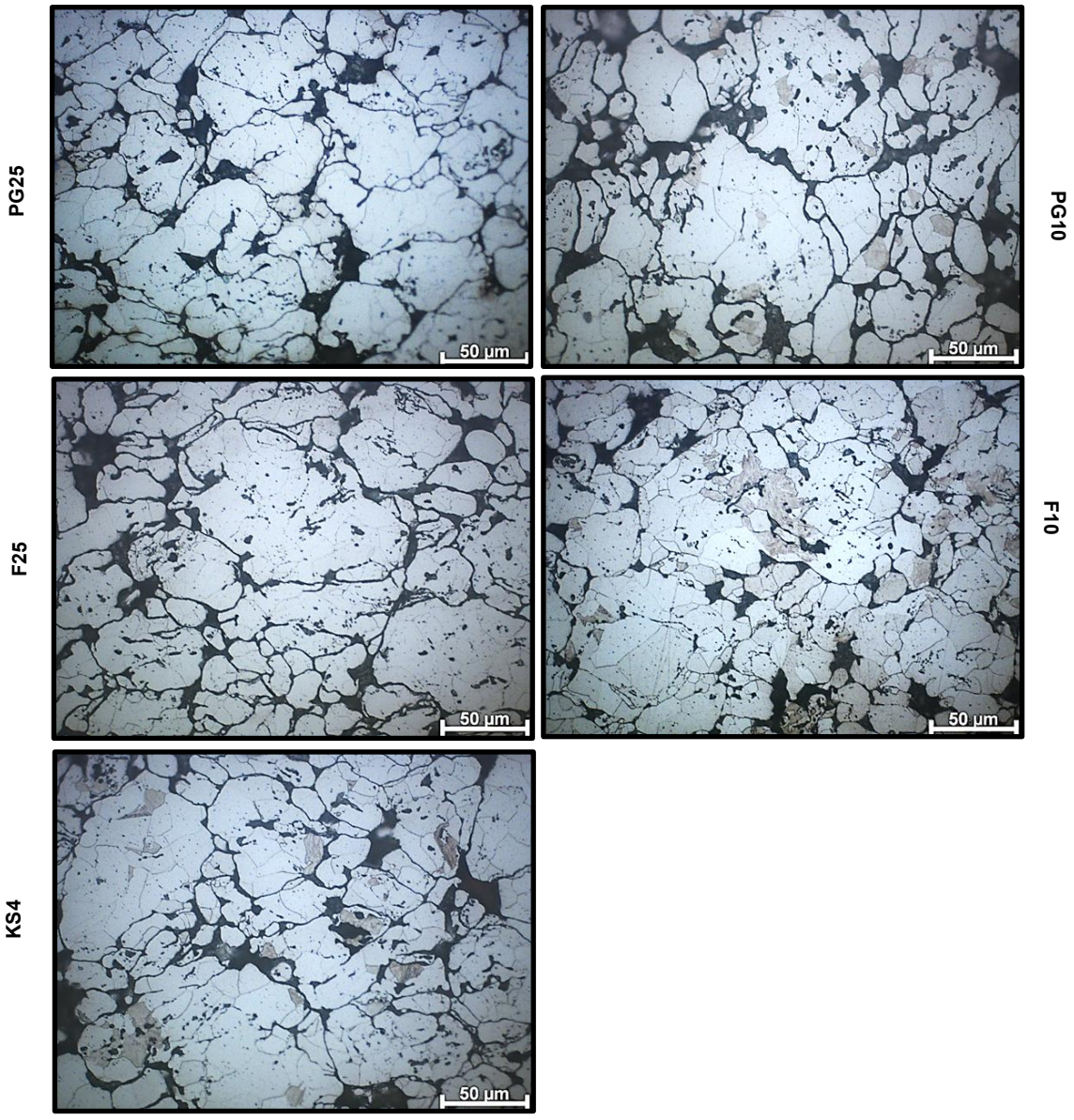

Fig. 4.2.3: Microstructure of specimens with different grade of graphite heated to 900˚C in N_2/10%H_2 (centre of specimens).

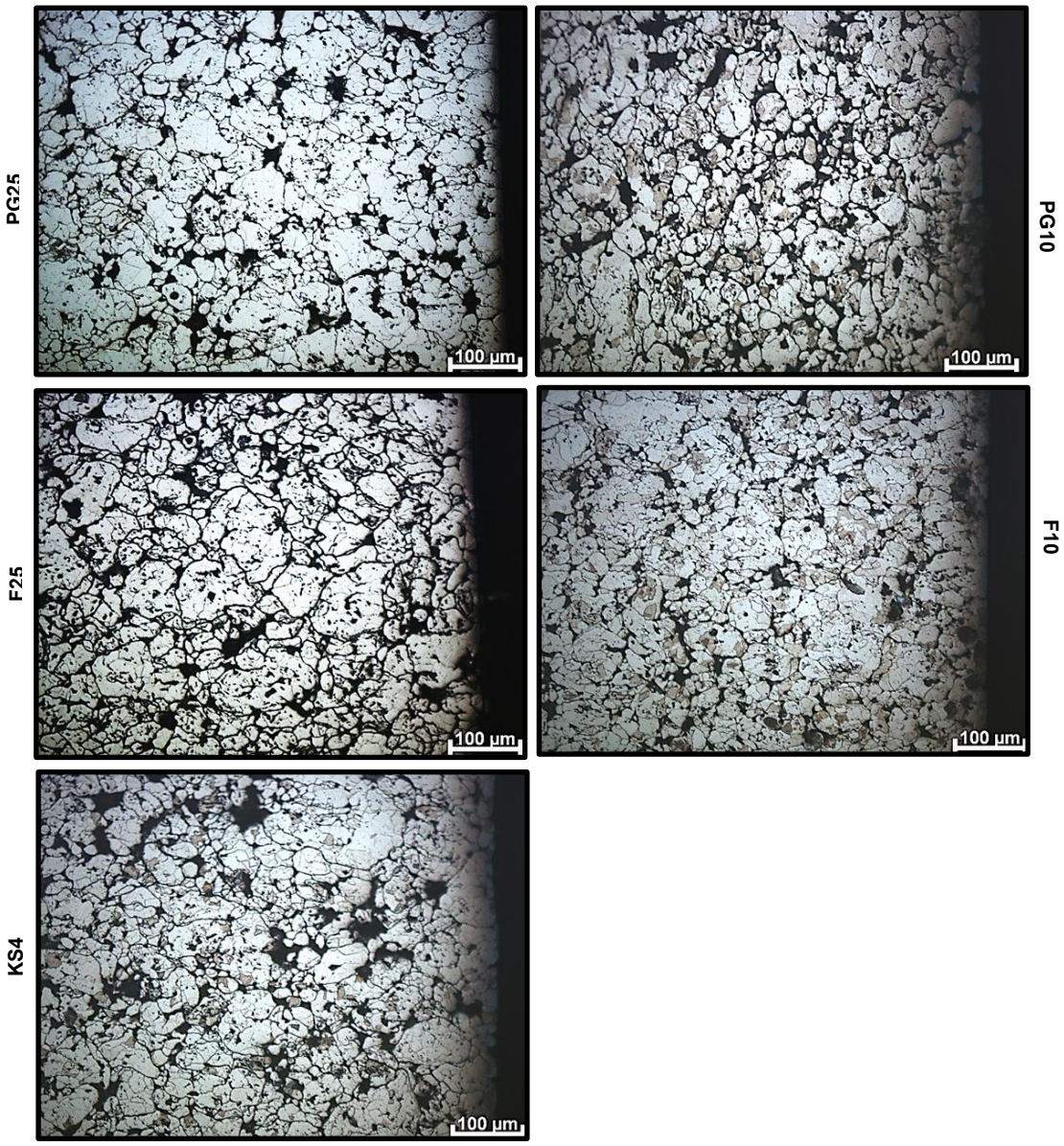

Fig. 4.2.4: Microstructure of specimens with different grade of graphite heated to 900˚C in N_2/10%H_2 (edge of the specimens).

Interrupted sintering at 900˚C (Ar/10%H_2) DIL

This set of experiments was done under conditions with better atmosphere control. In this case, carbon dissolution was registered for all samples except ENSACO 250. As shown in the **Fig. 4.2.5**, the amount of pearlite formed was slightly higher for KS4 than for F10 and PG10. Furthermore, it is comparable to the previous case, see **Fig. 4.2.3**. F25 and PG25 show traces of pearlite formation. At the edge of the samples, **Fig. 4.2.6**, bainite formation was observed for all samples except ENSACO 250. The extent of bainite formation in decreasing order is noticed for KS4, F10, PG10, PG25, F25.

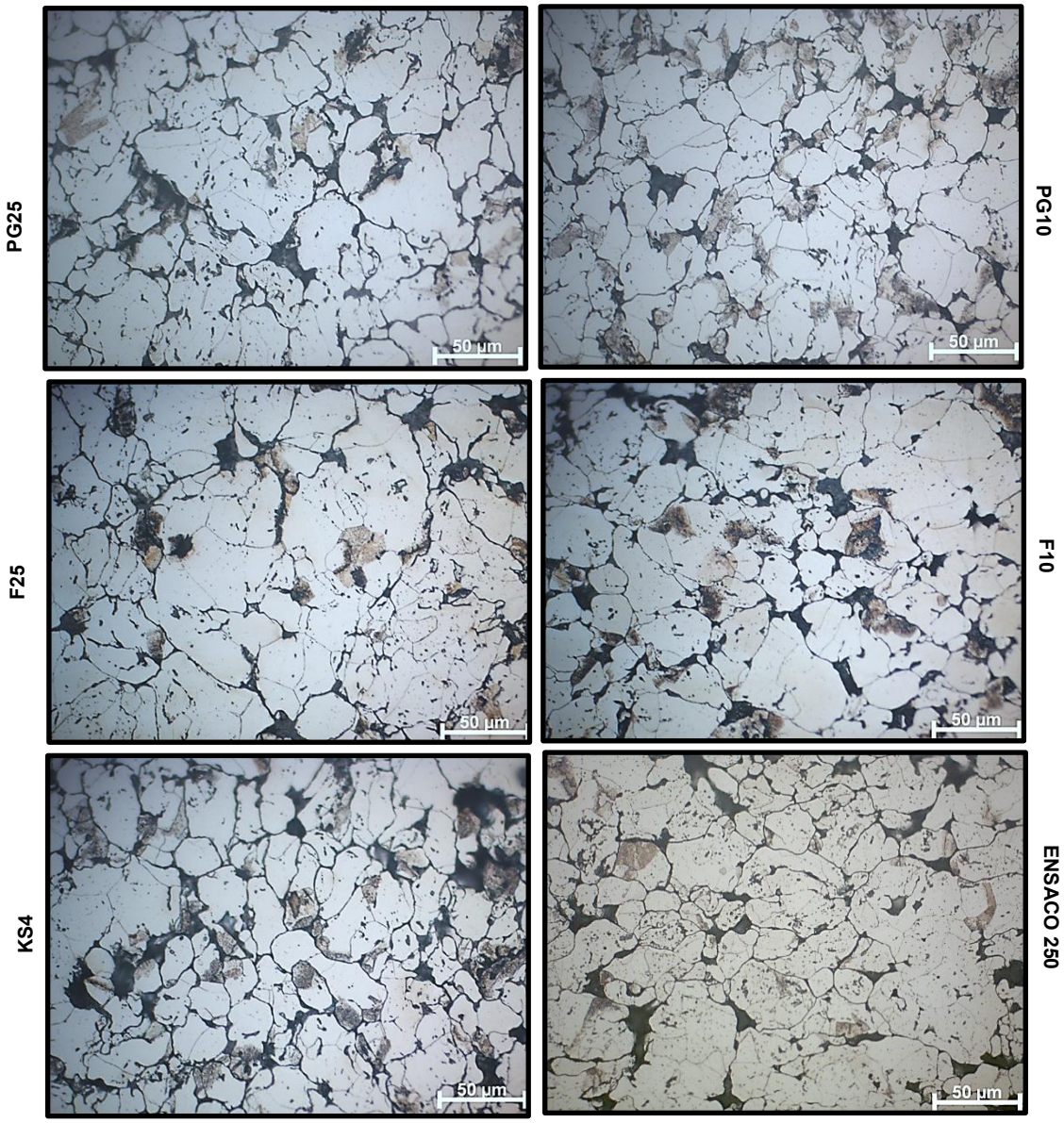

Fig.4.2.5: Microstructure of specimens with different carbon sources heated to 900˚C in Ar/10%H_2-DIL (centre of the specimens).

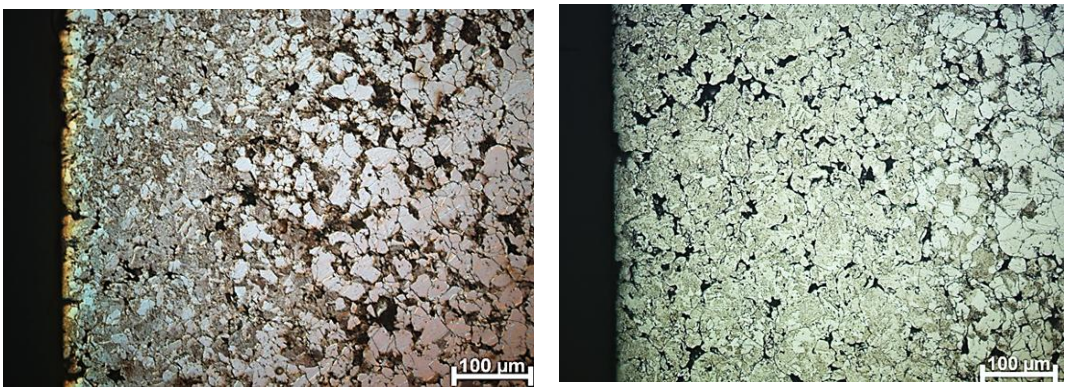

(PG25) (PG10)

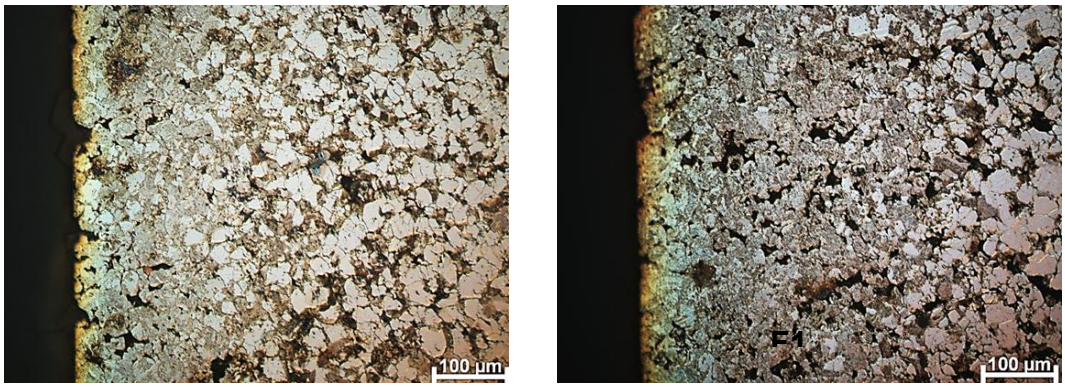

(F25) (F10)

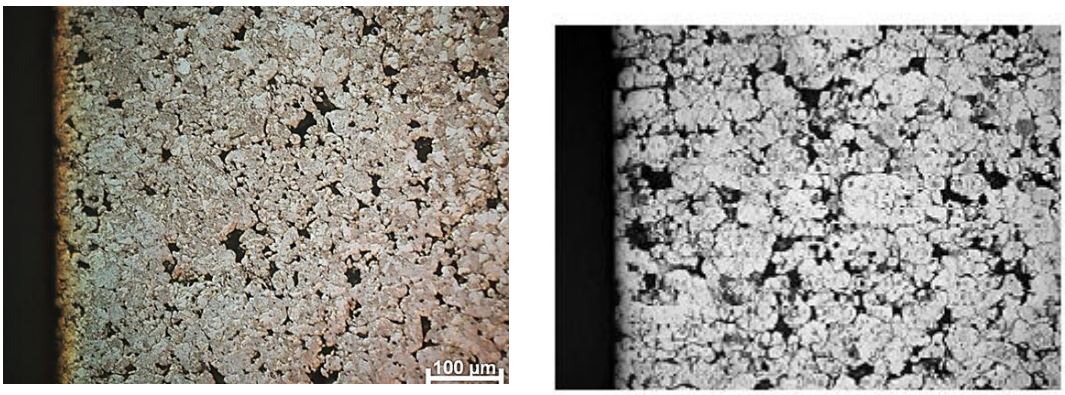

(KS4) (ENSACO 250)

Fig.4.2.6: Microstructure of specimens with different carbon sources heated to 900˚C in Ar/10%H_2-DIL (edge of the specimens).

Interrupted sintering at 1120˚C (N_2/10%H_2)

At this temperature bainite and trace amount of martensite formation were observed in the centre of the samples for the all carbon sources, see **Fig. 4.2.7**. ENSACO 250 shows different structure, possibly caused by larger martensite content in comparison with rest.

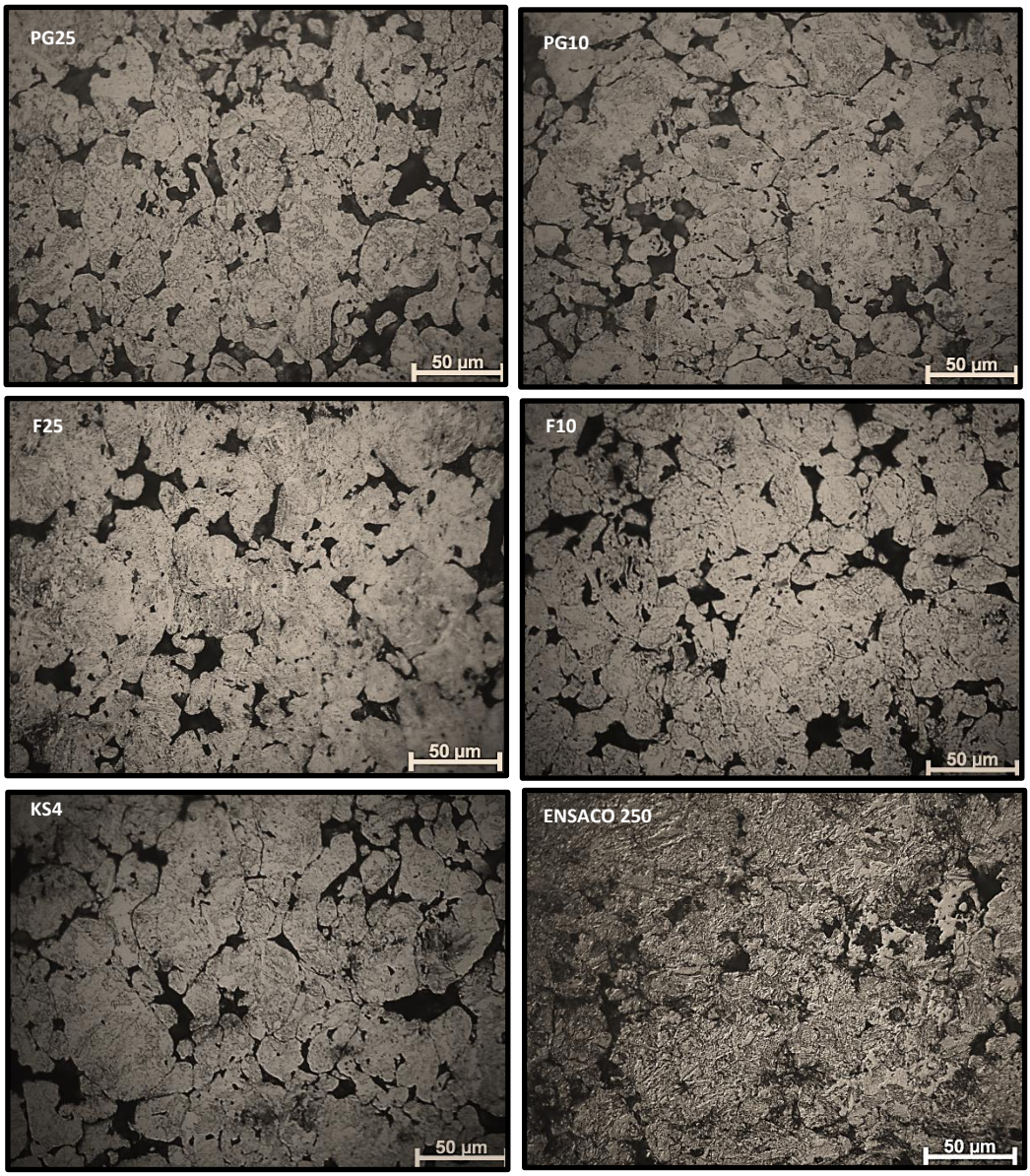

Fig.4.2.7: Microstructure of specimens with different carbon sources heated to 1120˚C in N_2/10%H_2, except ENSACO 250 in Ar/10%H_2-DIL (centre of the specimens).

Sintering at 1120˚C (N_2/10%H_2) for 30 min

Increase in the amount martensite in comparison to heated samples was observed for sintered at 1120˚C (N_2/10H_2) for KS4, F25, F10 and PG10, insignificant increase was observed for PG25, whereas ENSACO 250 shows almost no change, see **Fig. 4.2.8**.

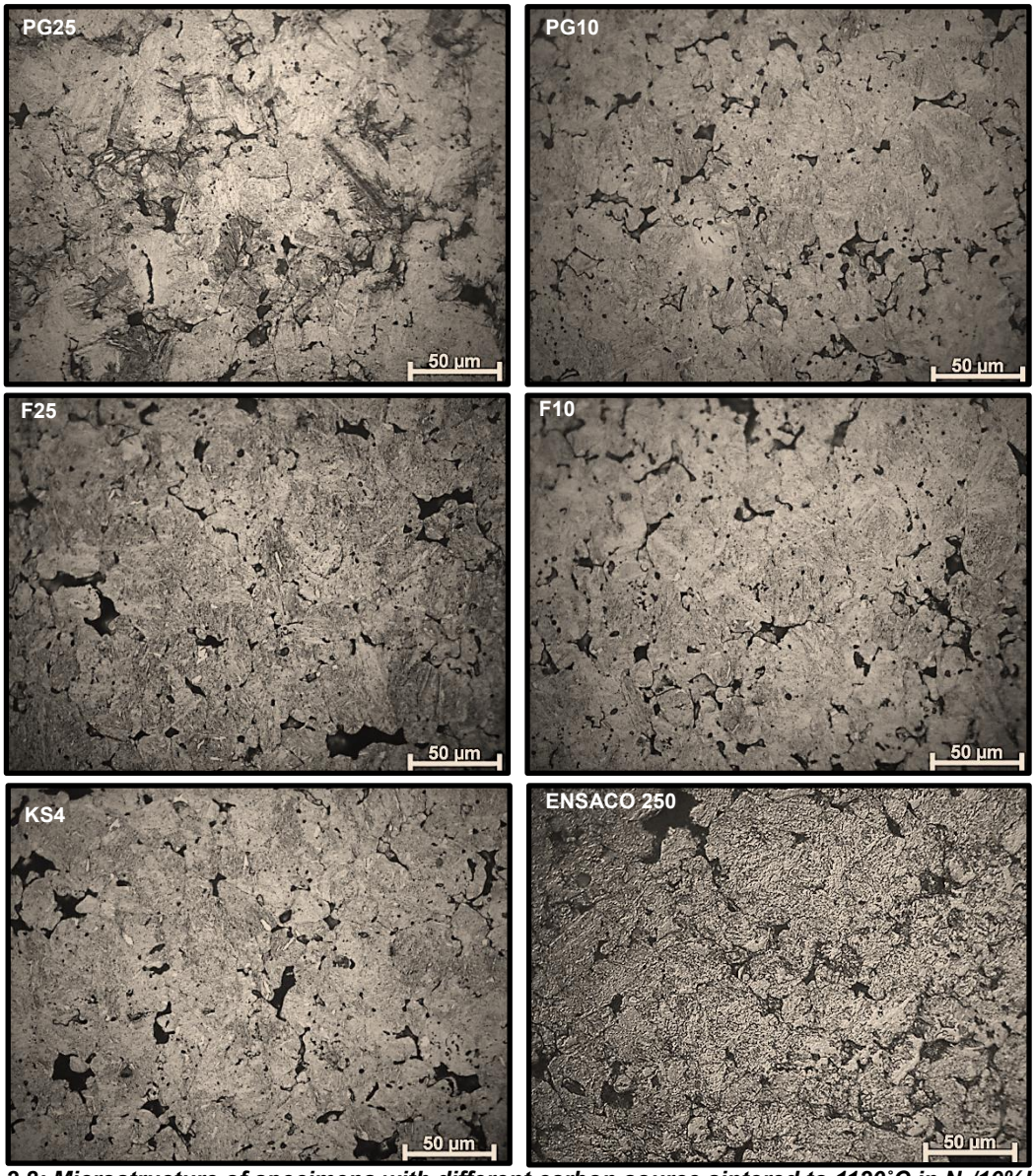

Fig.4.2.8: Microstructure of specimens with different carbon source sintered to 1120˚C in N_2/10%H_2 for 30min, except ENSACO 250 in Ar/10%H_2-DIL (centre of the specimens).

4.3. Fractography (SEM+EDX)

Interrupted sintering at 700˚C (N_2/10%H_2)

The fracture surfaces (from the centre of samples) at different magnifications of the samples heated up to 700°C are presented in **Figs. 4.3.1** and **4.3.2**. For all the specimens fracture surface observed was rough. Individual powder particles and their agglomerates can be easily distinguished for all samples, **Fig. 4.3.1**. The presence of graphite or carbon black was evident in all samples. The fracture surface close to the edge of the samples that can be found in Appendix shows similar result to that obtained from the centre of the samples. There was no indication of carbon activity in terms of the inter-particle necks development for all carbon sources at this stage as well.

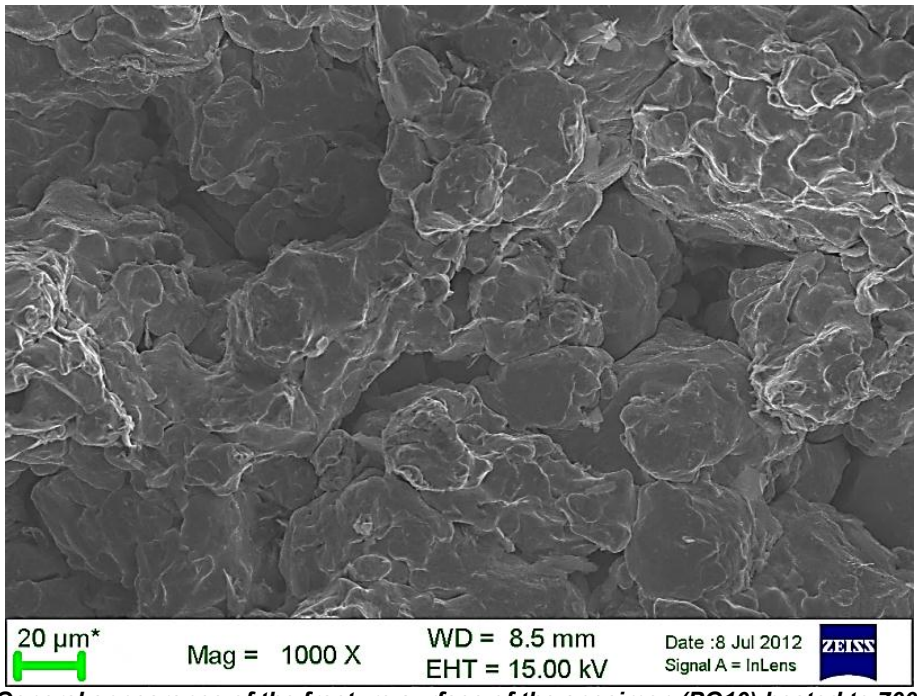

Fig.4.3.1: General appearance of the fracture surface of the specimen (PG10) heated to 700˚C in N_2/10%H_2.

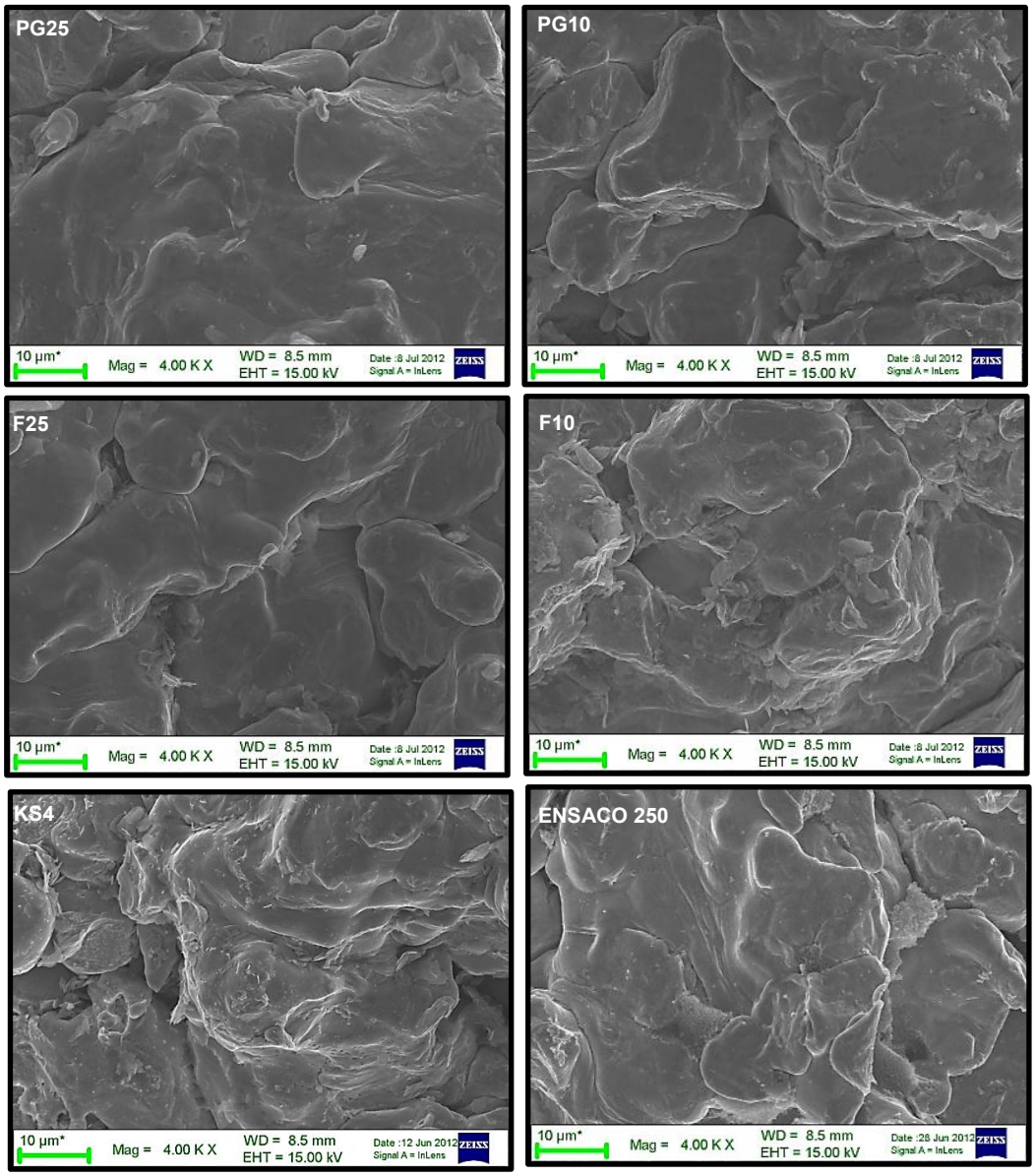

Fig.4.3.2: Fracture surface of specimens with different carbon sources heated to 700˚C in N_2/10%H_2, except ENSACO 250 in Ar/10%H_2-DIL (centre of the specimens).

Interrupted sintering at 900˚C (N_2/10%H_2)

The individual particles and their agglomerates also can be distinguished at this temperature as well as the presence of graphite for all three cases, see **Fig. 4.3.3**. At this stage, branched networks of inter-particle connections were only observed at the centre for KS4, F10 and PG10 indicating the reduction of the surface iron oxide layer, see **Figs. 4.3.4** and **4.3.5**. PG25 and F25 were still inactive at this temperature and atmosphere conditions. The edges of specimens show significant improvement in quality and amount of inter-particle connections for all three cases, see **Fig. 4.3.6**.

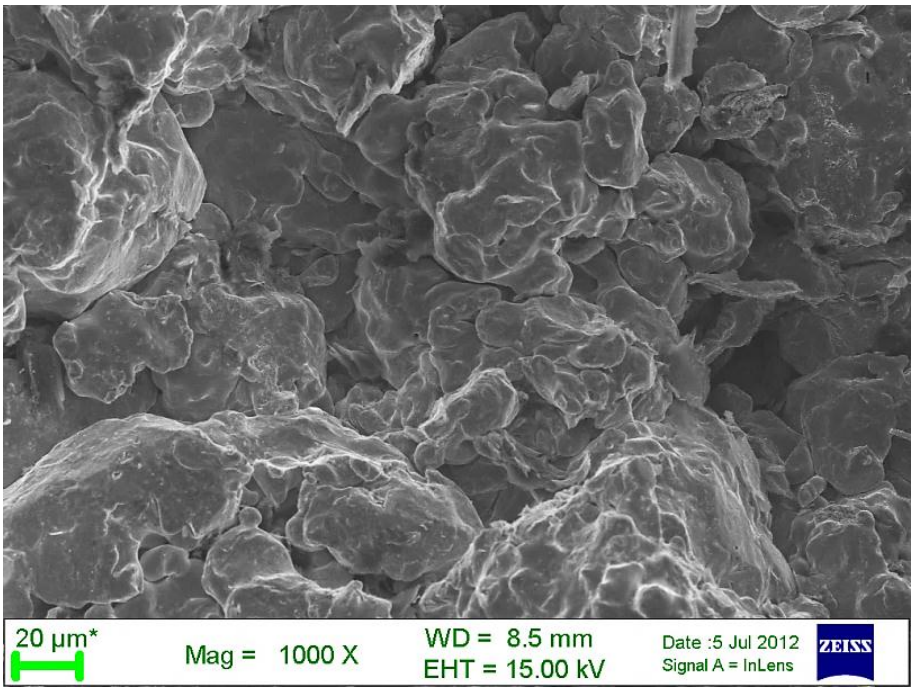

Fig.4.3.3: General appearance of the fracture surface of the specimen (F25) heated to 900˚C in N_2/10%H_2.

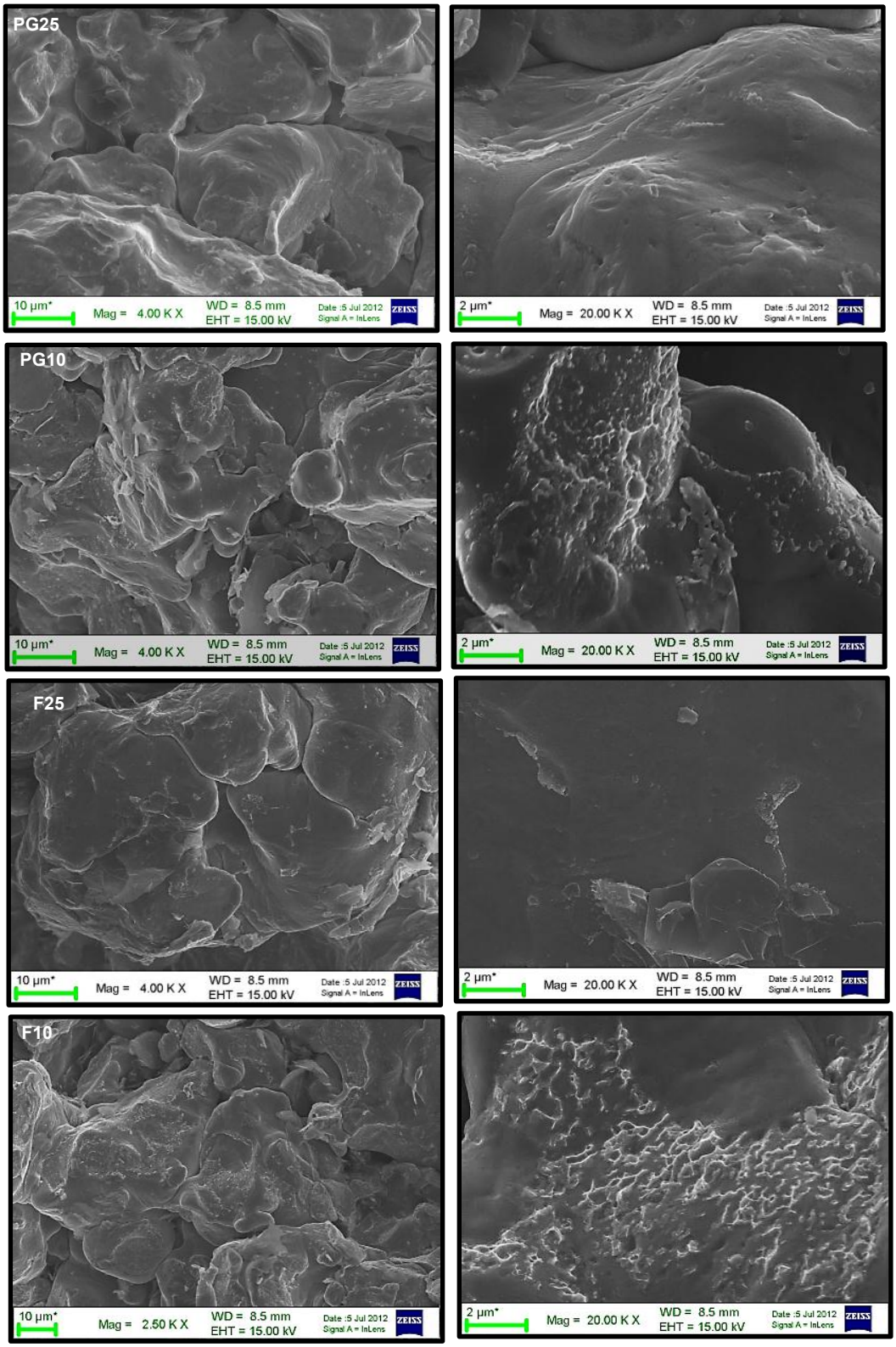

Fig.4.3.4: Fracture surface of specimens with different grade of graphite heated to 900˚C in N_2/10%H_2 (centre of the specimens).

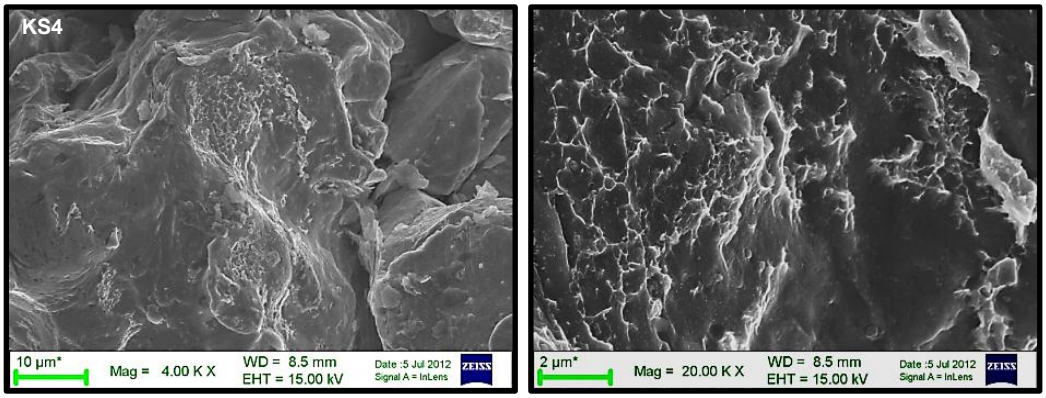

Fig.4.3.5: Fracture surface of specimens with KS4 heated to 900˚C in N N_2/10%H_2 (centre of the specimen).

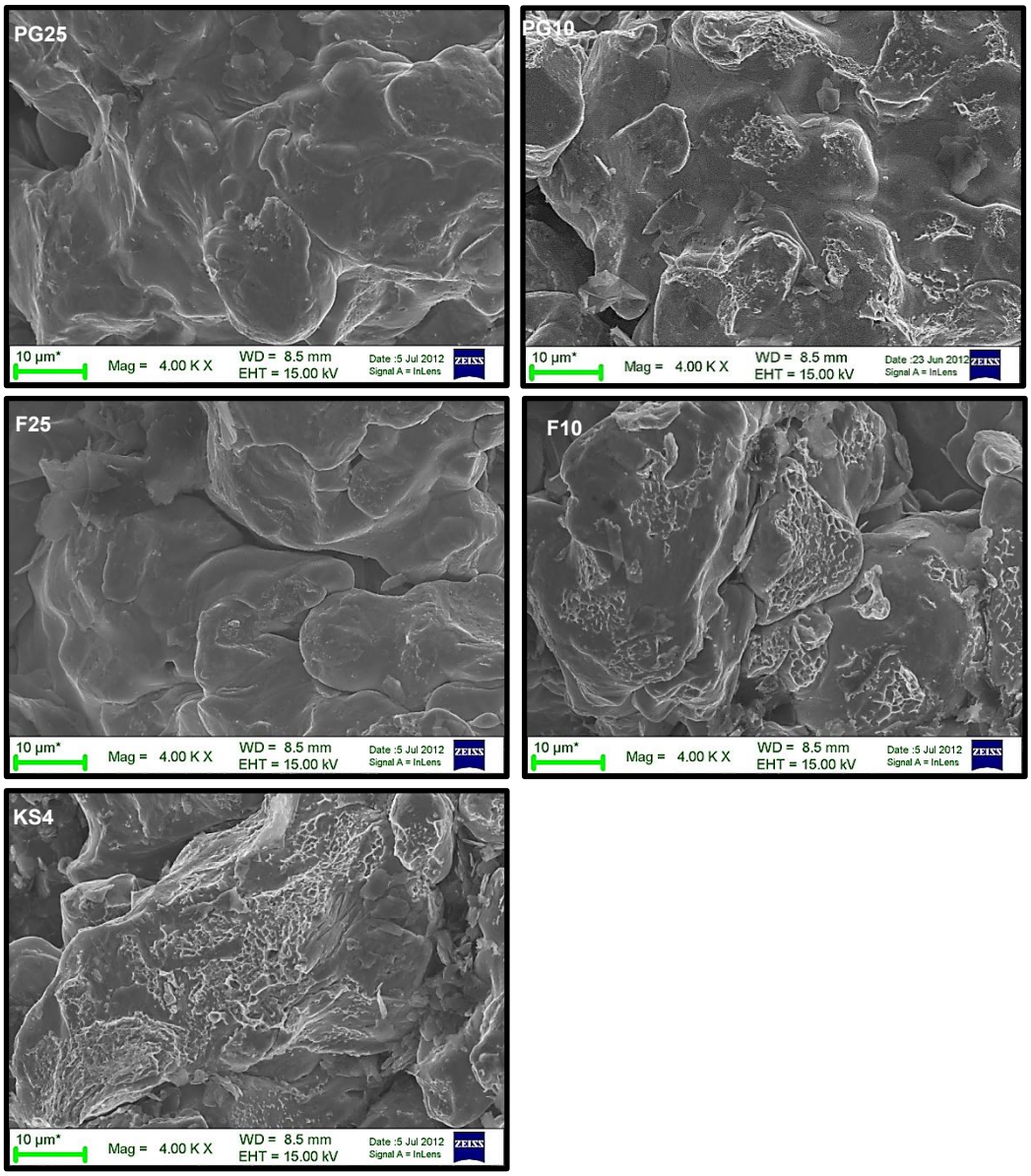

Fig.4.3.6: Fracture surface of specimens with different grade of graphite heated to 900˚C in N_2/10%H_2 (edge of the specimens).

Interrupted sintering at 900˚C (Ar/10%H_2)

The individual particles and their agglomerates can also be seen in this case, but with more inter-particle connection in comparison to previous case, see **Fig. 4.3.3** and **4.3.7**. Unlike the previous case, a network of line connections was observed for PG25 and F25 as well as short line inter-particle connections for ENSACO 250, see **Figs. 4.3.8** and **4.3.9**, indicating the carbon activity has started to some extent for the employed processing condition. Inter-particle ductile fracture with shallow dimples was observed in the case of KS4, F10 and PG10. As it was observed under the previous processing condition, for the present case larger amount of inter-particle connections and more developed necks were observed near the edge of the samples, except ENSACO 250, see **Fig. 4.3.10**. F25 and PG25 shows a comparable result in terms of the amount of inter-particle connections and neck formation development, whereas KS4, F10 and PG10 show much better developed necks and larger area fraction of contacts. The presence of large amount of un-dissolved graphite is evident in the cases of all graphite grades that have been used in this study at this temperature. Carbon black shows to be fully inert at this conditions, only seldom short-line inter-particle connection were observed. From the point of view of inter-particle connection, amount and strength, carbon black shows to be the worst up to this stage.

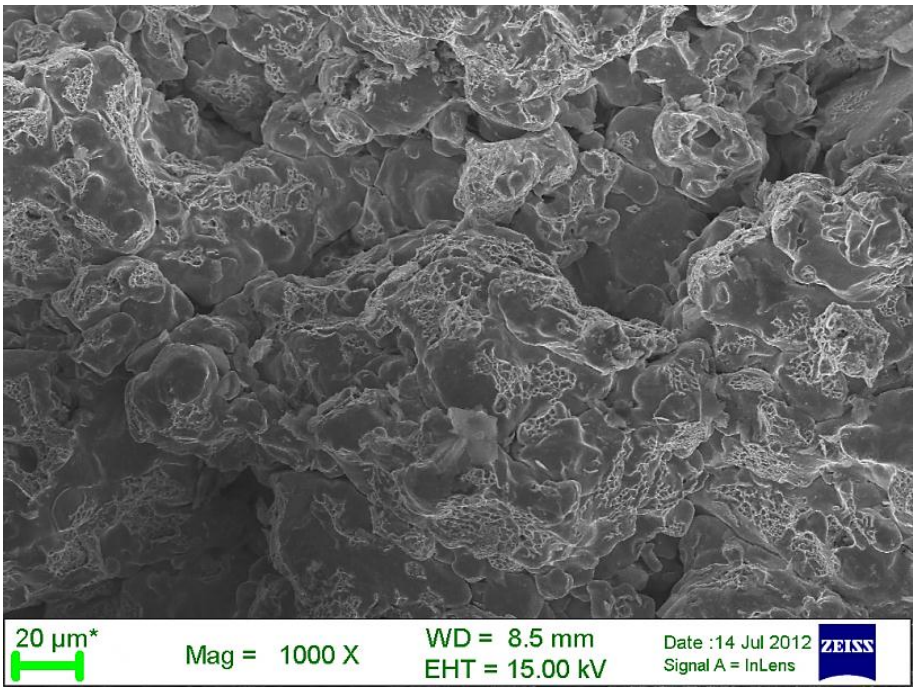

***Fig. 4.3.7: General appearance of the fracture surface of specimen (KS4) heated to 900˚C* in N_2/10%H_2.**

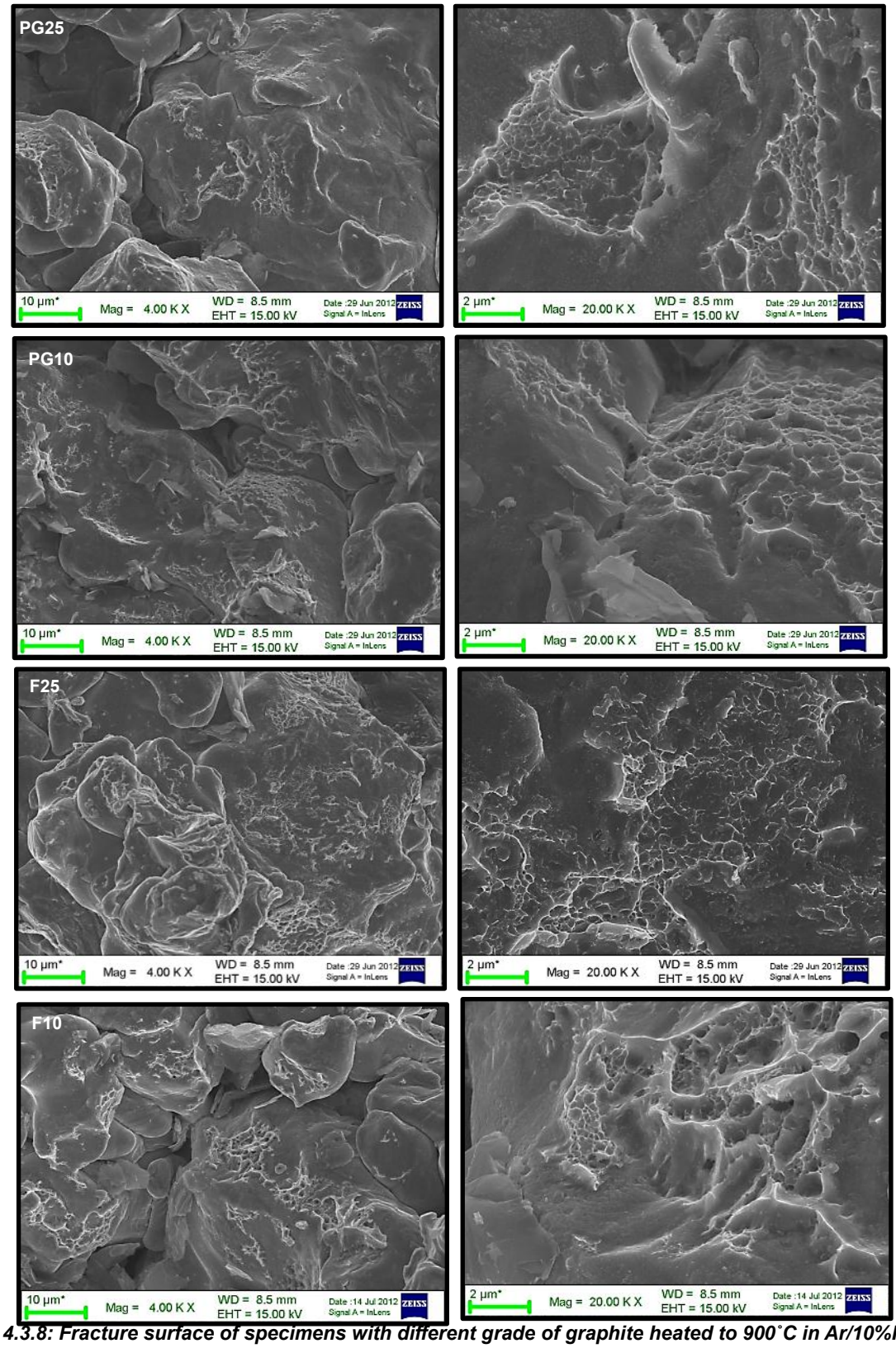

Fig. 4.3.8: Fracture surface of specimens with different grade of graphite heated to 900˚C in Ar/10%H_2, (centre of the samples).

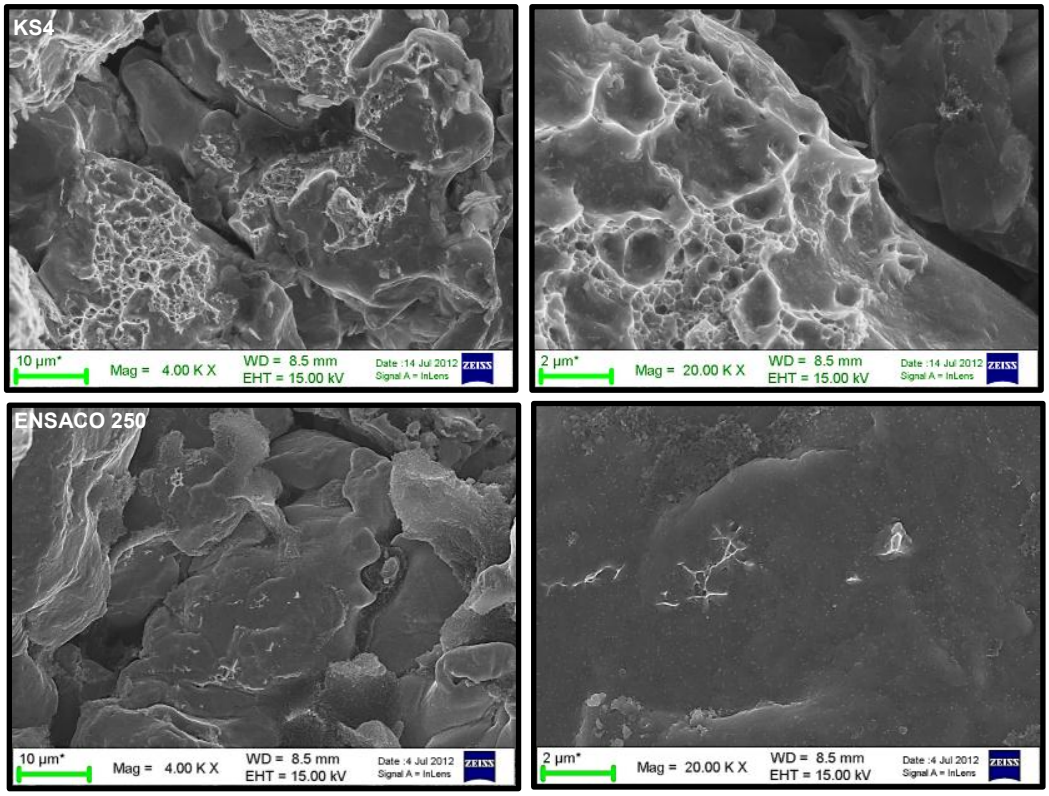

Fig. 4.3.9: Fracture surface of specimens with KS4 and ENSACO250 heated to 900˚C in Ar/10%H_2 (centre of the sample).

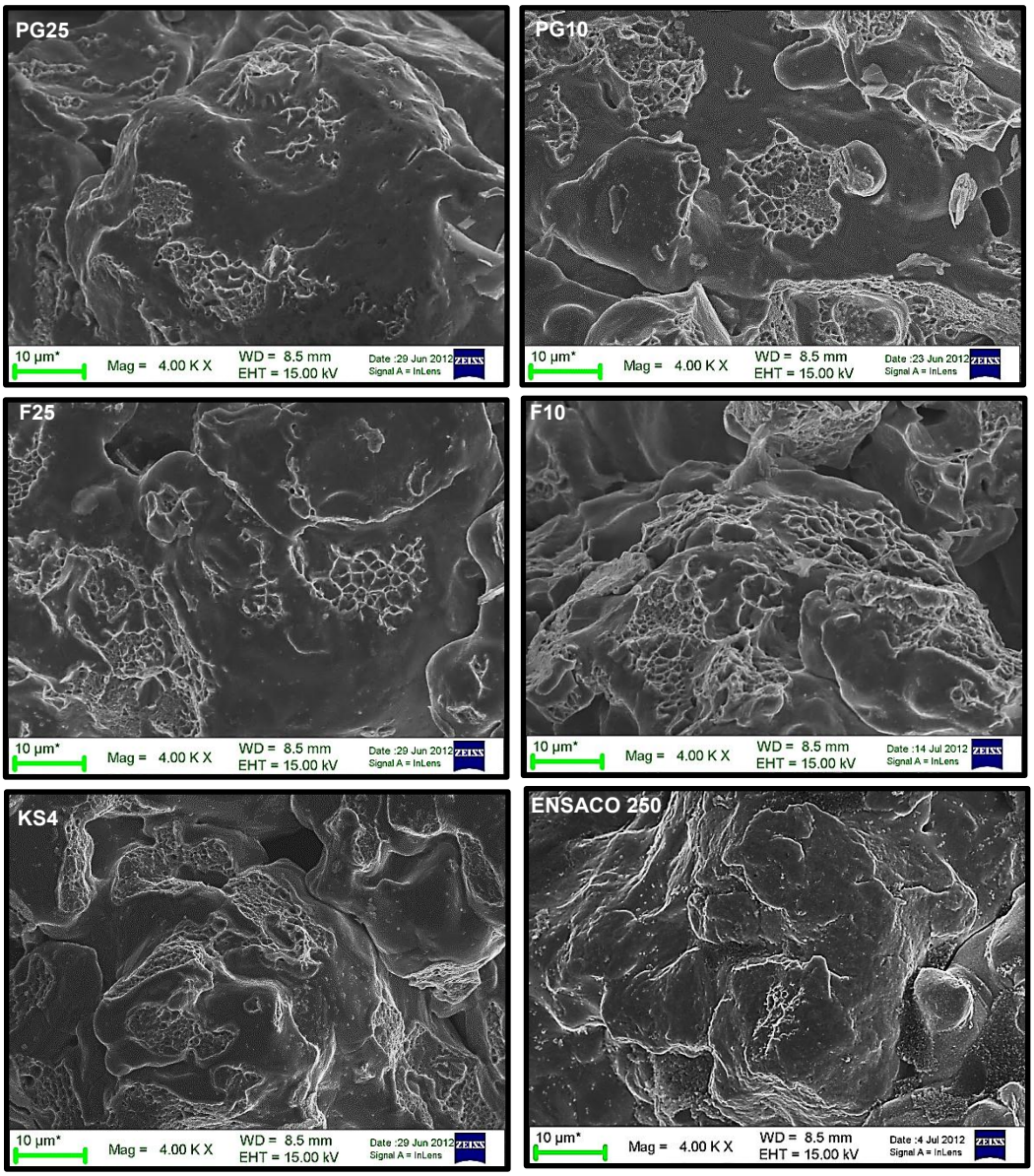

Fig. 4.3.10: Fracture surface of specimens with different carbon source heated to 900˚C in Ar/10%H_2 (edge of the sample).

Interrupted sintering at 1120°C (N_2/10%H_2)

At this temperature the main focus was to find indications of the presence of carbon source and evaluate the free powder surface condition. As the **Fig. 4.3.11** shows, the presence of residual graphite is evident for the cases of KS4, F10, F25, PG25 and PG10. Furthermore the powder surface still contains particulate oxides. ENSACO 250 on the other hand shows opposite result, with no indication of carbon black or particulate oxides on powder surface. For all samples the main failure mechanism was inter-particle dimple ductile fracture. EDX analysis shows that primary oxide inclusions inside the necks are rich in strong oxide forming elements Cr and Mn with ratio 2:1 and Si-oxide see **Fig. 4.3.12**.

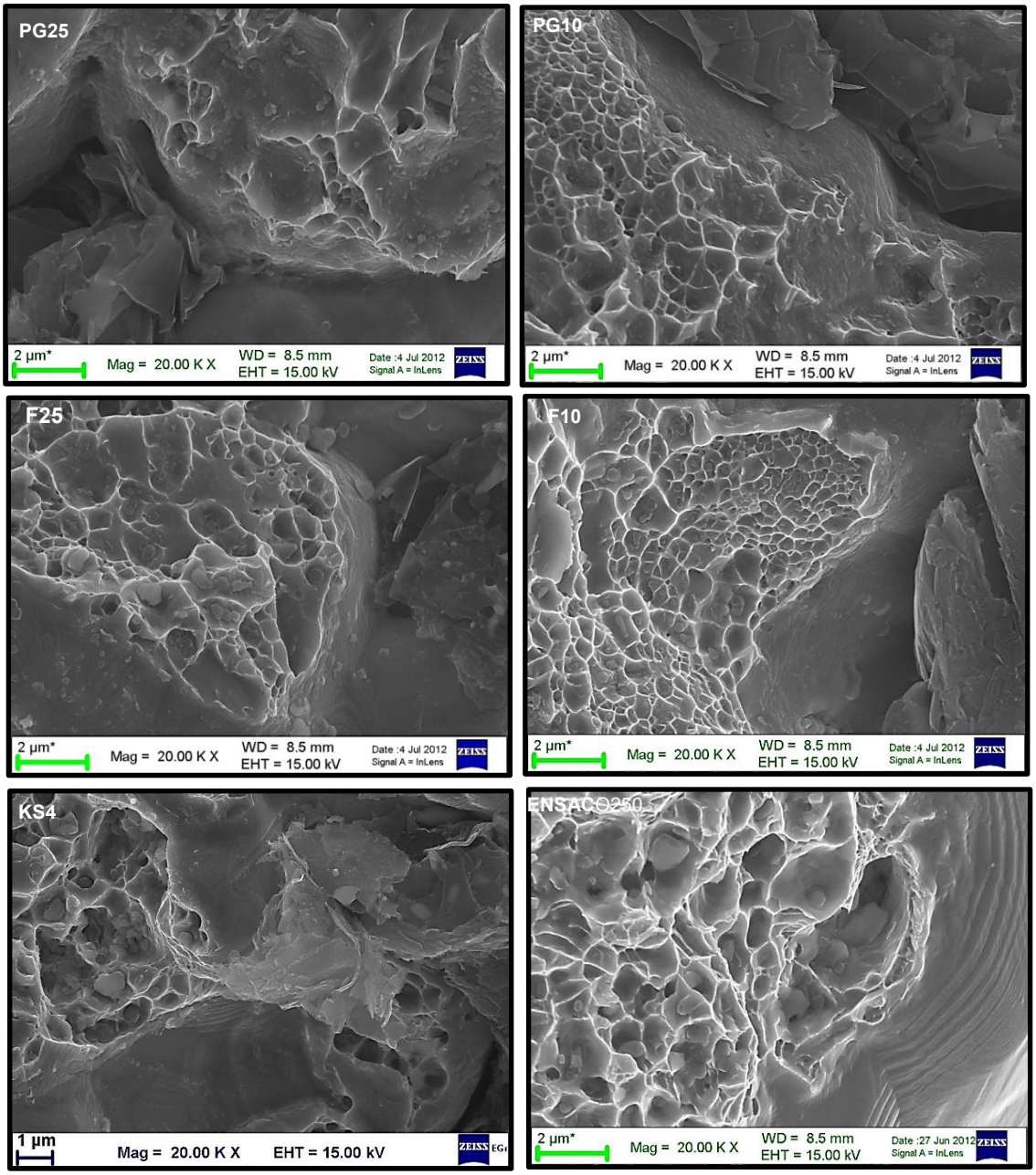

Fig.4.3.11: Appearance of the fracture surface for the specimens heated to 1120˚C in N_2/10%H_2 indicates presence of residual graphite.

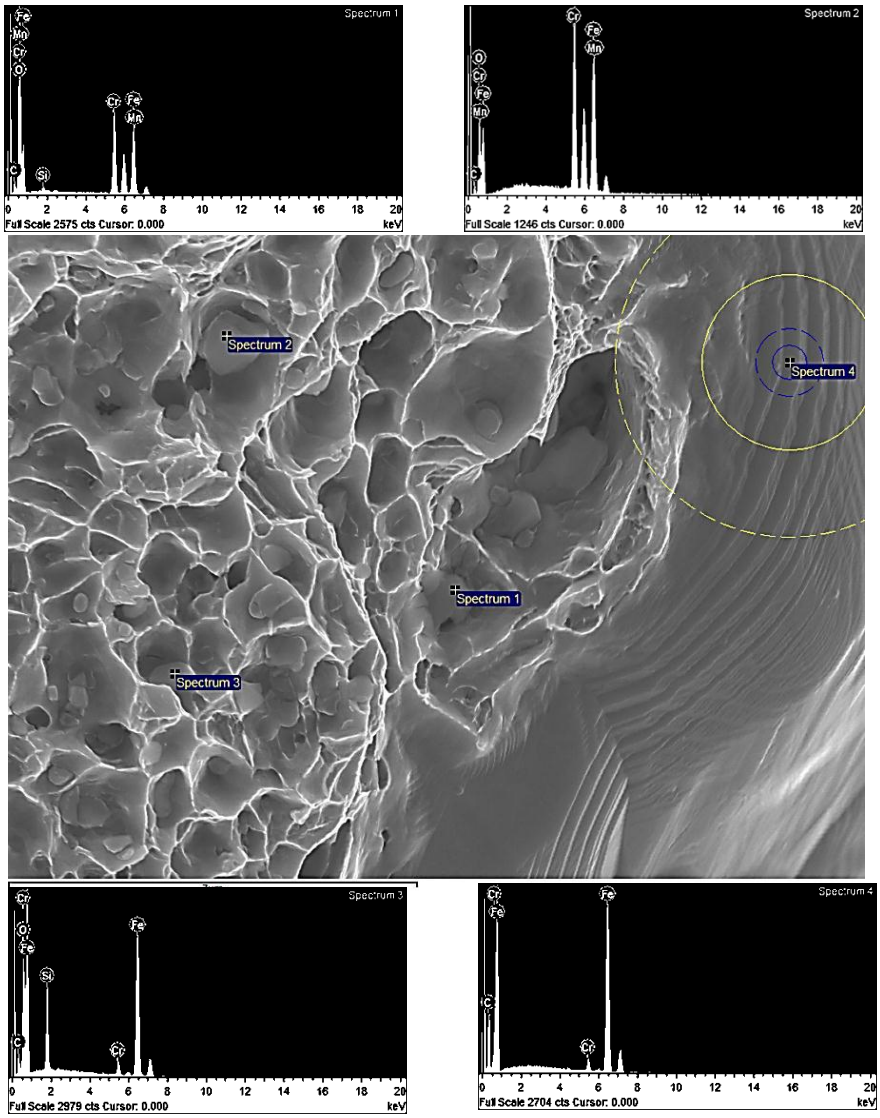

Spectrum	O	Si	Cr	Mn	Fe
1 [at.%]	43.78	0.74	20.07	10.35	25.07
2	12.21		33.35	15.80	38.64
3	32.02	10.38	3.08		54.52
4			3.54		96.46

Spectrum	Si	Cr	Mn	Fe
1 [at.%]	1.40	35.51	18.36	44.73
2		37.96	17.98	44.06
3	15.79	4.48		79.73
4		3.54		96.46

Fig.4.3.12: SEM+EDX analysis on particulate features observed on the fracture surface of the specimen heated to 1120˚C in Ar/10H_2.

Sintering at 1120°C (N_2/10H_2) for 30 min

After sufficient time is given, KS4, F10, F25, and PG10 were fully dissolved and the free surface of the powder was oxide free, while large amount of residual graphite for PG25 was registered. Moreover free powder surface contains un-reduced particulate oxides in the case of PG25, see **Figs. 4.3.13** and **4.3.14**. SEM+EDX analysis indicates that even if after sintering amount of oxides decreased, their chemical composition does not change so much indicating presence of Cr-Mn oxide, see **Fig. 4.3.15**. Therefore, it is assumed that these oxide inclusion are Cr-Mn spinal oxides which have high thermodynamic stability.

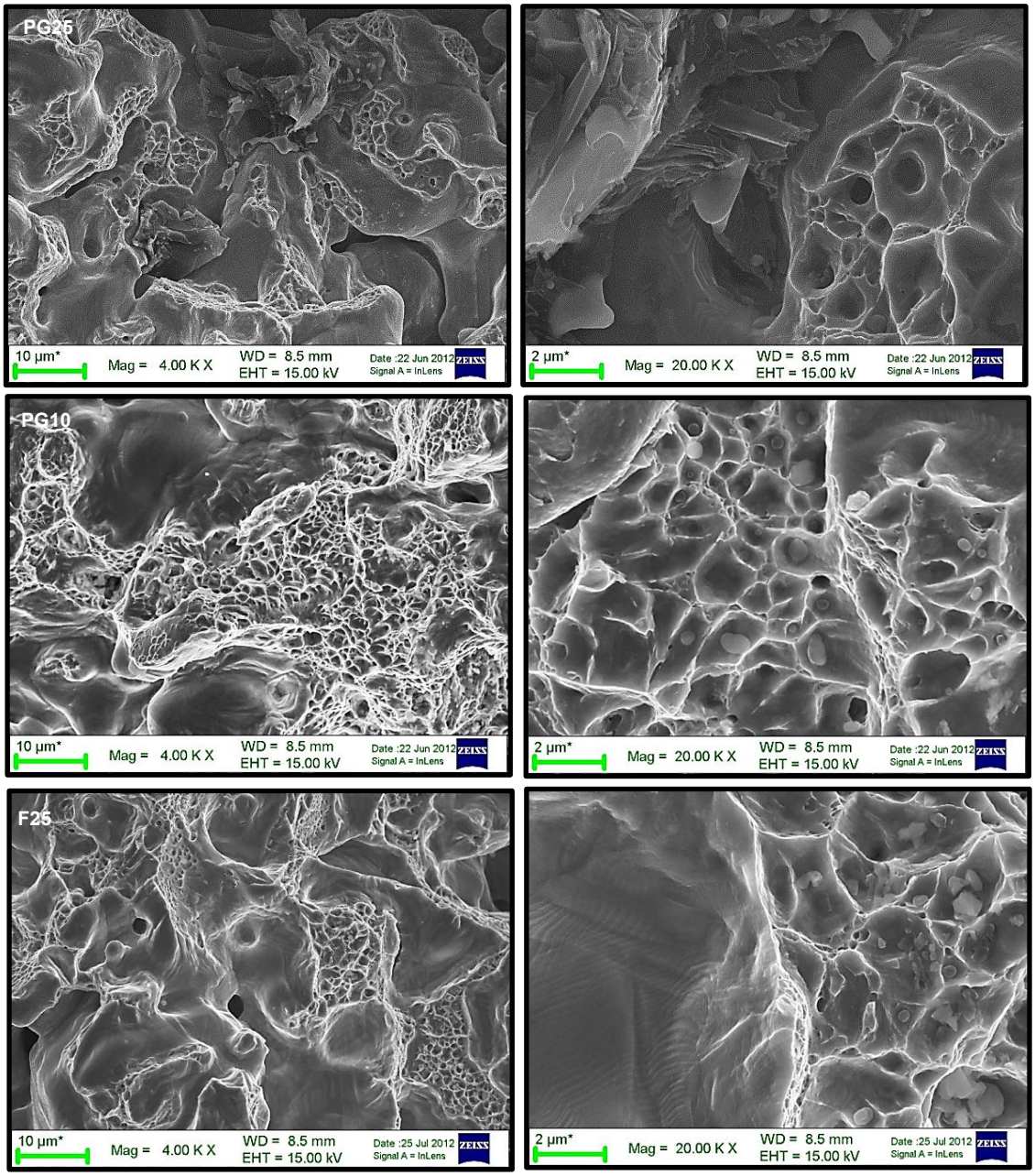

Fig.4.3.13: Fracture surface of specimen with different carbon sources heated to 1120˚C in N_2/10%H_2 for 30min, except ENSACO 250 in Ar/10%H_2-DIL showing free powder surface, necks and residual graphite.

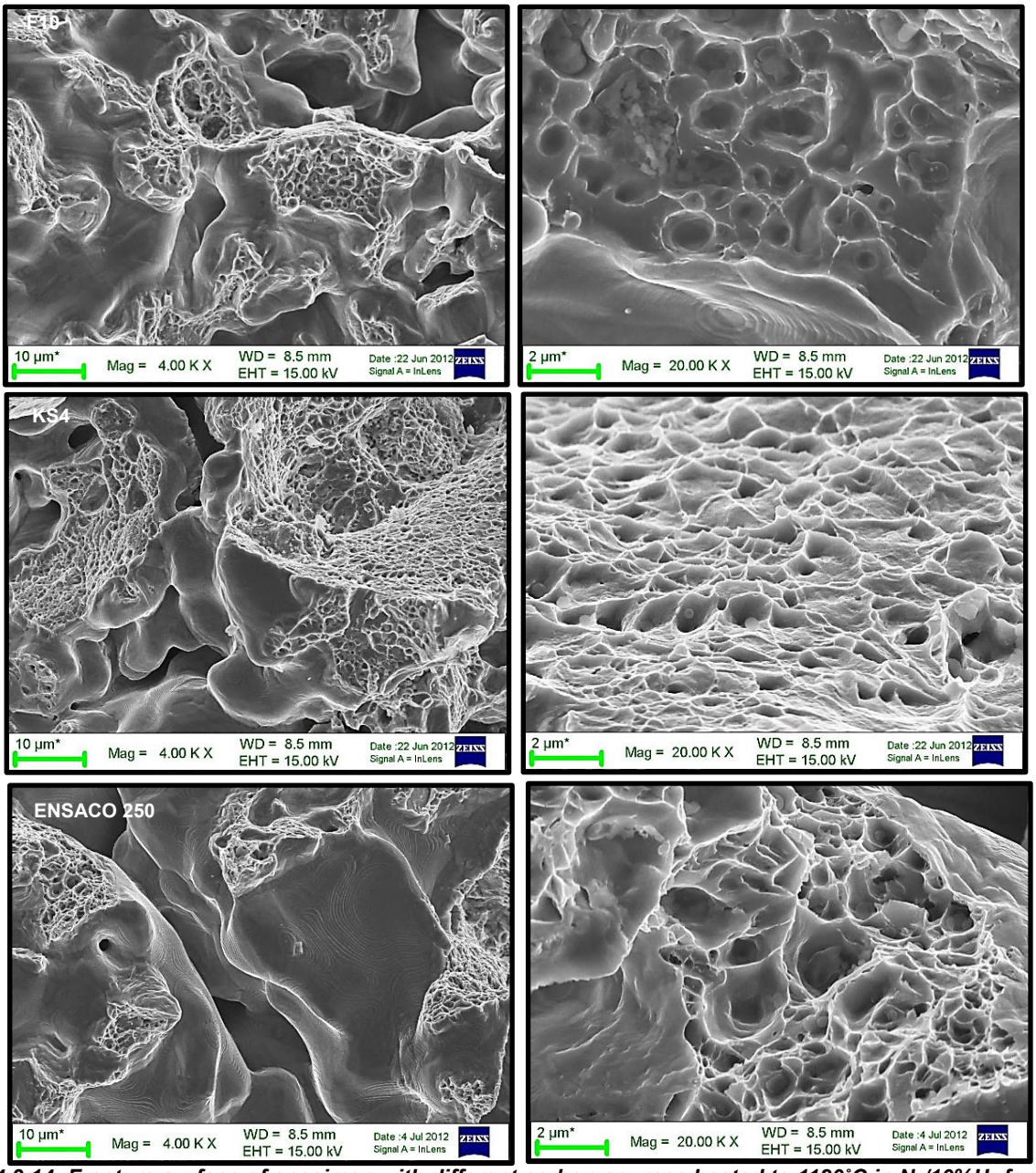

Fig.4.3.14: Fracture surface of specimen with different carbon sources heated to 1120˚C in N_2/10%H_2 for 30min, except ENSACO 250 in Ar/10%H_2-DIL showing free powder surface, necks and residual graphite.

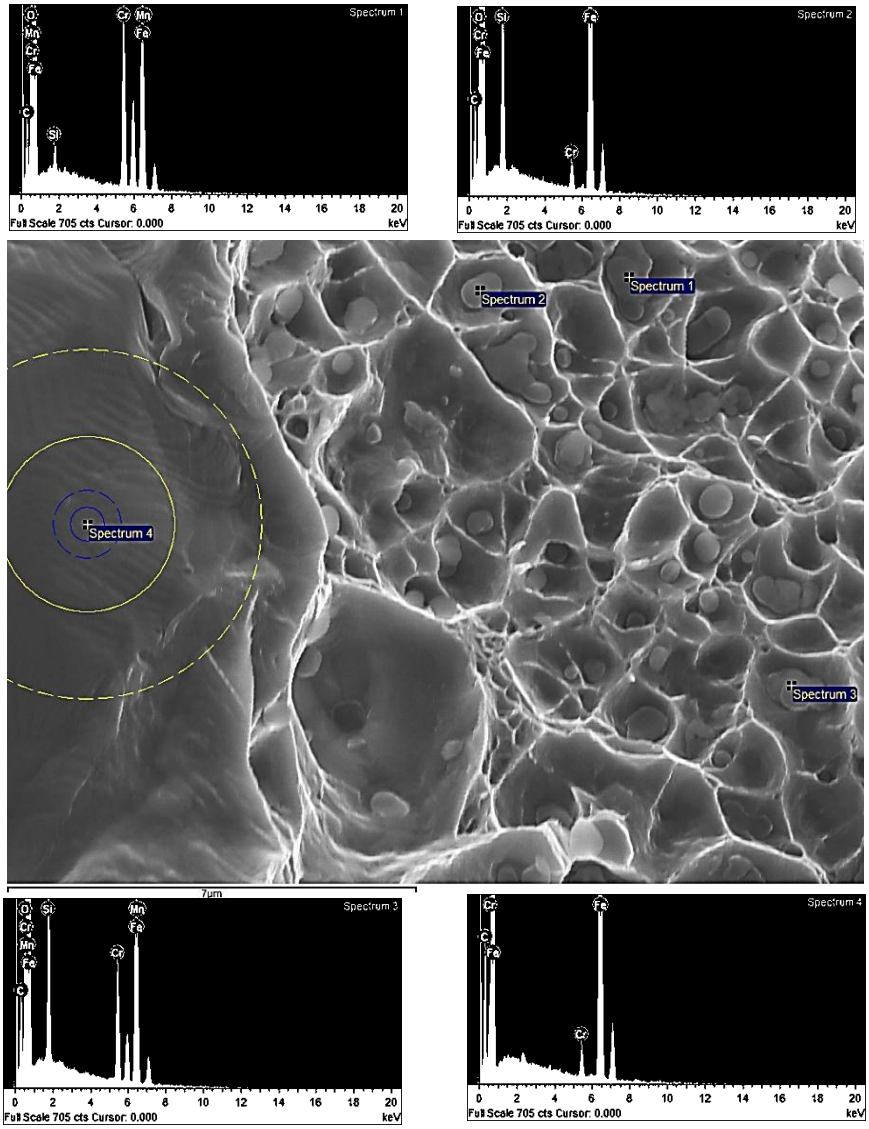

Spectrum	O	Si	Cr	Mn	Fe
1 [at.%]	49.95	0.91	15.72	7.47	25.94
2	36.00	12.10	1.97		49.93
3	52.23	7.66	8.35	3.67	28.10
4			3.36		96.64

Spectrum	Si	Cr	Mn	Fe
1 [at.%]	1.96	31.19	14.88	51.97
2	19.61	3.03		77.36
3	17.03	17.15	7.58	58.24
4		3.38		96.64

Fig.4.3.15:SEM+EDX analysis on particulate features observed on the fracture surface of the specimen sintered to 1120˚C in N_2/10%H_2 for 30min.

5. Discussion

Evaluation of activity/reactivity of different carbon sources and establishment the carbon source that has better carbon activity in terms of carbon dissolution and reducing ability, particularly at low temperatures, was the main aim of this work. Metallographic analysis gives information on carbon dissolution based on change in the microstructure – fraction of the pearlitic/bainitic phase. As the carbon can dissolve only after reduction of the iron oxide layer, metallography was used to determine which carbon source has the ability to reduce iron oxide layer and so dissolve more efficiency. SEM analysis gives information about reducing ability which can be indicated by the amount of residual oxides, quality and amount of inter-particle connections and their strength between the powder particles. At high temperatures more attention was given to the amount of residual graphite and carbon black that left in the matrix.

As was expected, for all carbon sources there was no indication for carbon dissolution in term of pearlite formation at 700˚C. During the heating of the steel powder up to this temperature only ferrite was observed that is in agreement with the theory. The solubility of carbon is limited in ferrite region which means that the admixed graphite cannot dissolve in the steel powder at this temperature. However, it still can react with the atmospheres or/and surface iron oxide layer covering powder particle. However, SEM results also show that there was no indication of carbon activity at this stage from the development of inter-particles necks point view which means that the carbon sources used are still inert at this temperature. Absence of inter-particle connections between the powder particles indicates that the reducing activity of the atmosphere used was also too low, meaning high (H_2O/H_2) ratio.

In principle, increase in the temperature above the boudouard equilibrium (> 720˚C) increases the carbon activity. However, the carbon activity of carbon source is also strongly governed by its properties. At 900˚C in N_2/10%H_2 atmospheres of rather low purity some amount of pearlite formation is registered in both sites of the sample (centre and edge) for KS4, F10 and PG10, indicating starting of the carbon dissolution. However PG25, F25 and carbon black are still inactive at this temperature. The amount of pearlite that forms in the centre of the samples was lower comparably to the edges of the samples in all three cases, indicating the influence of hydrogen-containing atmospheres on the reduction of the surface iron oxide layer on the powder particle. The difference in amount of pearlite formed between KS4, F10 and PG10 was low in both sites of the samples, confirming low purity of the sintering atmospheres applied. Additionally it means that KS4, F10 and PG10 are comparable in terms of carbon dissolution and so activity with slightly higher reactivity registered for KS4. SEM results confirmed the results of metallography for fine graphite grades only, namely KS4, F10 and PG10. A weak branched network of inter-particle connections was observed, indicating reduction of the surface iron oxide layer between the particles. Nevertheless, these inter-particle connections were weak, indicating insufficient reduction of surface iron oxides and thus low carbon activity at this temperature. Again, KS4, F10 and PG10 were comparable in terms of amount and strength of inter-particle connections. This result was unexpected as there was considerable difference in particle size distribution between these grades of graphite as well as the type of graphite and based on previous

observation [18] the synthetic graphite with smaller powder particle has the tendency to dissolve faster. Therefore, KS4 was expected to dissolve more efficiency than F10 and PG10. However, in our case differences between KS4 and other carbon grade were lower than expected. One of the important factors affecting carbon activity is the “poisoning” of the graphite powder surface by the presence of ash layer/particulates that was also observed during SEM analysis for all powders, even for KS4. During SEM investigation edges of some the KS4 particles were covered by some amorphous phase that most probably reduces carbon activity and hence dissolution. Therefore this might explain why KS4 was roughly comparable to F10 and PG10. However, amount of such sites was extremely low and so it can’t be claimed as the main reason responsible for lower activity.

Another important effect observed was the much better developed inter-particle necks in the case of good controlled atmosphere meaning lower carbon reactivity with respects to surface iron oxide reduction in the case of poor atmosphere control. The reason of it can be high amount of the samples in the furnace - high “furnace load” meaning high amount of water vapour/carbon dioxide produced during oxide reduction leading to considerable decrease in atmosphere reducing ability. Atmosphere purity can be also locally deteriorated by absorbed in carbon source moisture. All these effects negatively influence the microclimate inside the pores and thus the carbon activity. The influence of the atmospheres was confirmed by trials in dilatometer at 900 °C in controlled Ar/10%H_2 atmosphere. The results show large amount of bainite formed close to the edges of the samples, indicating sufficient reduction of surface iron oxide and significant amount of carbon dissolved in the matrix. Due to the strong contribution of gas atmospheres, the comparison was difficult. Nevertheless, intensive investigation was carried out to determine which of studied graphite grades has better carbon activity. The result shows that KS4 has the best carbon activity, F10 and PG10 slightly lower and PG25 and F25 the worst ones. Additionally results show an insignificant increase in the amount of pearlite formation as well as the amount of inter-particle connection in the centres of the specimens – emphasizing the same problem with atmosphere purity. This implies that the sintering atmospheres conditions have the major role on the reduction of the surface iron oxide layer, not the carbon activity of graphite at this temperature. Despite the same atmospheres conditions that were used for graphite grades were also used for ENSACO 250, there was no indications for carbon activity at this temperature for ENSACO 250. This was evident throughout all the sample where there was no indication of carbon dissolution or inter-particle connections between the powder particles. This could be the result of the bad microclimate due to possibly high moisture in carbon black. The distribution of fine carbon black powder was more homogenous than in case of graphite powder.

Large amount of residual graphite was observed for all graphite grades even after heating to 1120°C. As we were expecting, the centre of the samples has the highest amount of residual graphite, while the edges has much less for all cases. The particulate oxides on the pore surfaces were also evident in all cases of graphite admixing, indicating that the carbon activity for all the graphite grades was not high enough to reduce these oxides at this temperature. Unexpected results from carbon black were obtained: i) there was no indication of any residual carbon black left in the matrix; ii) surprisingly all the particulate oxides are reduced, indicating that the carbon activity in this case was significantly large in comparison with graphite grades studied. However, large amount of agglomerated oxides inside the inter-particle necks was observed for ENSACO 250 at this temperature as well. This could be a result

of the kinetics of inter-particle neck growth that was higher than the kinetics of the surface oxide layer reduction which led to enclosure of residual iron-based oxide inside inter-particle neck. Hence, because carbon black was inert up to 900°C, large amount of residual surface oxide was present when intensive inter-particle necking started to take place.

After sintering at 1120°C for 30 min only for PG25 there was residual graphite left in the matrix as well as particulate features on the open powder surface. This indicates that even at this stage the carbon activity for PG25 was not high enough to reduce the particulate oxides. However, KS4, F10, F25, PG10 and ENSACO 250 were fully dissolved and their free powder surface was clean. This makes the carbon source characteristics for KS4, F10, F25, PG10 and ENSACO 250 do not show significant differences after this stage, particularly in terms of carbon dissolution.

6. Conclusions

- Astaloy CrM was tested with different carbon sources of various properties in order to evaluate their carbon activity in terms of carbon dissolution and reducing ability based on metallographic and SEM analyses;

- All carbon sources show to be inert up to 700°C;

- Graphite grades KS4, F10 and PG10 were comparable in terms of carbon dissolution up to 900°C, despite of their various properties, while F25 and PG25 showed to be much less active and ENSACO 250 is inert up to 900°C;

- The quality of sintering atmosphere (composition, purity, flow, etc.) has the major role in reduction of surface iron oxide layer on powder particles, not the carbon activity of graphite, particularly at low temperatures;

- Better coverage of the powder by carbon black was registered;

- Uncompleted dissolution for both synthetic and natural graphite grades during heating up to 1120°C was registered. Moreover, the free powder surface contained unreduced particulate oxides, indicating that the carbon activity was not high enough for all graphite grades;

- Carbon black was completely dissolved during heating up to 1120°C and particulate features on the free powder surface were fully reduced;

- When sufficient time is given (1120˚C-30min), most of the graphite grades (KS4, F10, PG10 and F25 were fully dissolved in the steel matrix and free powder surface was oxide-free. Only for PG25 there was residual graphite left in pores and particulate features were present on the free powder surface, indicating that PG25 has the lowest carbon activity among the all carbon sources studied.

References

1. Schatt, W and K.P. Wieters, Powder Metallurgy, Processing and Materials. 1997, Shrewsbury, European Powder Metallurgy Association. 492.
2. German, R.M., Powder Metallurgy Science. 1994, Princeton, New Jersey 085406692, U.S.A, Metal Powder Industries Federation. 472.
3. Chasoglou, D., E. Hryha, and L. Nyborg, Effect of Atmosphere Composition on the Surface Interactions during Sintering of Chromium-alloyed PM Steels, in Euro PM2011 Congress and Exhibition 2011, Barcelona, Spain. P. 111-117.
4. Hryha, E. and L. Nyborg, Changes in Oxide Chemistry during Consolidation of Cr/Mn Water Atomized Steel Powder. Powder Metall. Prog., 2011. 11(1-2): p.42-50.
5. European Powder Metallurgy Association; www.epma.com.
6. Nyborg, L, Metal Powder and Their Properties-*Fundamentals behind Physical and Chemical Properties*. PM Summer School, Kosice, june 23-29, 2007.
7. Höganäs Handbook for Sintered Components. 2004, Höganäs AB, Sweden.
8. Bergman, O., Key Aspects of Sintering Powder Metallurgy Steel Prealloyed with Chromium and Manganese, in Department of Materials and Manufacturing Technology 2011, Chalmers University of Technology, Gothenburg.
9. Ortiz, P. and F. Castro, Thermodynamic and Experimental Study of Role of Sintering Atmospheres and Graphite Additions on Oxide Reduction in Astaloy CrM Powder Compacts. Powder Metal., 2004. 47(3): p. 291- 298.
10. Hryha, E., E. Dudrova, and L. Nyborg, On-line Cnotrol of Processing Atmospheres for Proper Sintering of Oxidation-Sensitive PM Steel. J Mater process Tech, 2012. 212(4): p. 977-987.
11. Chasoglou, D., E. Hryha, and L. Nyborg, Methodology for Evaluating the Oxide Distribution in Water Atomized Steel Powder, in Department of Materials and Manufacturing Technology 2012, Chalmers University of Technology, Gothenburg.
12. Dudrova, E. and M. Kabatova, Fractographic of Sintered Iron and Steels. Powder Metall. Prog., 2008. 8(2): p. 59-75.
13. Höganäs Handbook for Sintered Components – 2. Production of sintered components, Höganäs AB, 1997.
14. Sintering of Steels, in Furnace Atmospheres. 2011, The Linde Group.
15. Chasoglou, D., E. Hryha, and L. Nyborg, Fractographic Investigation of Chromium alloyed PM Steels Sintered in Atmospheres with Varying Hydrogen Content. Powder Metall. Prog., 2011. 11(1-2): p. 59-75.
16. Smallman, R.E and A.H.W. Ngan, Physical Metallurgy and Advanced Materials. Seventh edition 2007, Elsevier Ltd.
17. Hermann, H, Schubert, W, Gruner and N, Mattern, Structure and Chemical Reactivity of Ball-Milled Graphite.Nanostructured materials, 1997, Vol. 8, No. 2. pp 215-229.
18. Luigi Alzati, Dr. Raffaele Gilardi, Dr. Simone Zurcher, Giovanni Pozzi, Stefano Fontana; Guidelines for Optimal Selection of Graphite Type for PM Parts Production.
19. Metzloff, K.E, Nelson, R.D, Loper,C.R, Carbon Dissolution in Cast Iron Metal Reexamind. American Foundry Society 2005. 05-168(05).p 1-10.

Appendices

SEM-N_2/10%H_2-700˚C-PG25-CENTRE

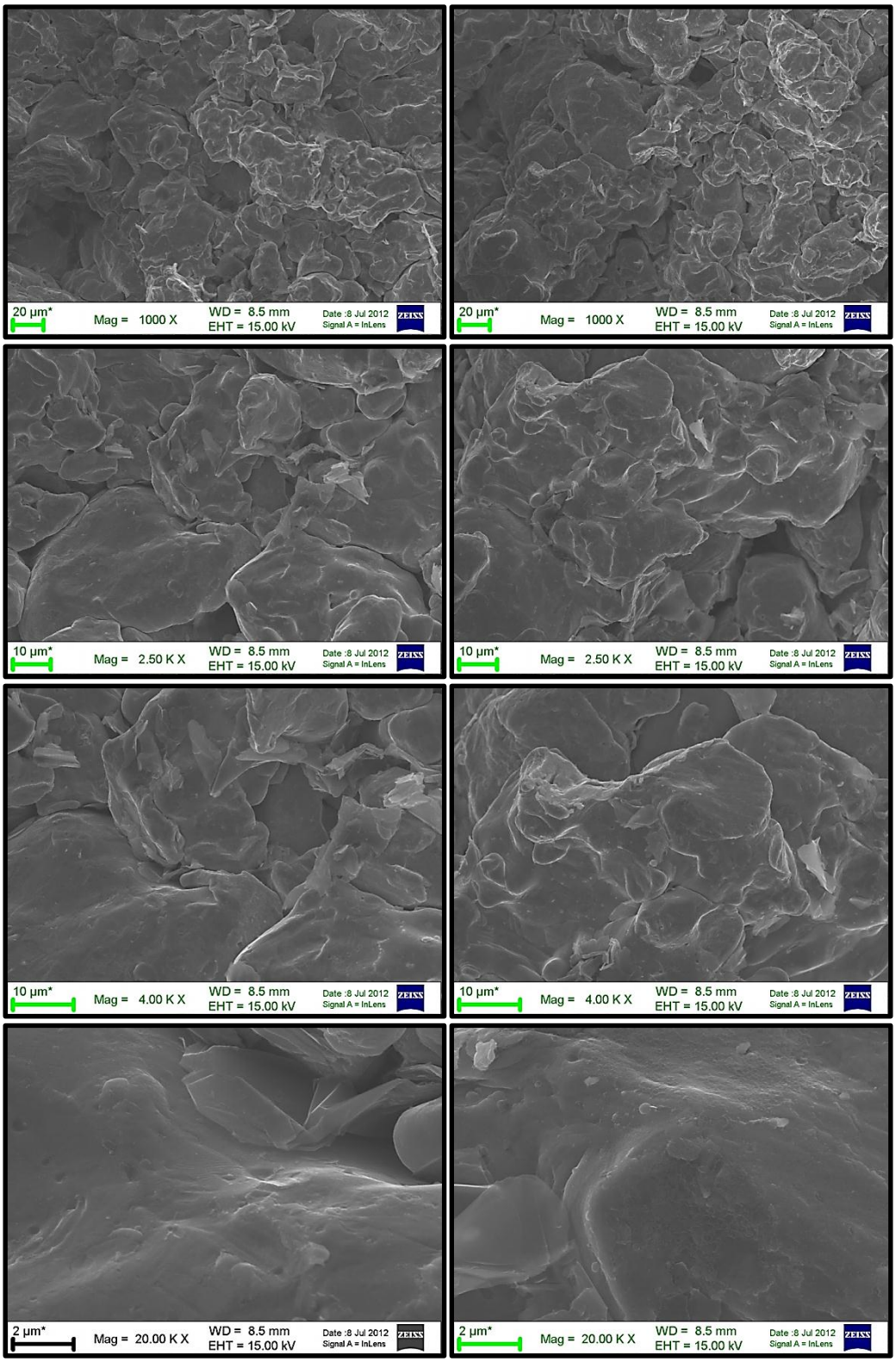

SEM-N_2/10%H_2-700˚C-PG10-CENTRE

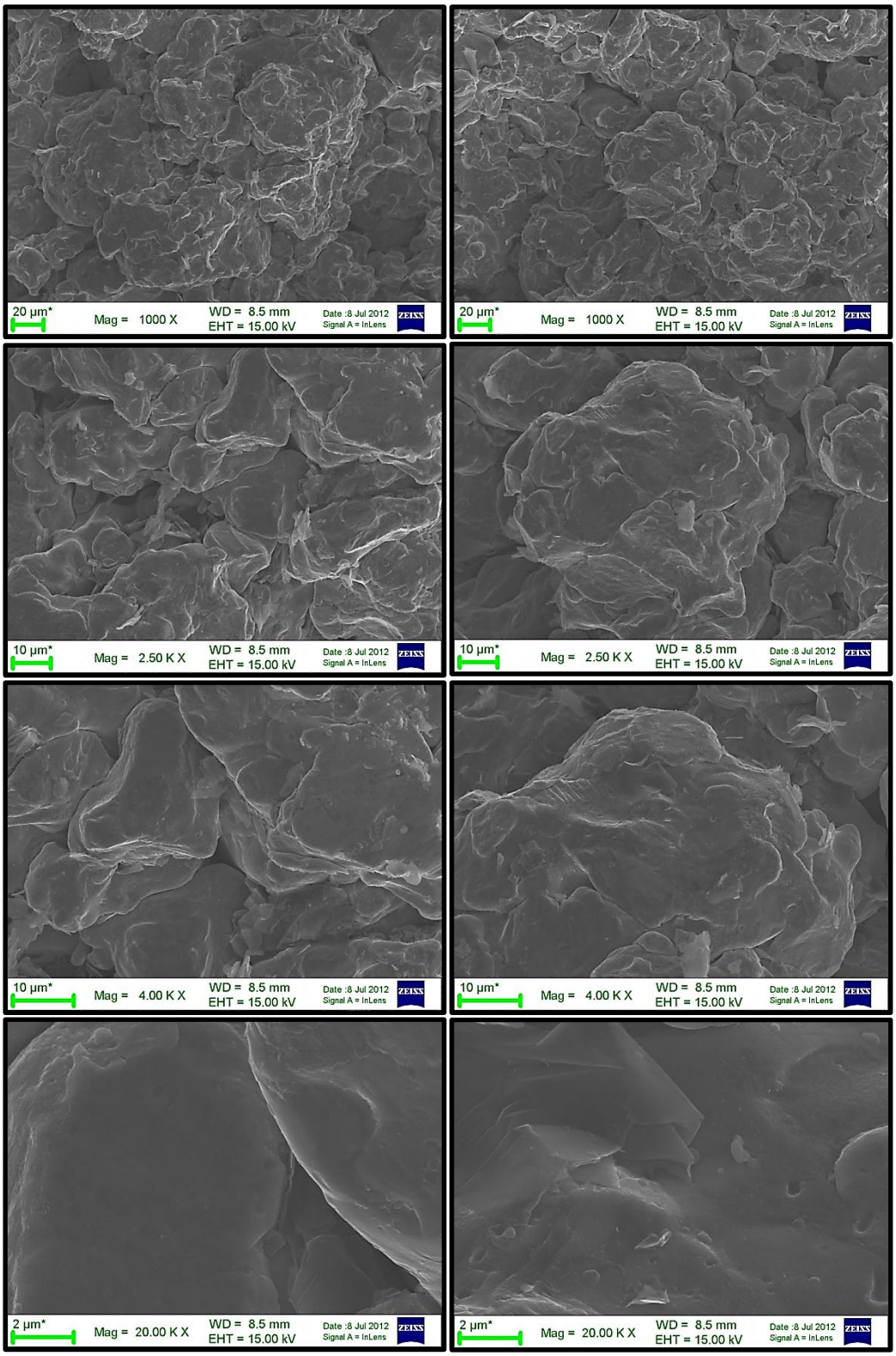

SEM-N_2/10%H_2-700˚C-F25-CENTRE

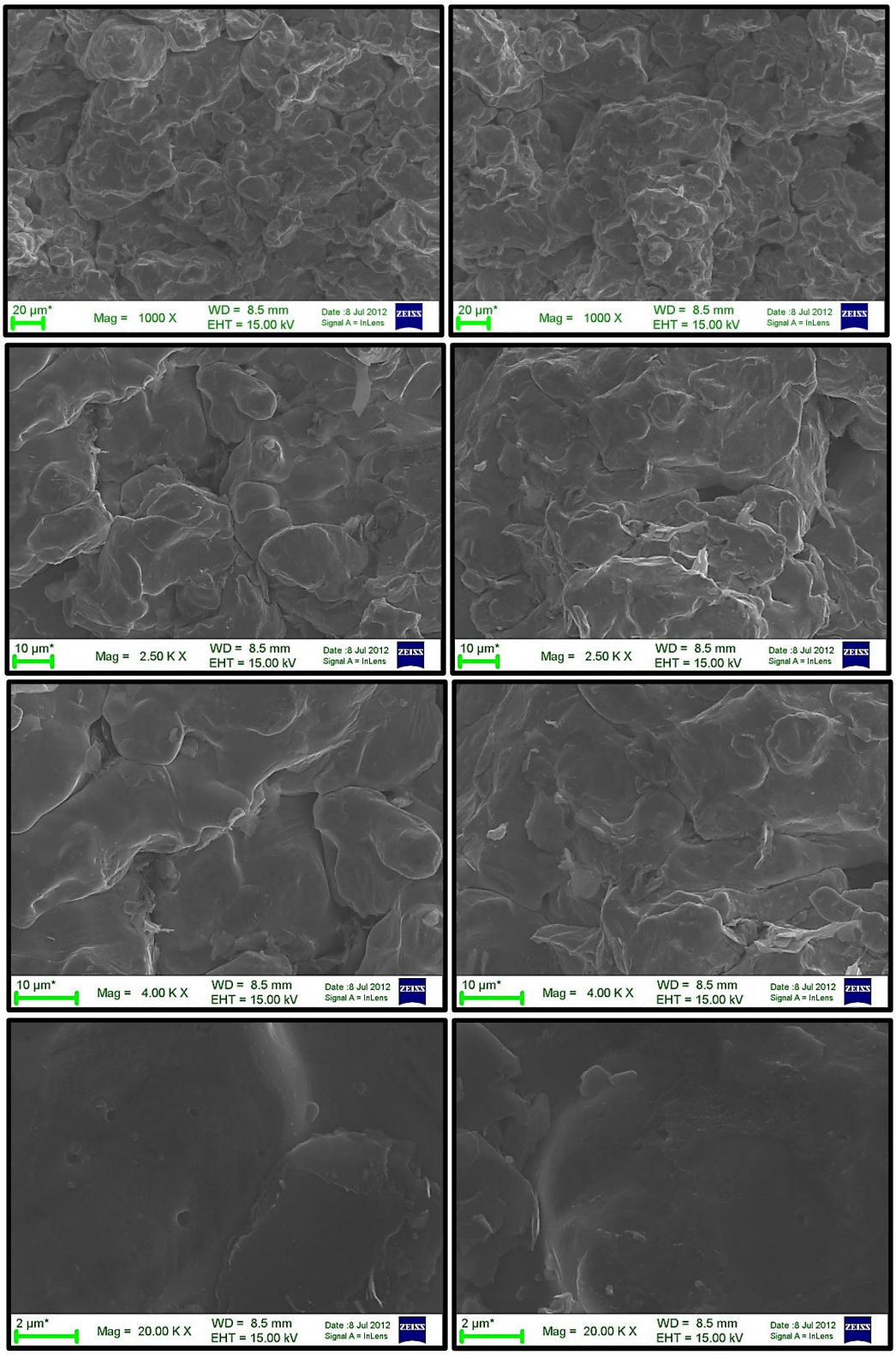

SEM-N_2/10%H_2-700˚C-F10-CENTRE

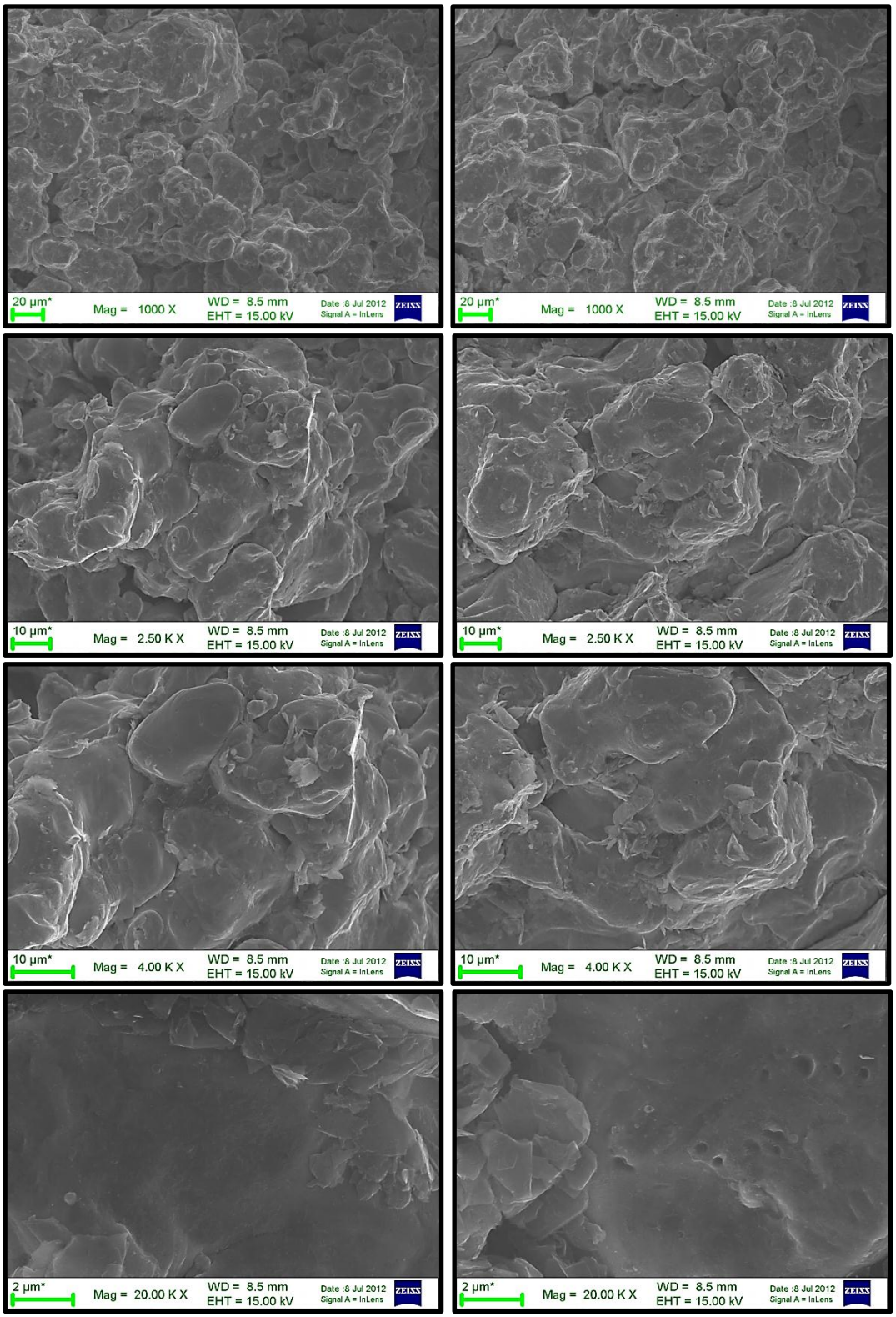

SEM-N_2/10%H_2-700˚C-KS4-CENTRE

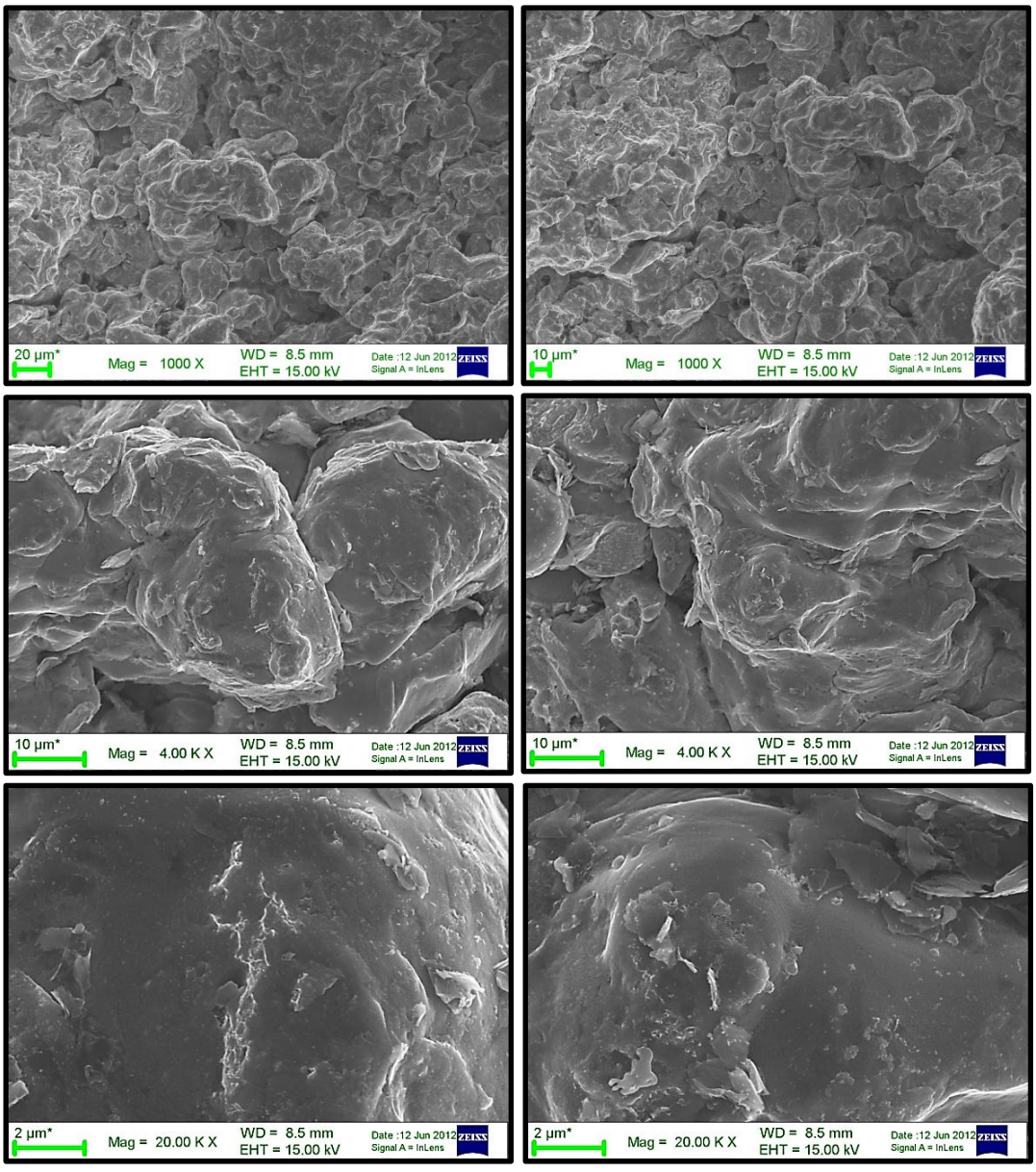

SEM-Ar/10%H_2-700˚C-DIL-ENSACO 250-CENTRE

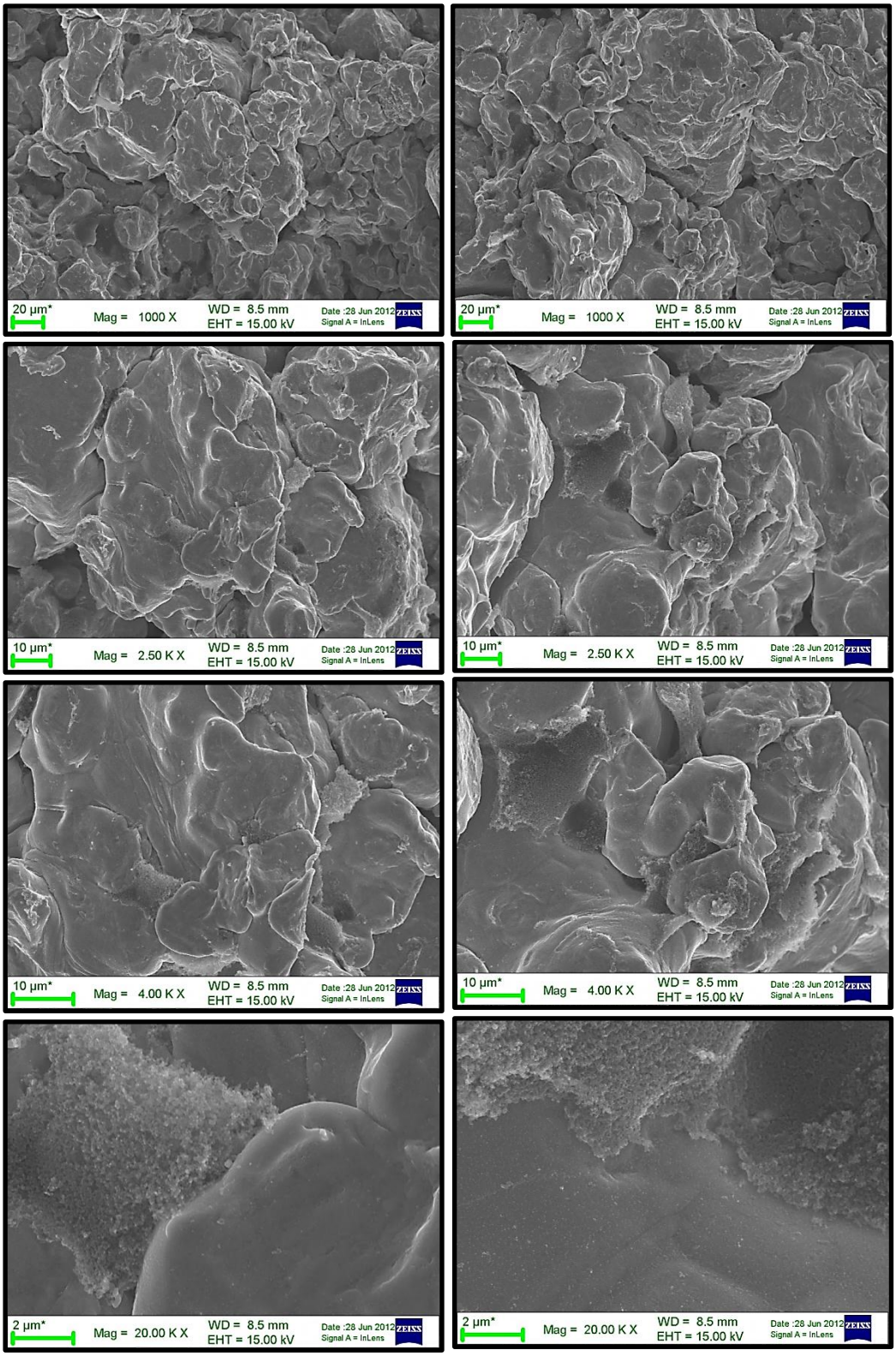

SEM-N_2/10%H_2 -900˚C-PG25-CENTRE

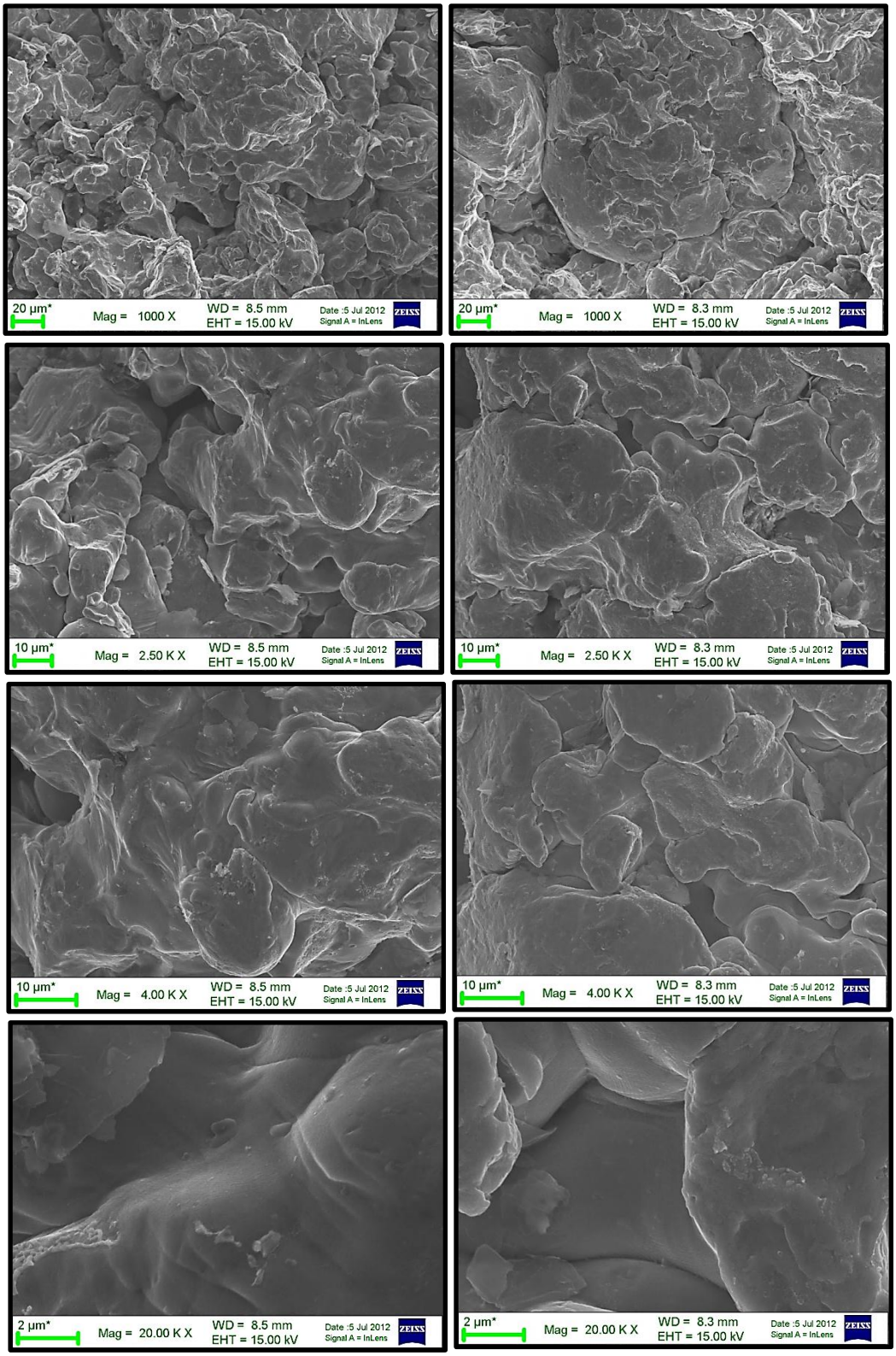

SEM-N_2/10%H_2 -900˚C-PG25-EDGE

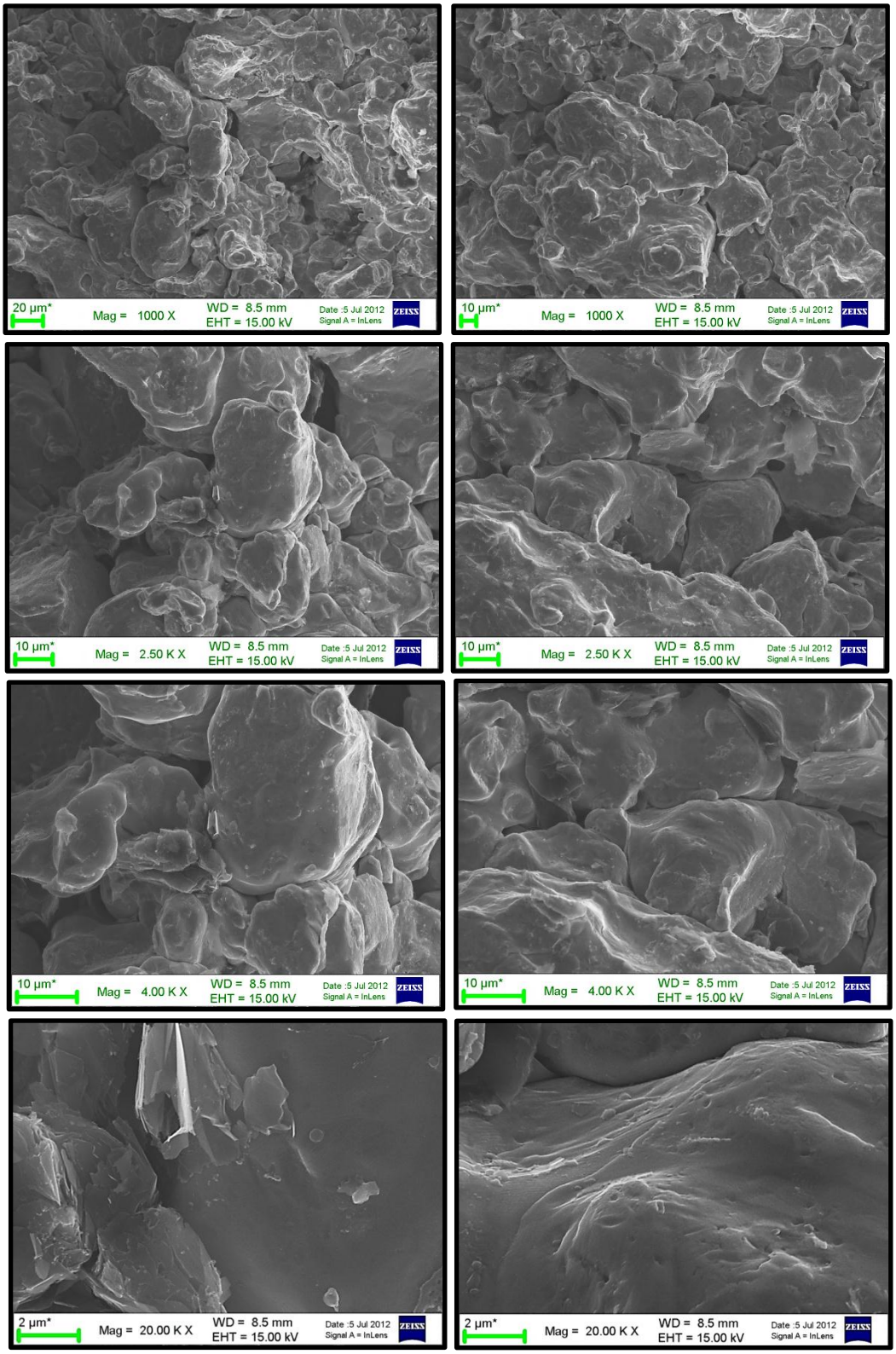

SEM-N_2/10%H_2 -900˚C-PG10-CENTRE

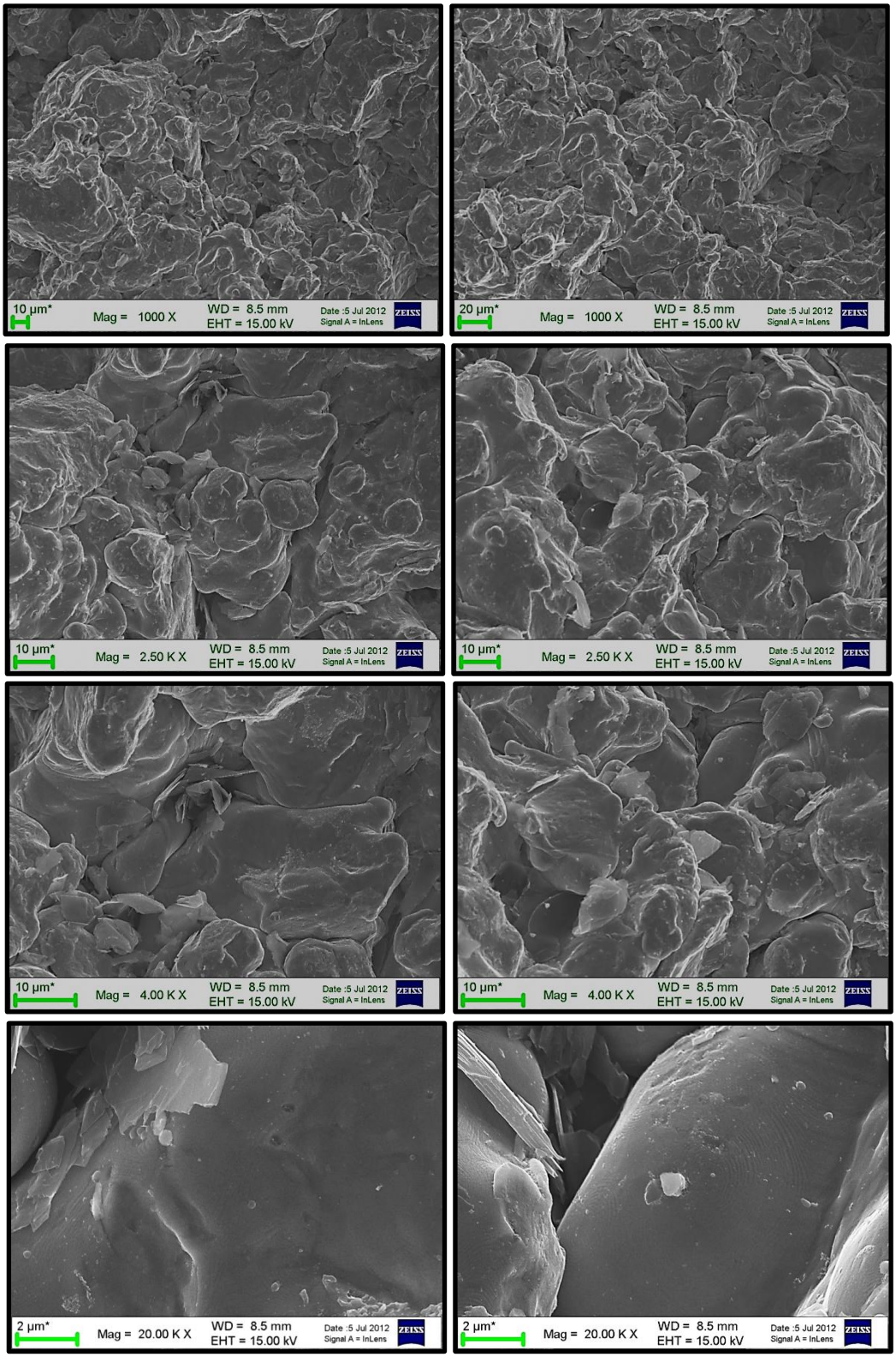

SEM-N_2/10%H_2 -900˚C-PG10-EDGE

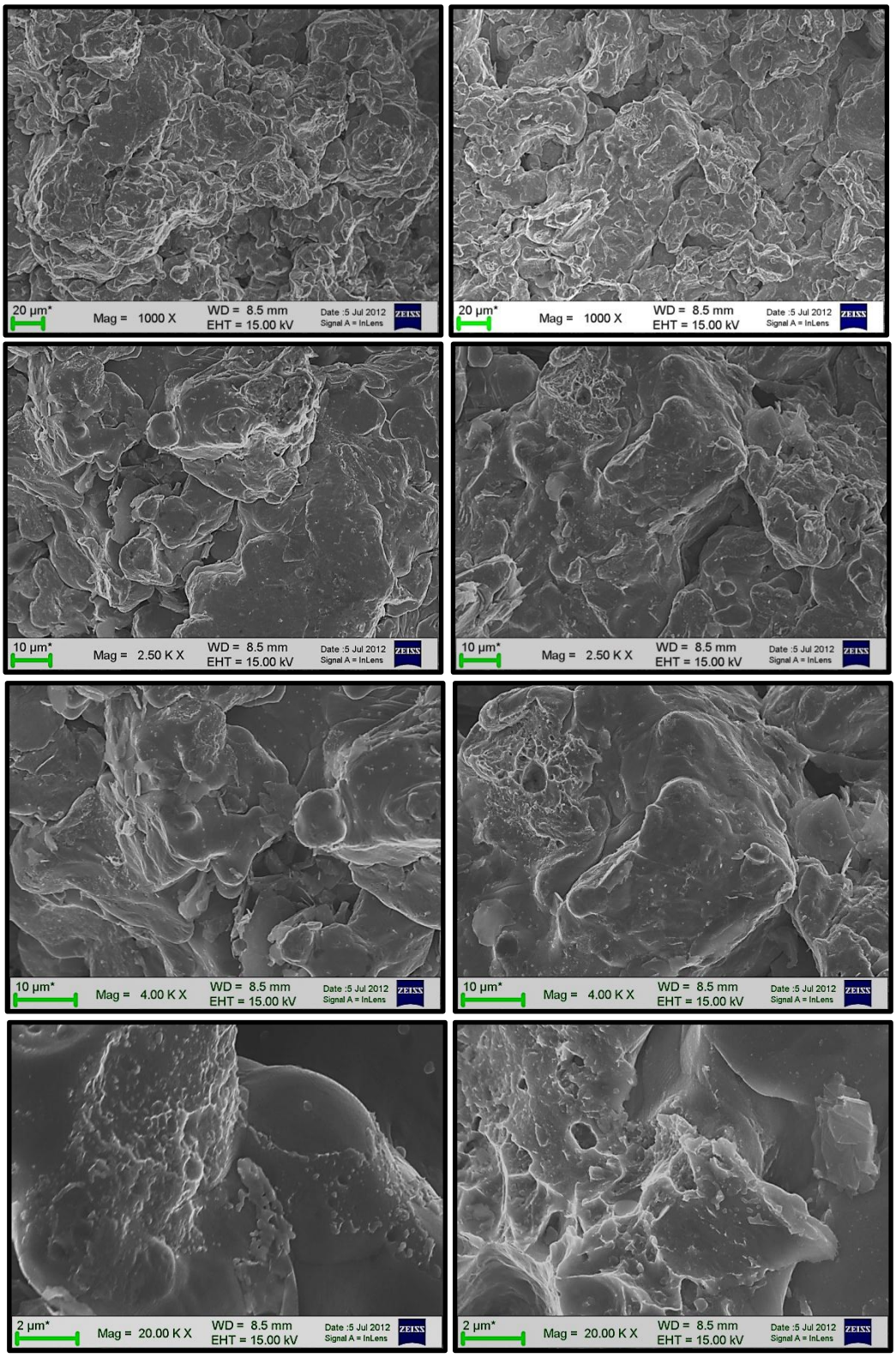

SEM-N_2/10%H_2 -900˚C-F25-CENTRE

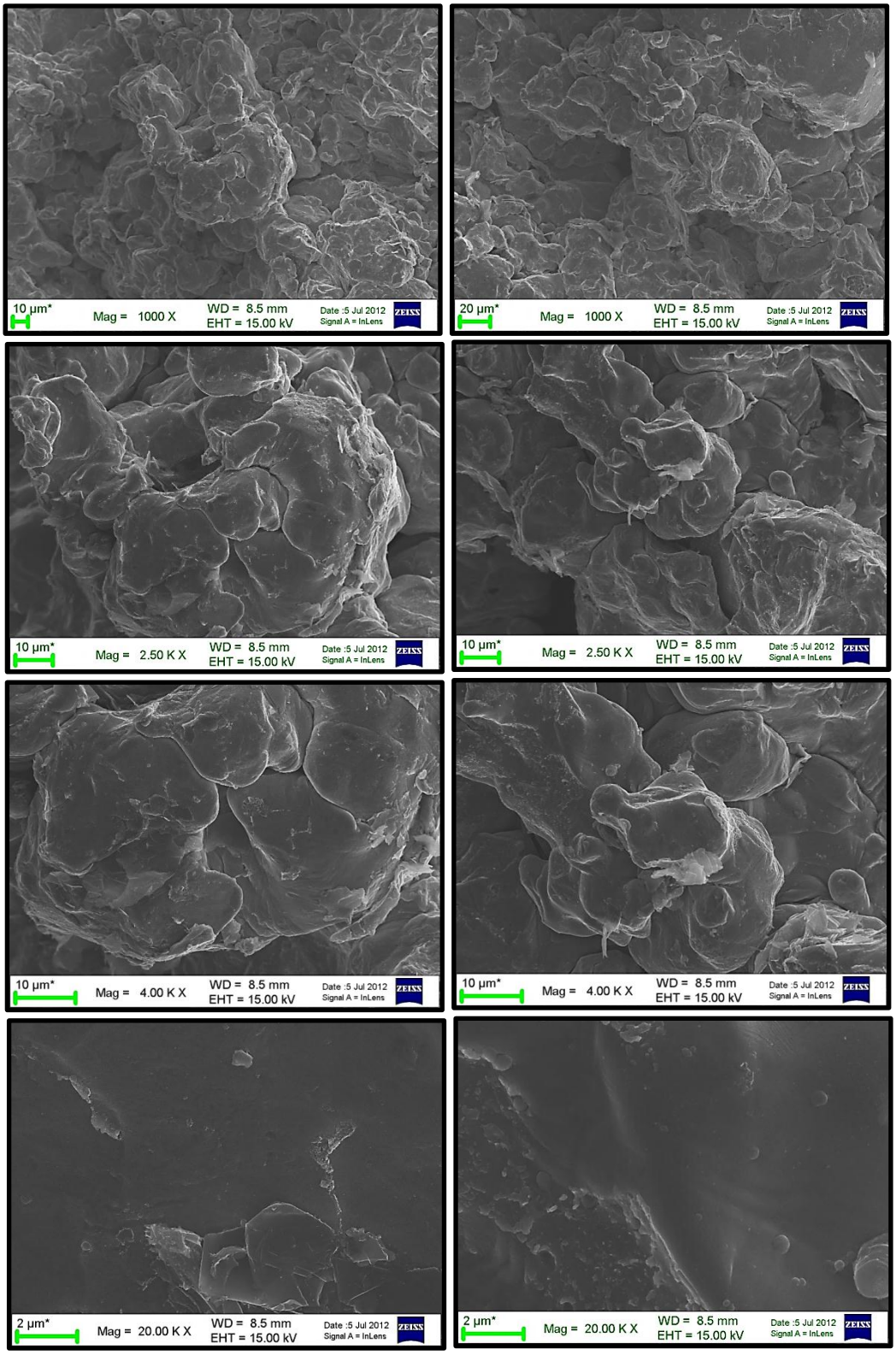

SEM-N_2/10%H_2-900˚C-F25-EDGE

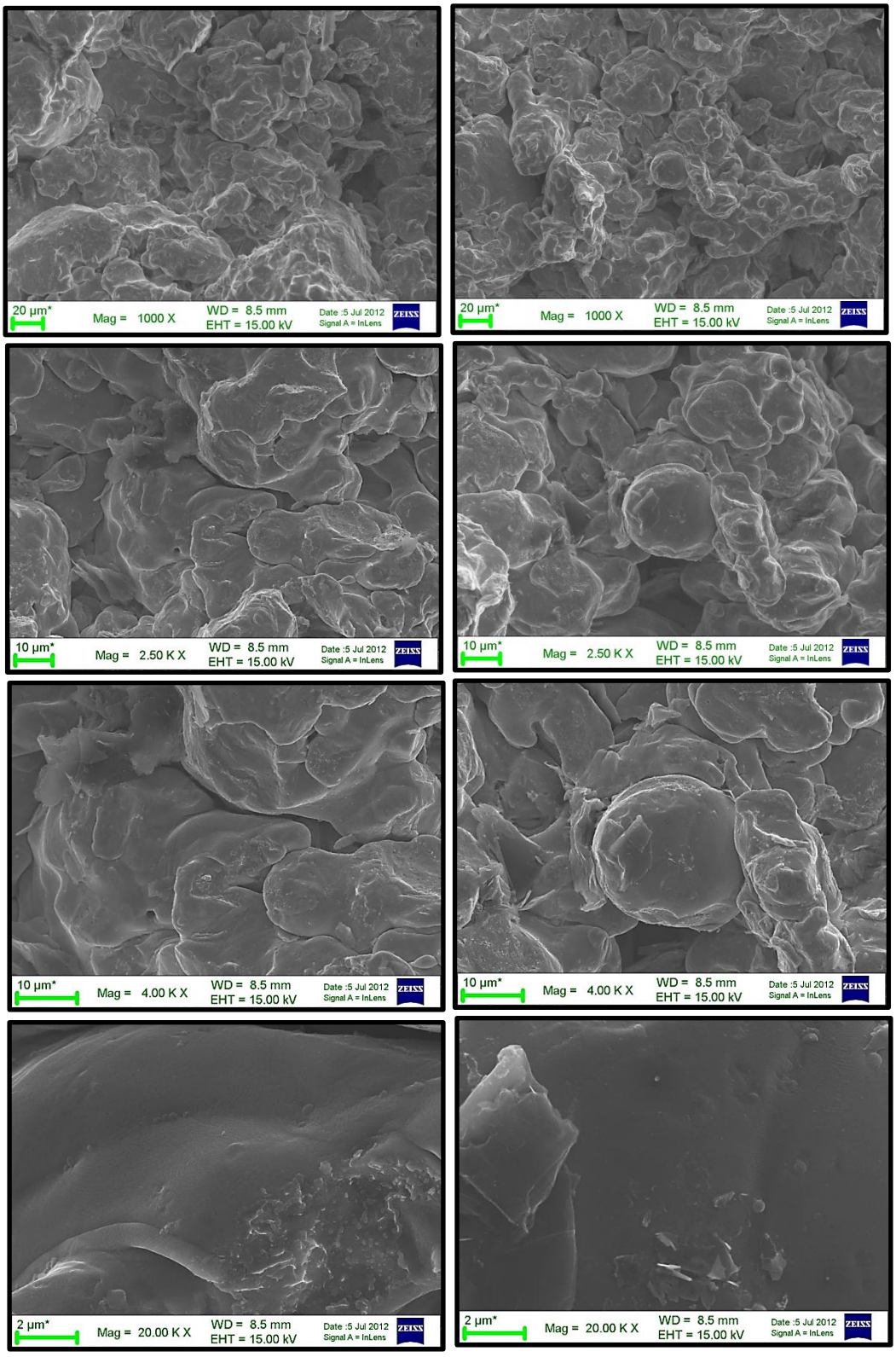

SEM-N_2/10%H_2-900˚C-F10-CENTRE

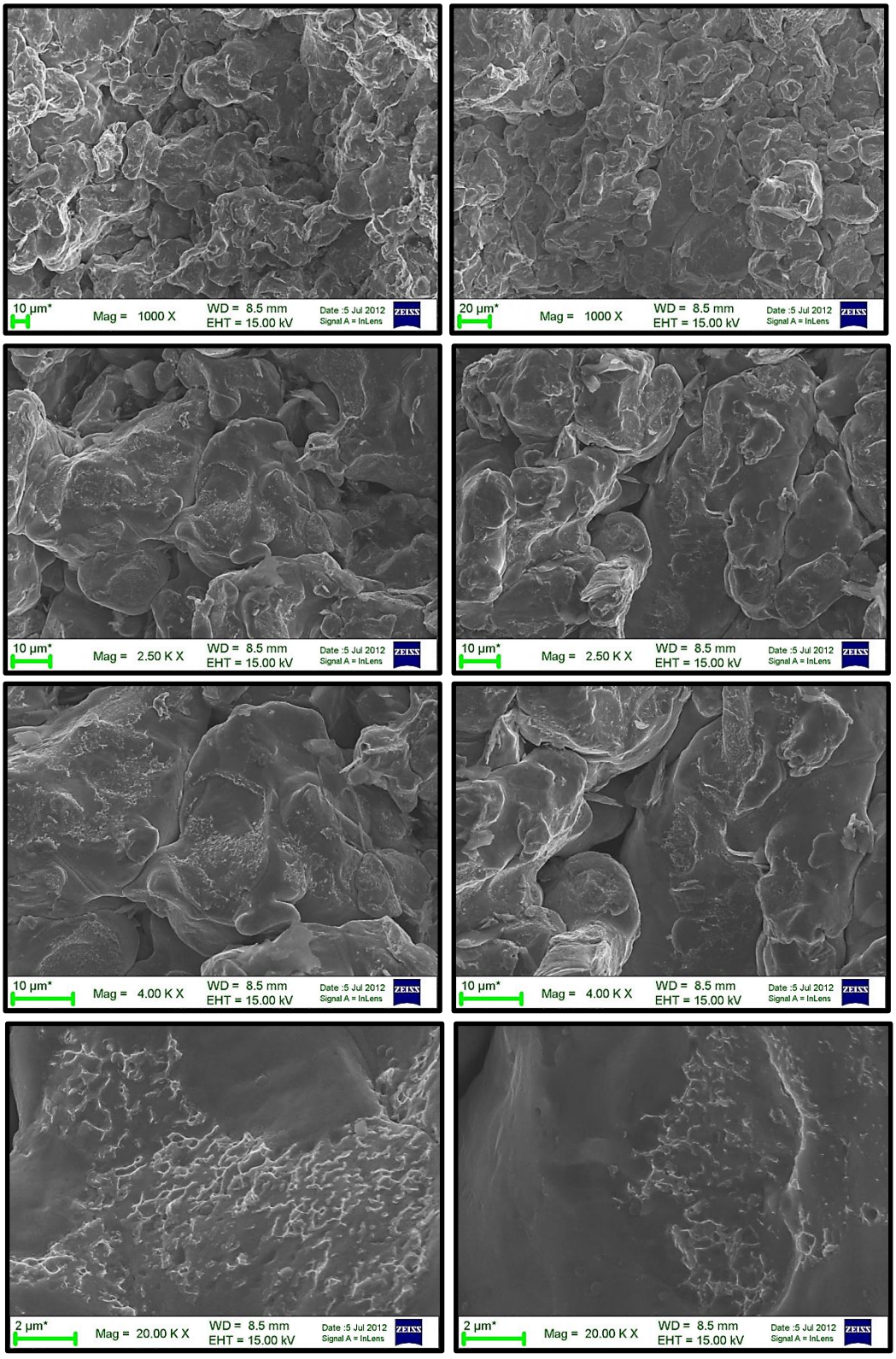

SEM-N_2/10%H_2-900˚C-F10-EDGE

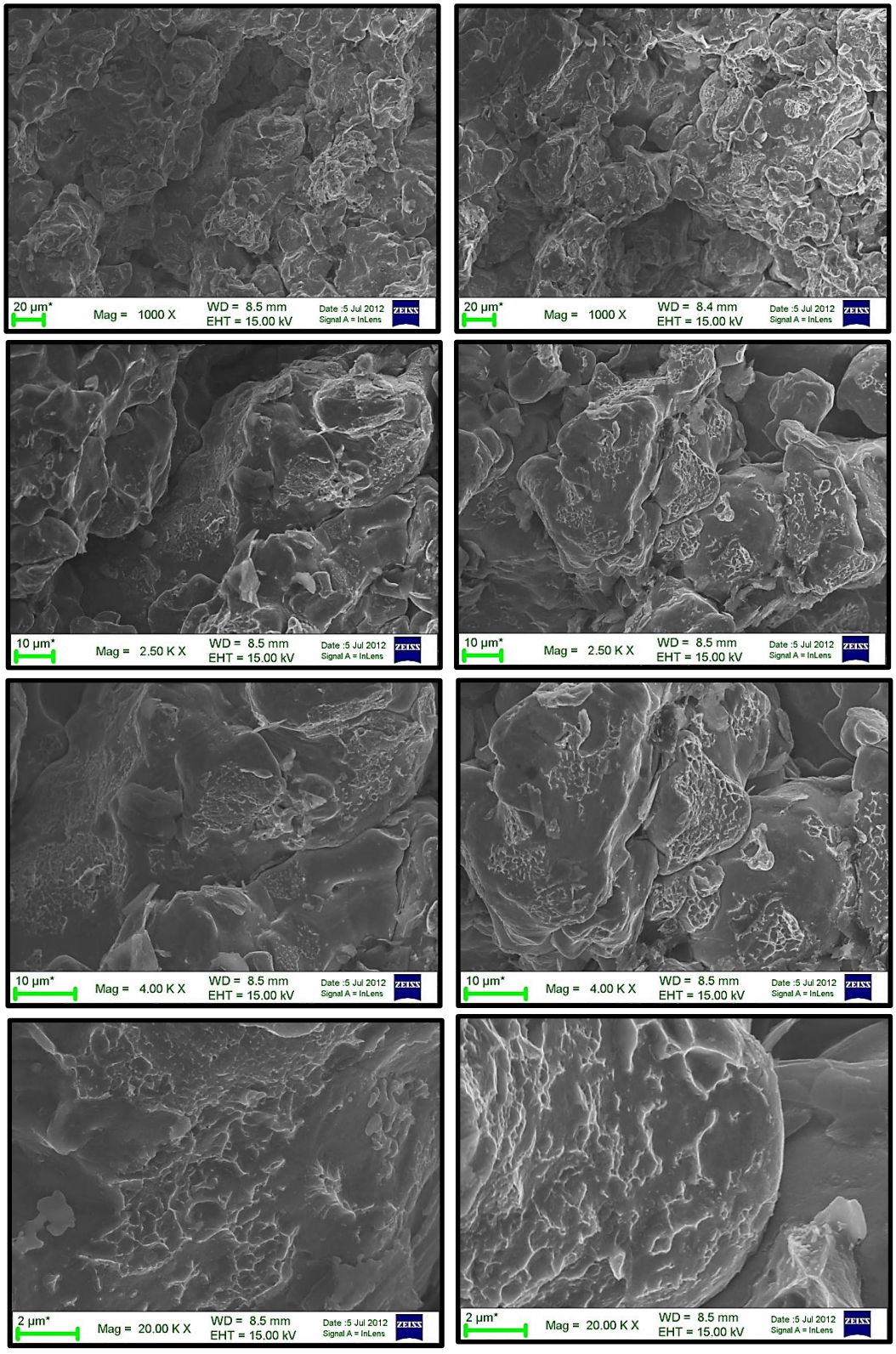

SEM-N_2/10%H_2-900˚C-KS4-CENTRE

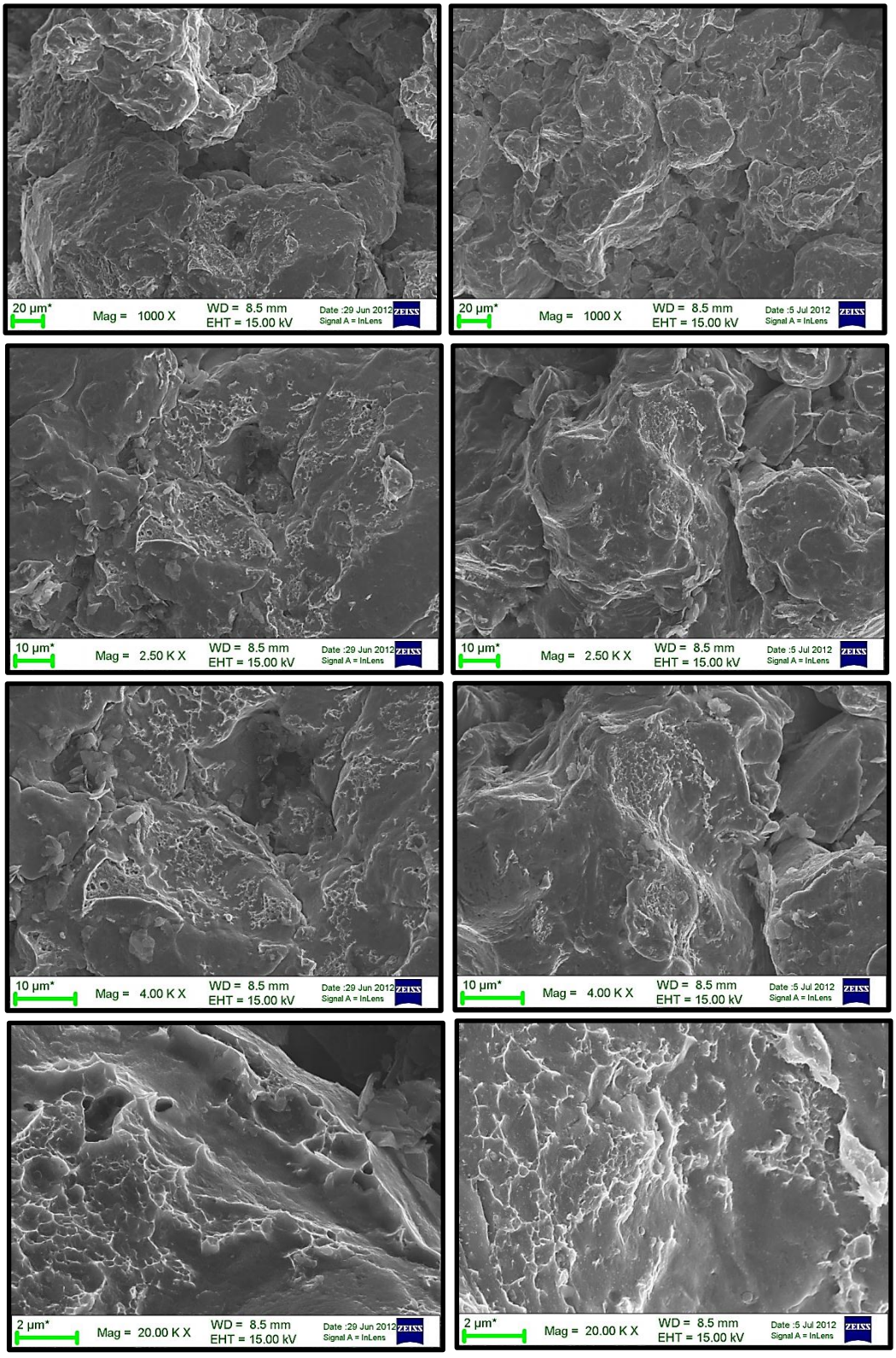

SEM-N_2/10%H_2-900˚C-KS4-EDGE

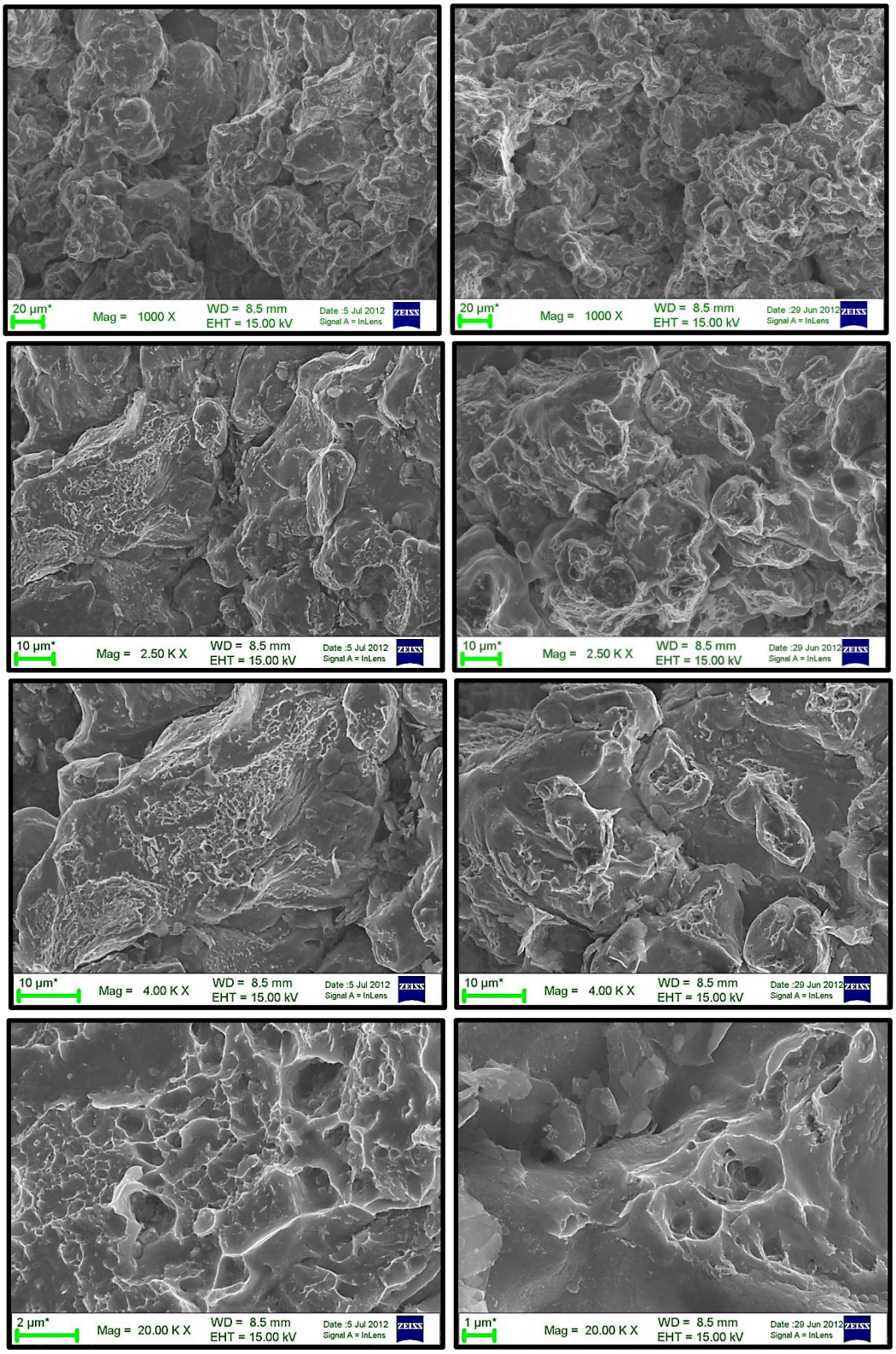

SEM-Ar/10%H_2-90O˚C.DIL-PG25-CENTRE

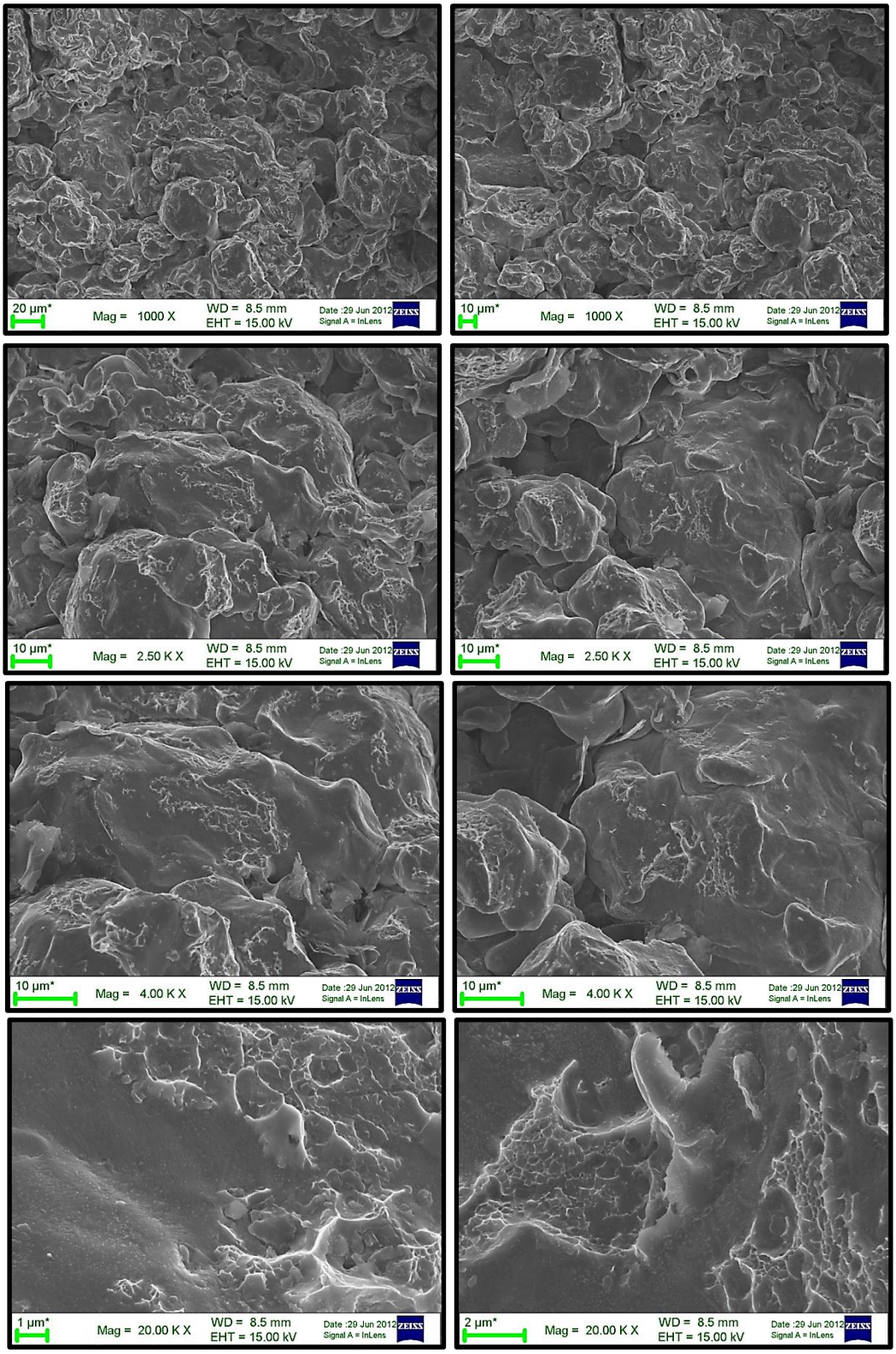

SEM-Ar/10%H_2-900˚C.DIL-PG25-EDGE

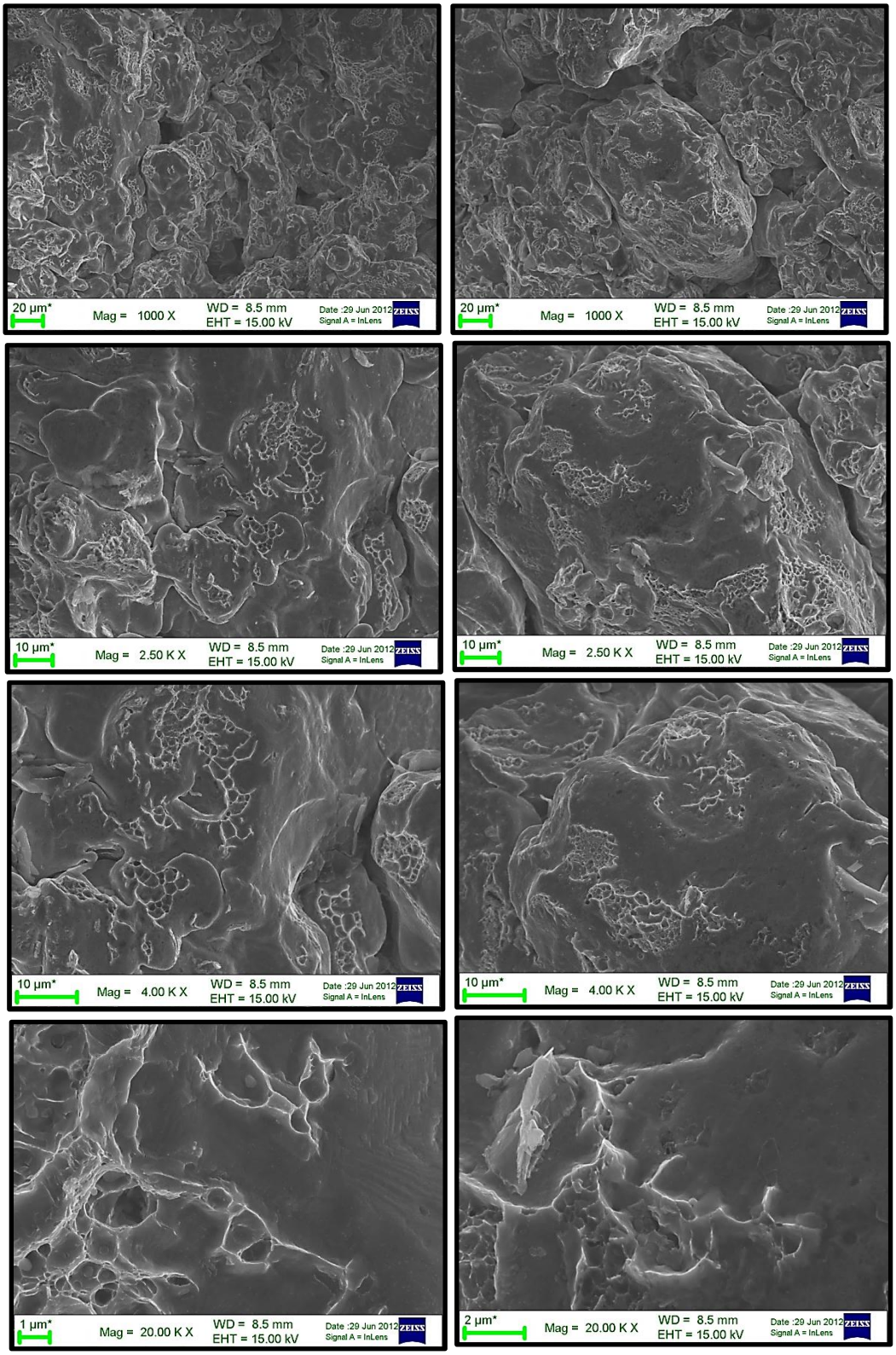

SEM-Ar/10%H_2-900˚C.DIL-PG10-CENTRE

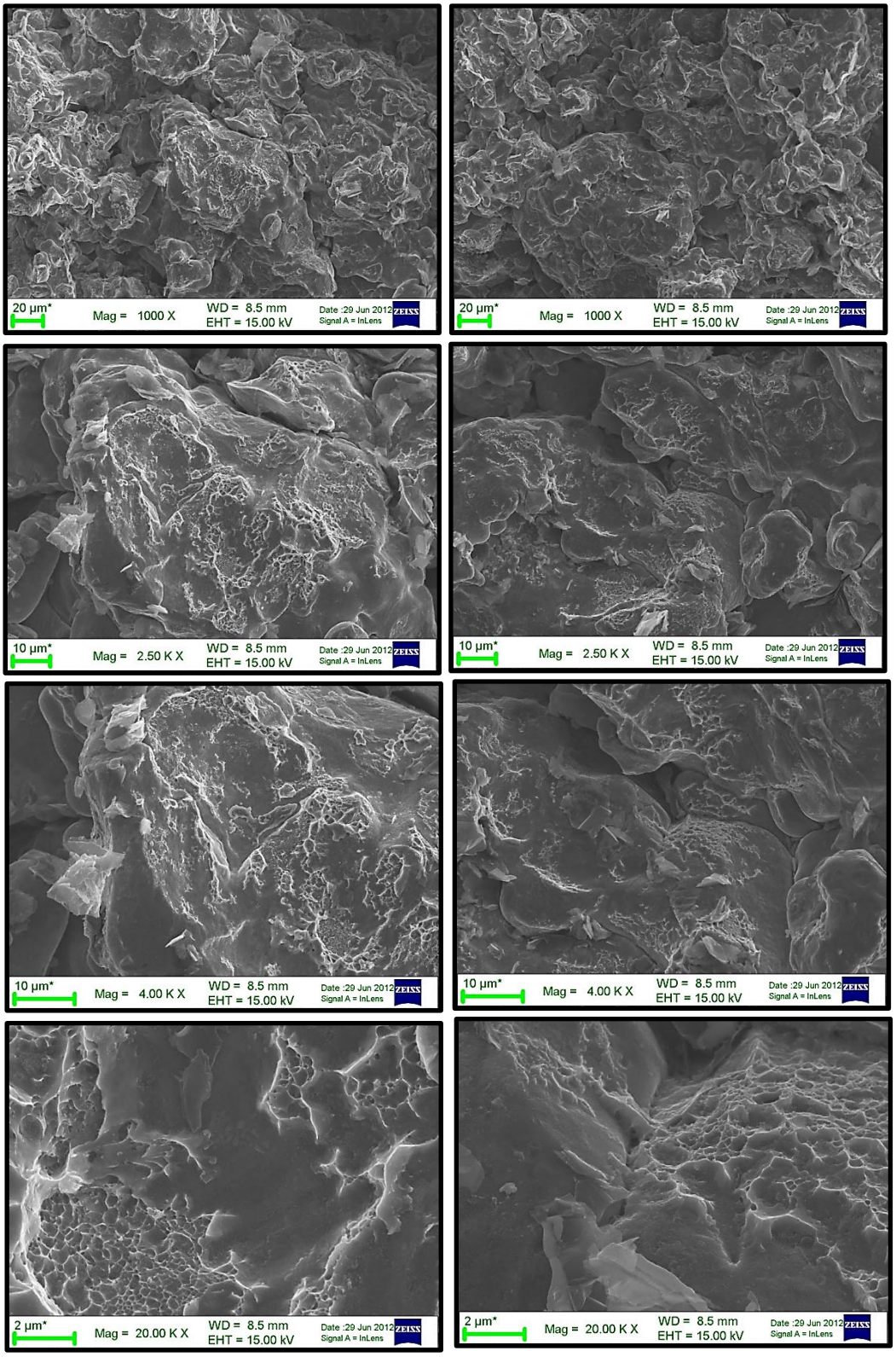

SEM-Ar/10%H_2-900˚C.DIL-PG10-EDGE

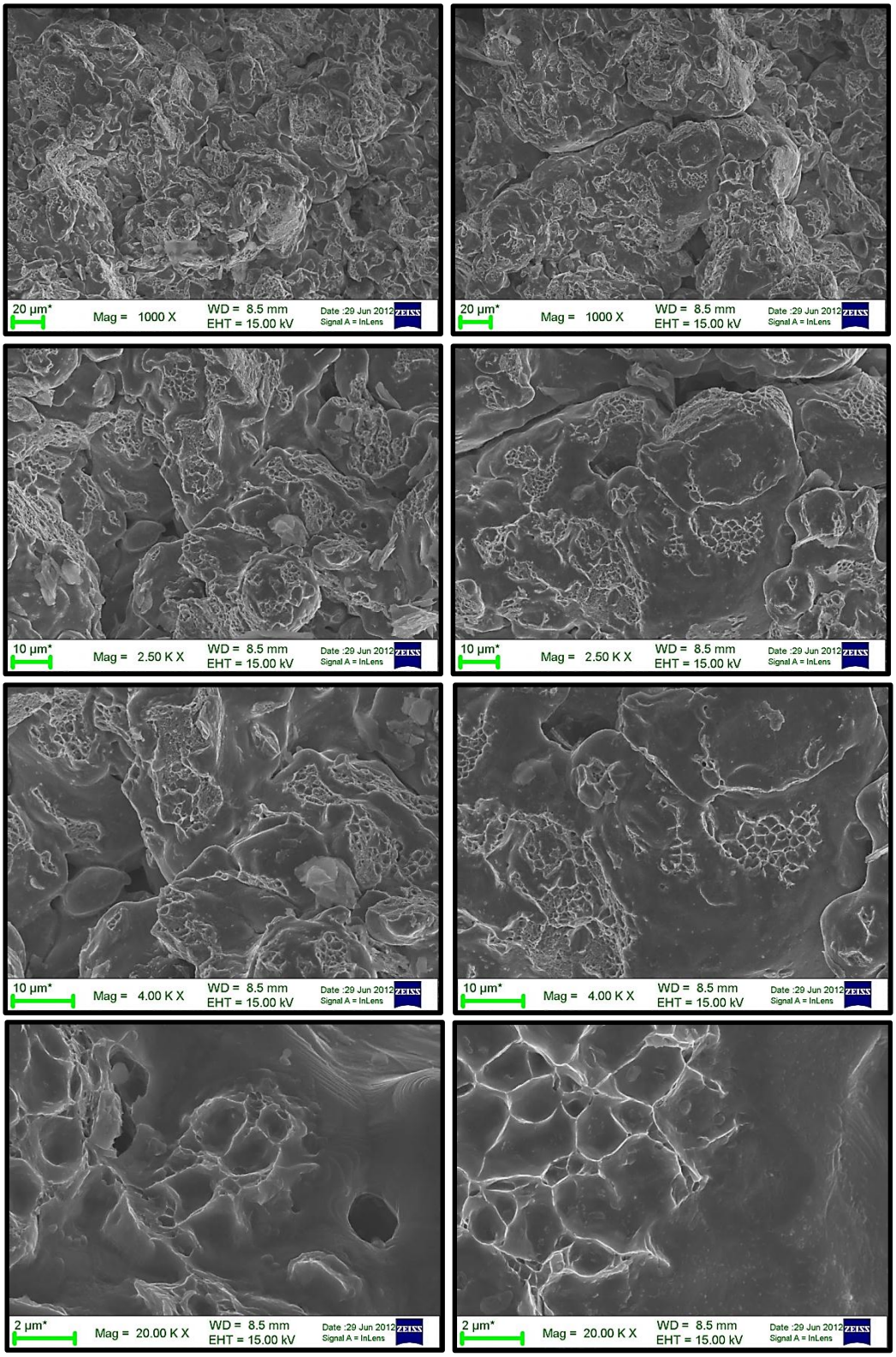

SEM-Ar/10%H_2-900˚C.DIL-F25-CENTRE

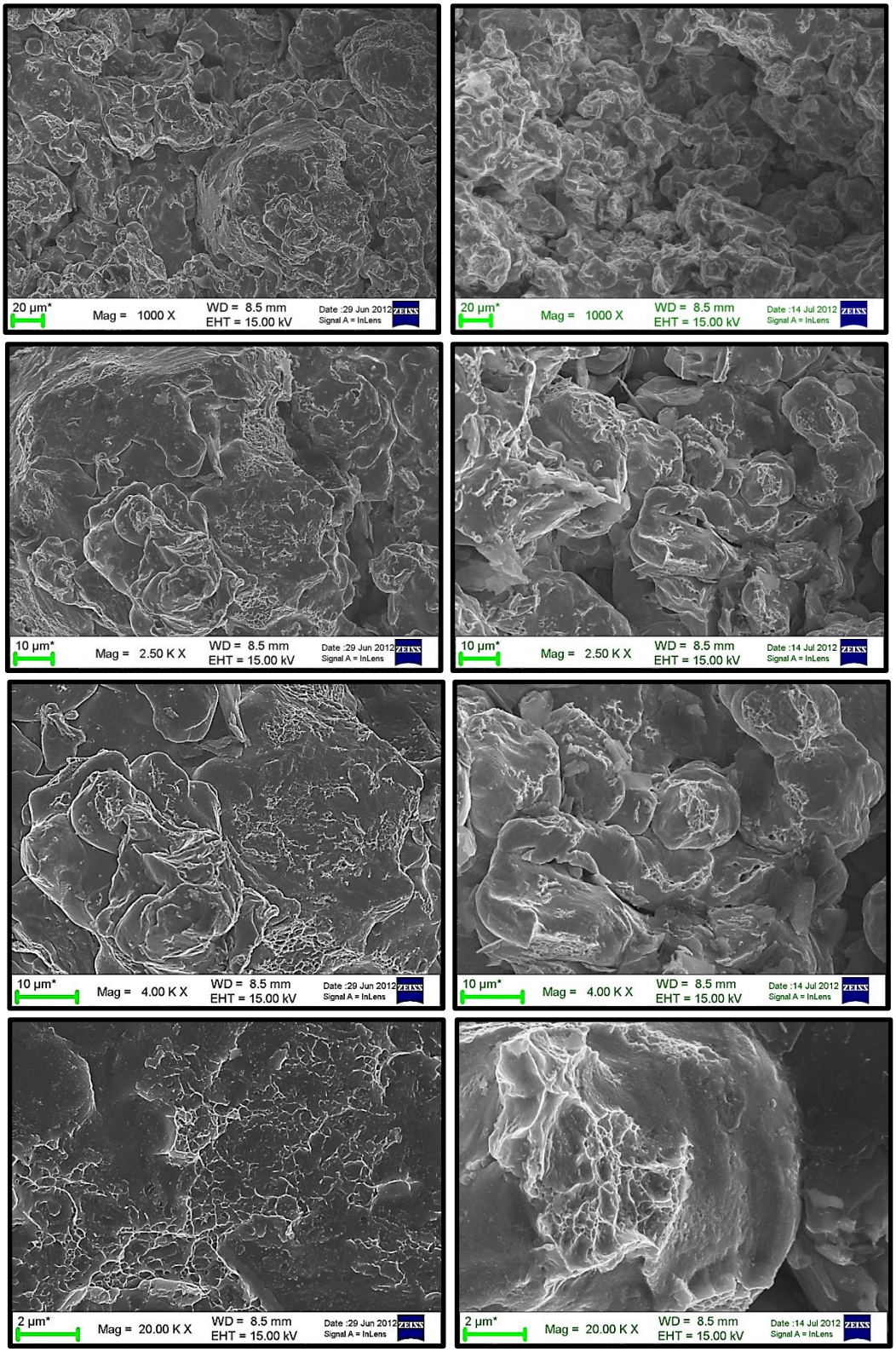

SEM-Ar/10%H_2-900˚C.DIL-F25-EDGE

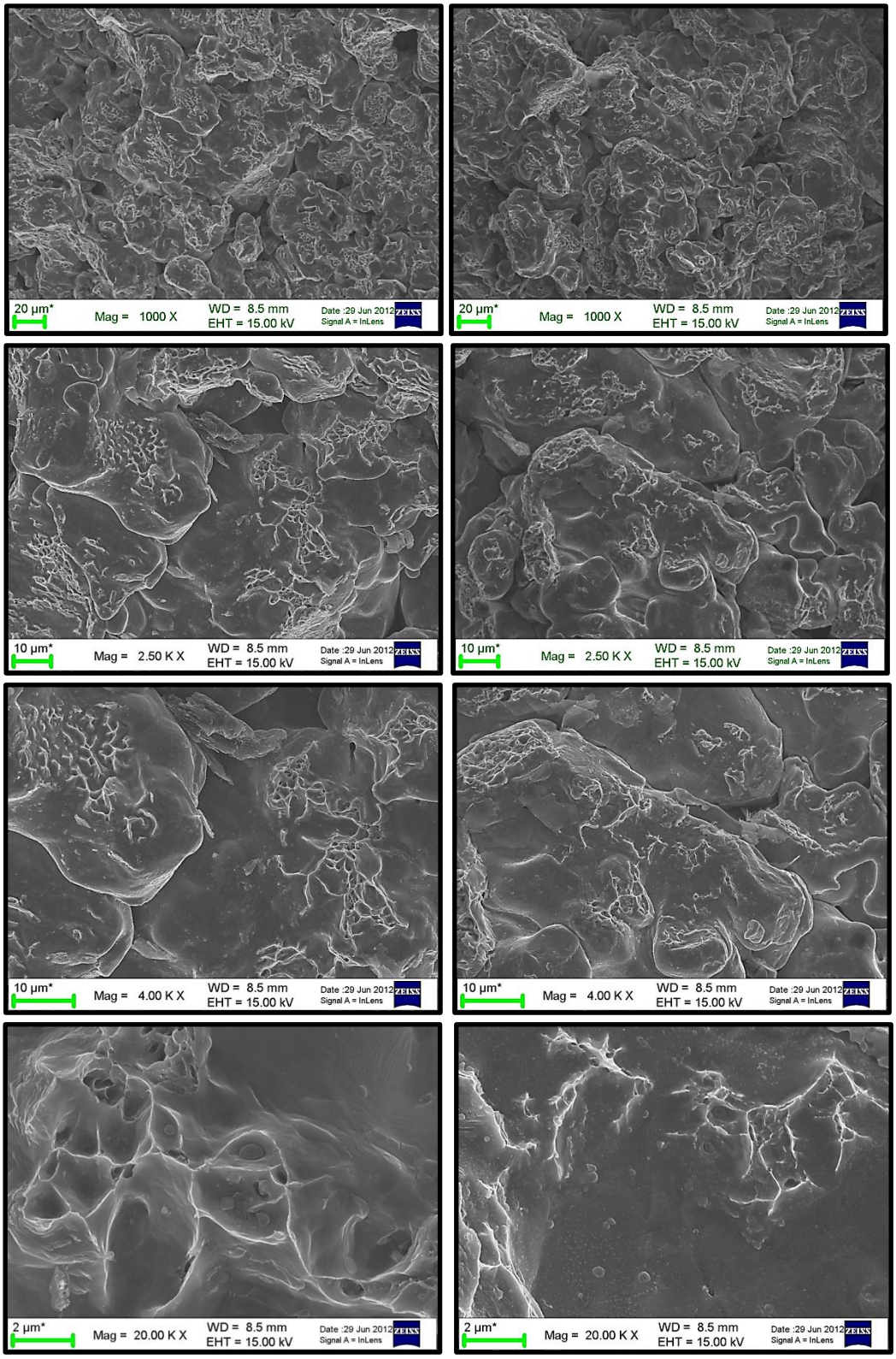

SEM-Ar/10%H_2-900˚C.DIL-F10-CENTRE

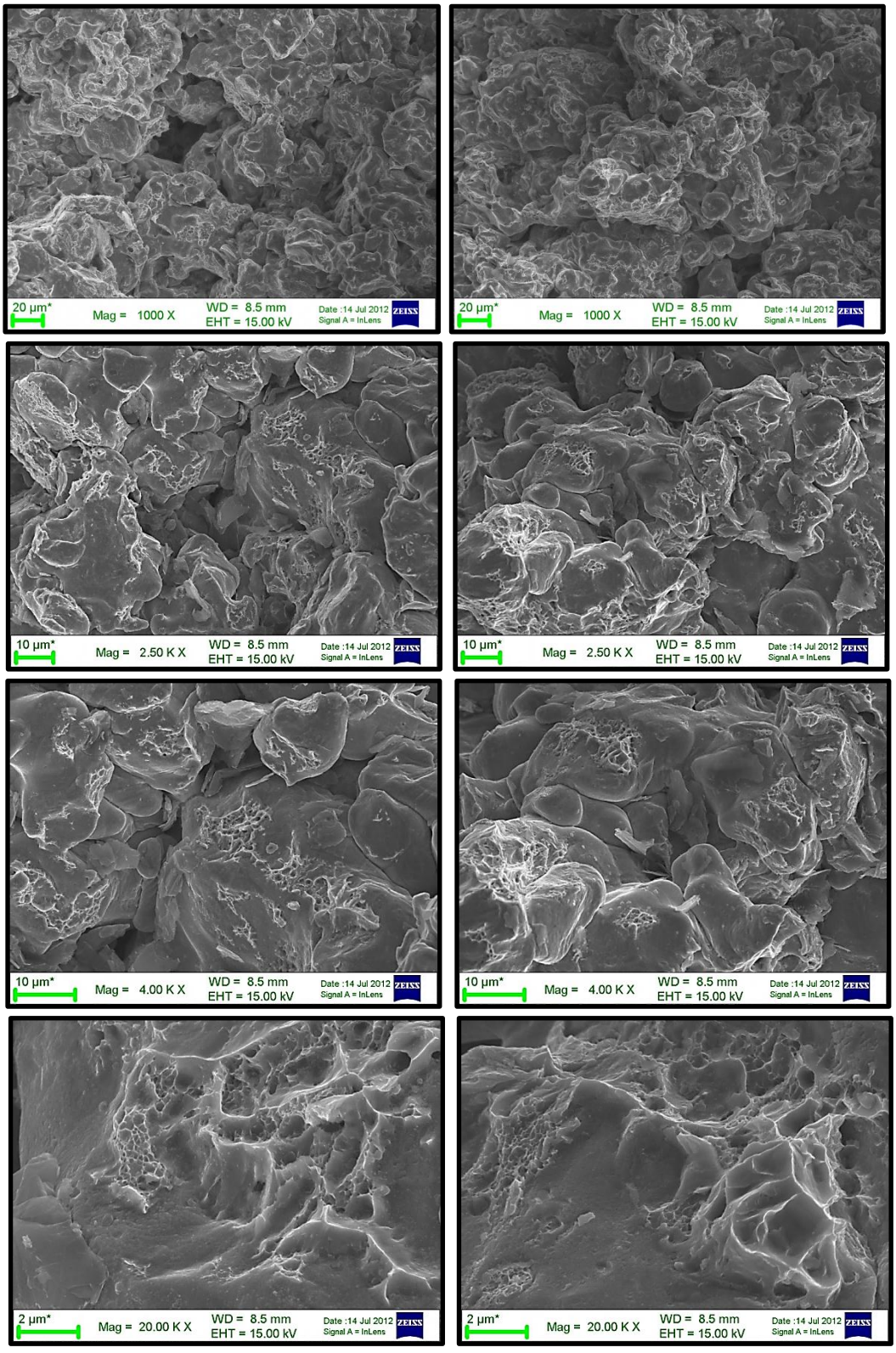

SEM-Ar/10%H_2-900˚C.DIL-F10-EDGE

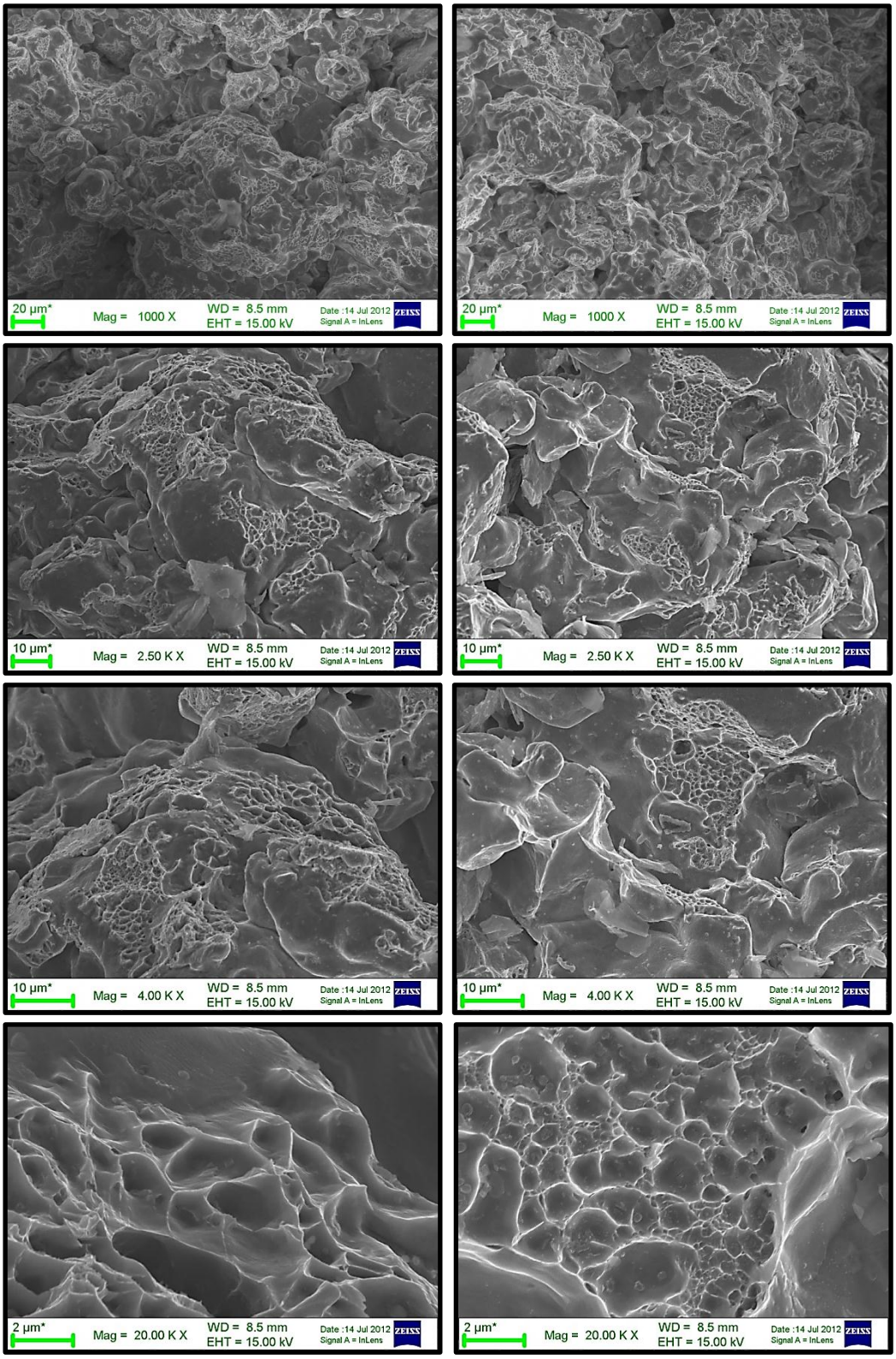

SEM-Ar/10%H_2-900˚C.DIL-KS4-CENTRE

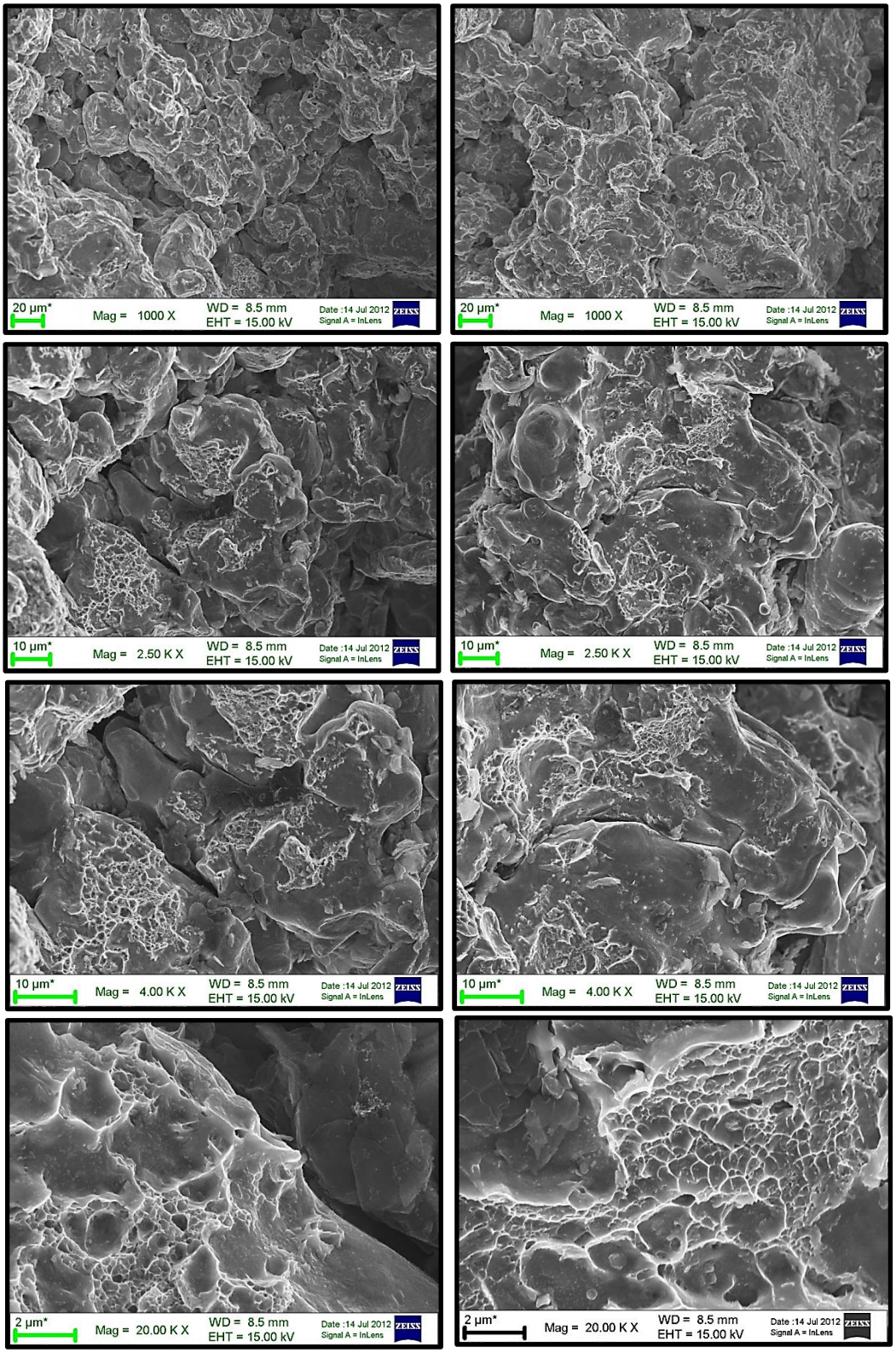

SEM-Ar/10%H_2-900˚C.DIL-KS4-EDGE

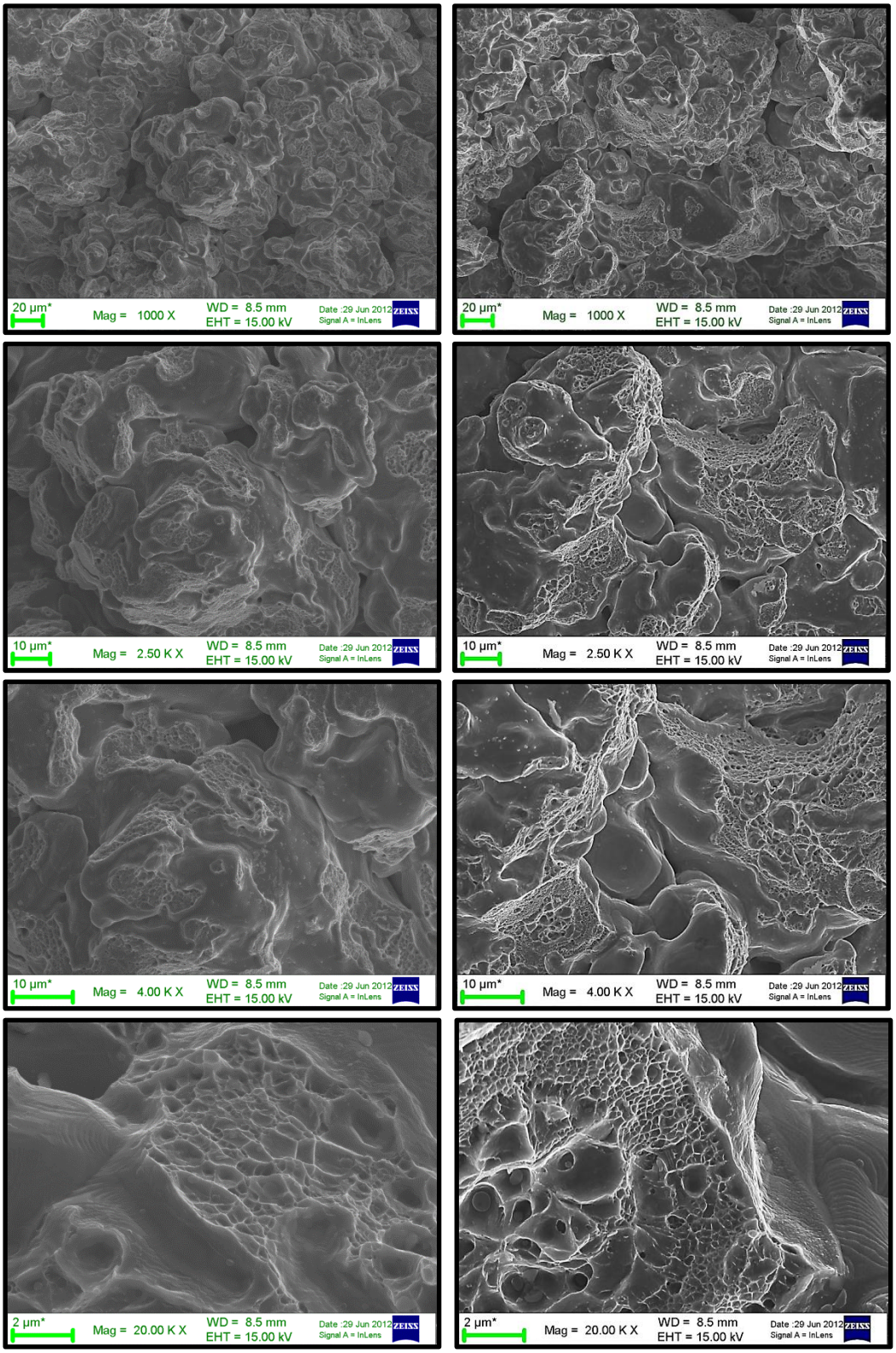

SEM-Ar/10%H_2-900˚C.DIL-ENSACO 250-CENTRE

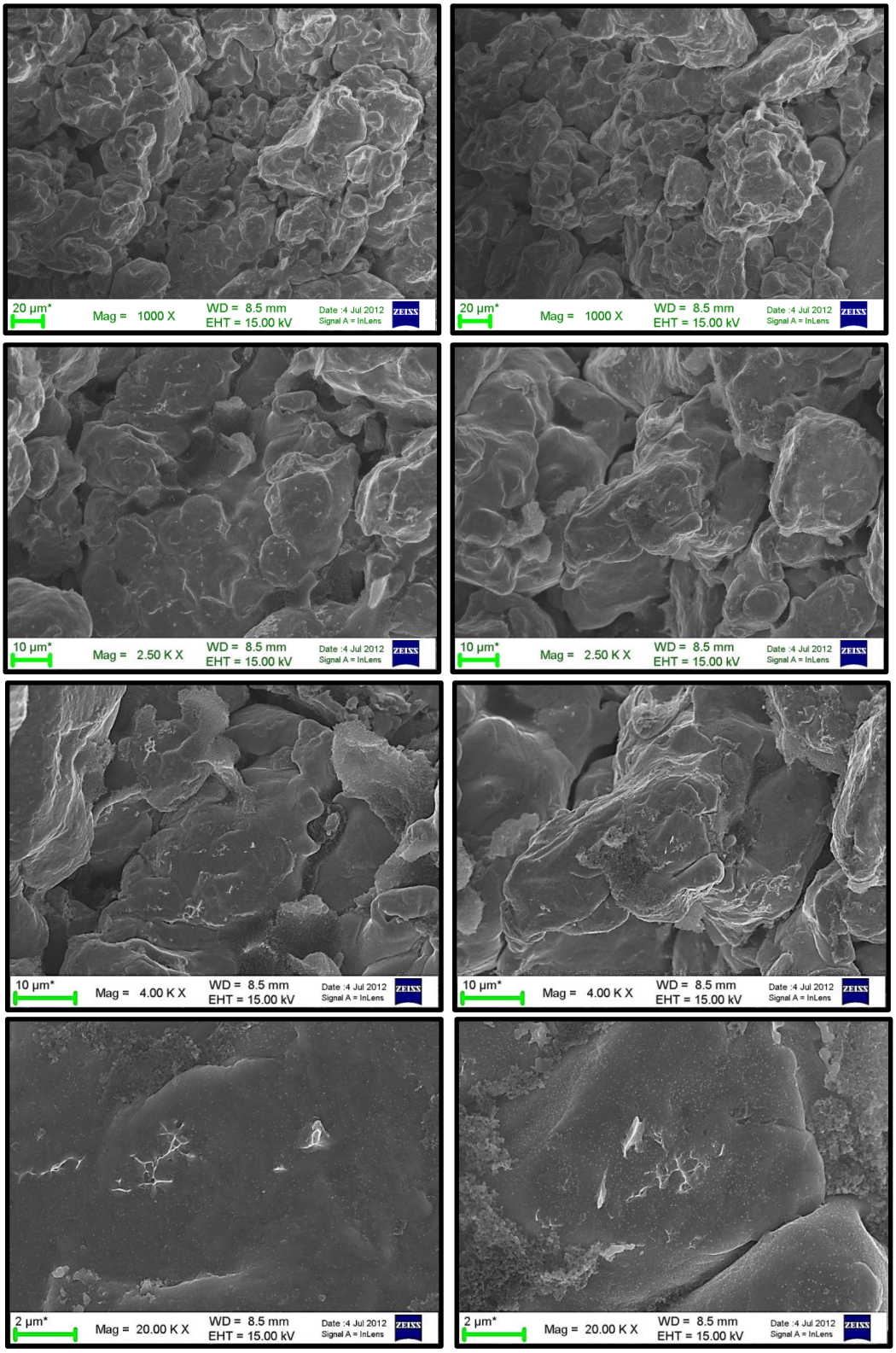

SEM-Ar/10%H2-900˚C.DIL-ENSACO 250-EDGE

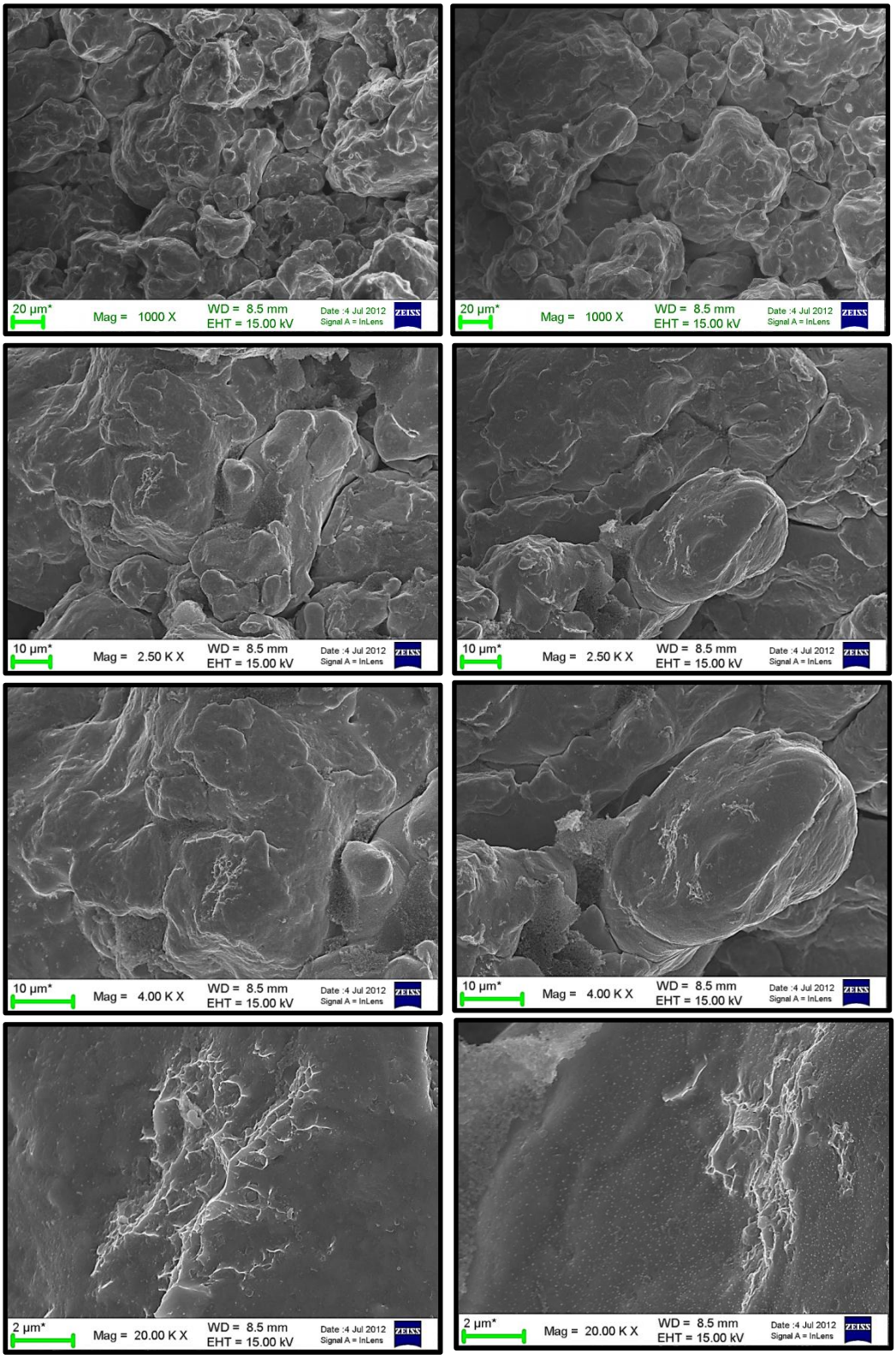

SEM-N_2/10%H_2-1120˚C-PG25

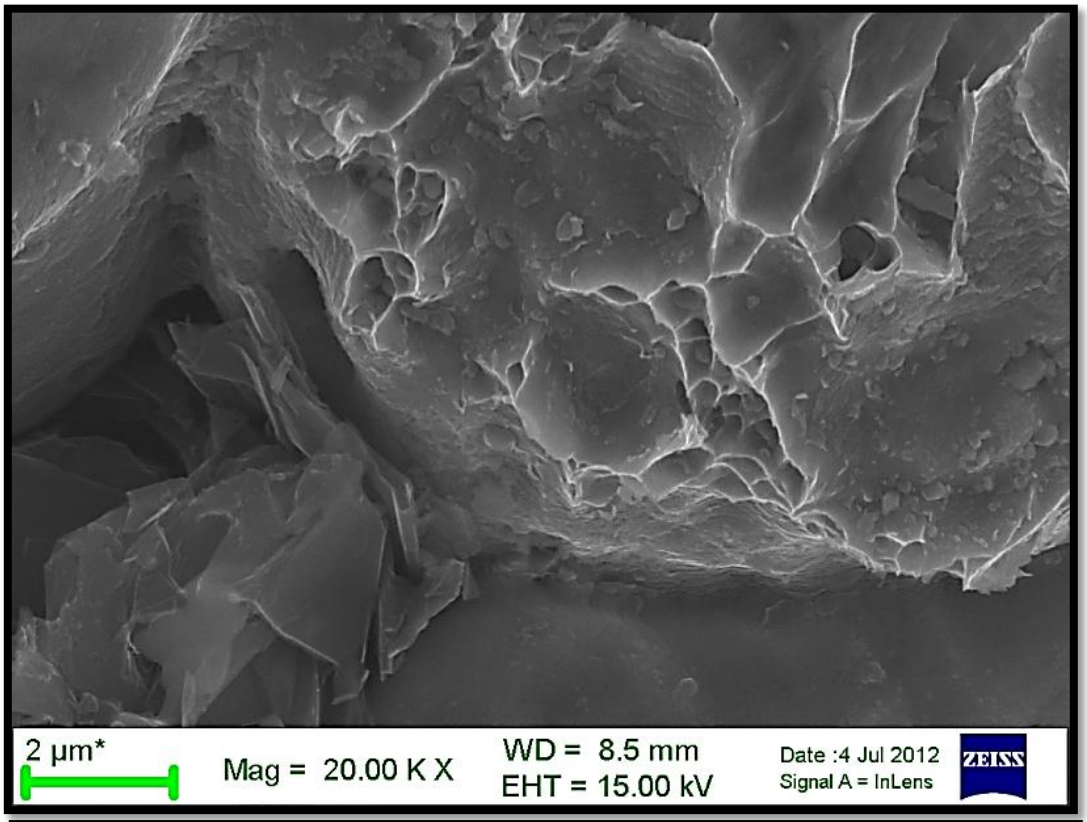

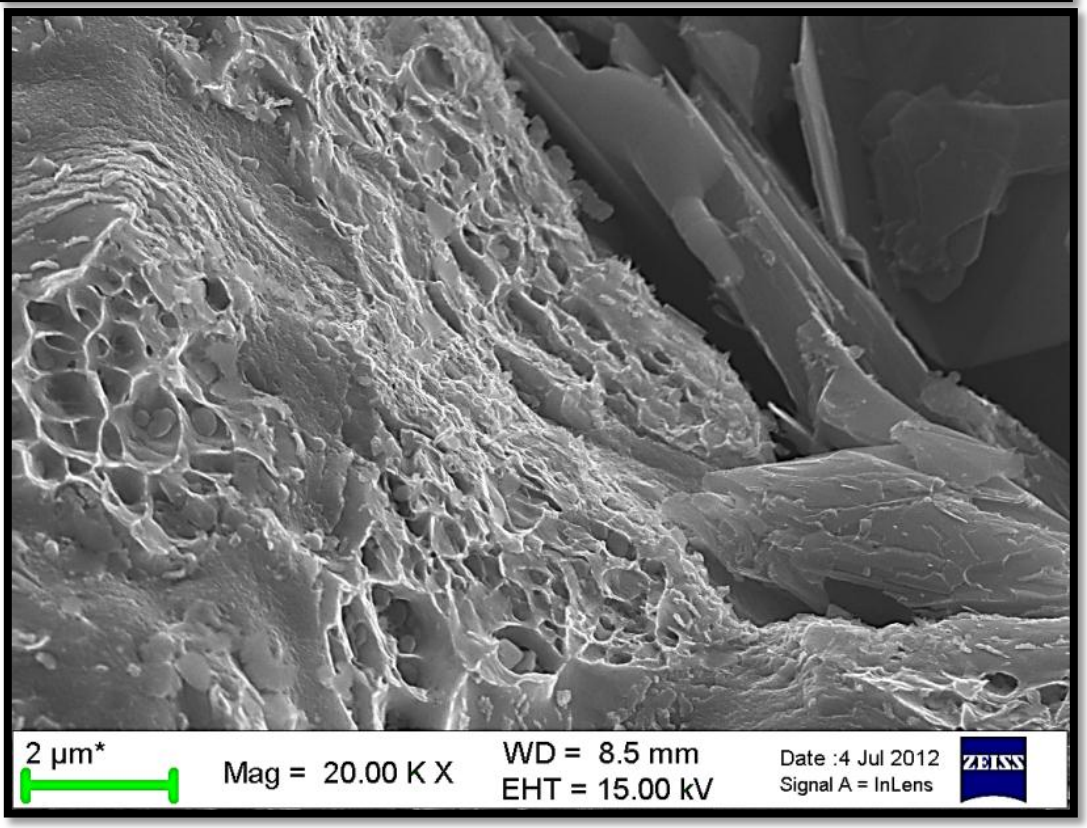

SEM-N_2/10%H_2-1120˚C-PG10

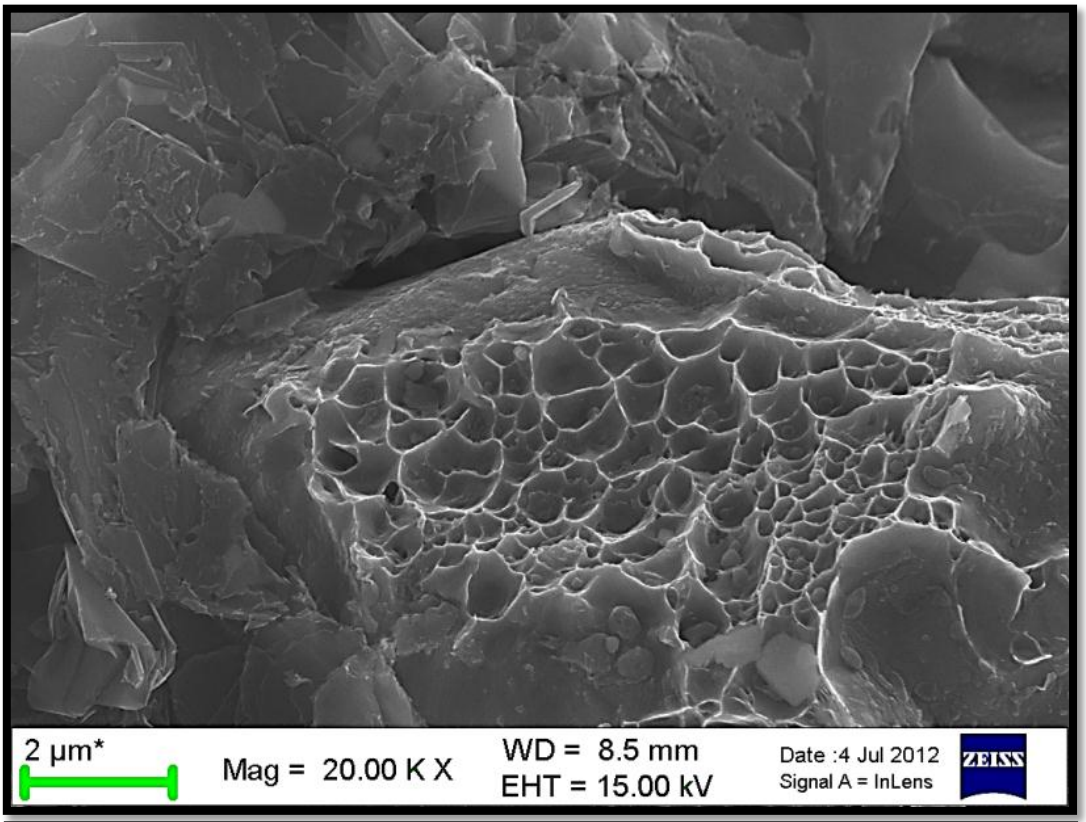

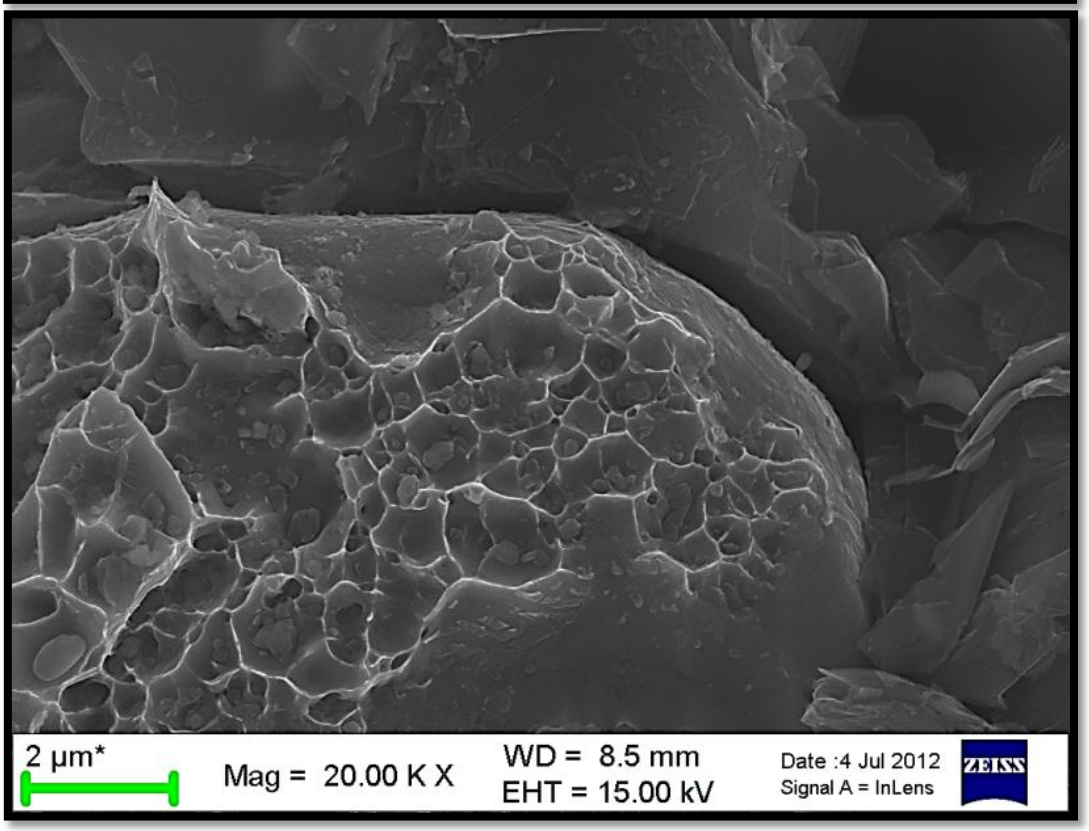

SEM-N_2/10%H_2 -1120˚C-F25

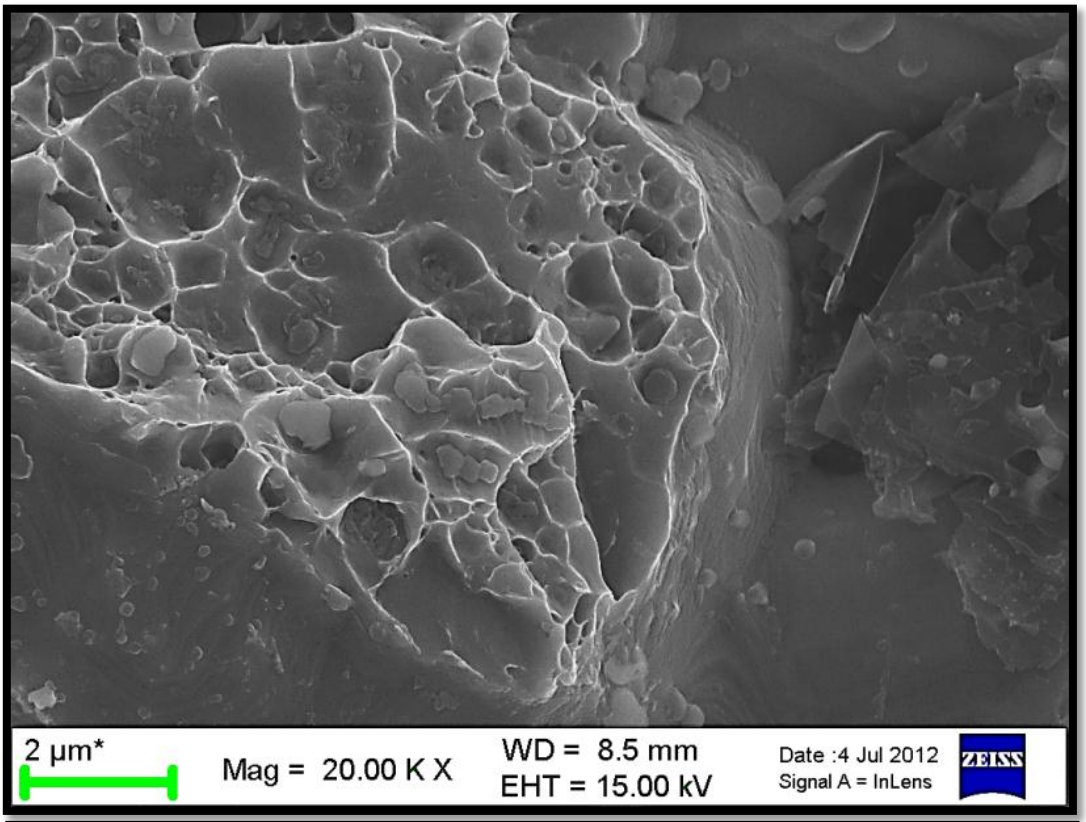

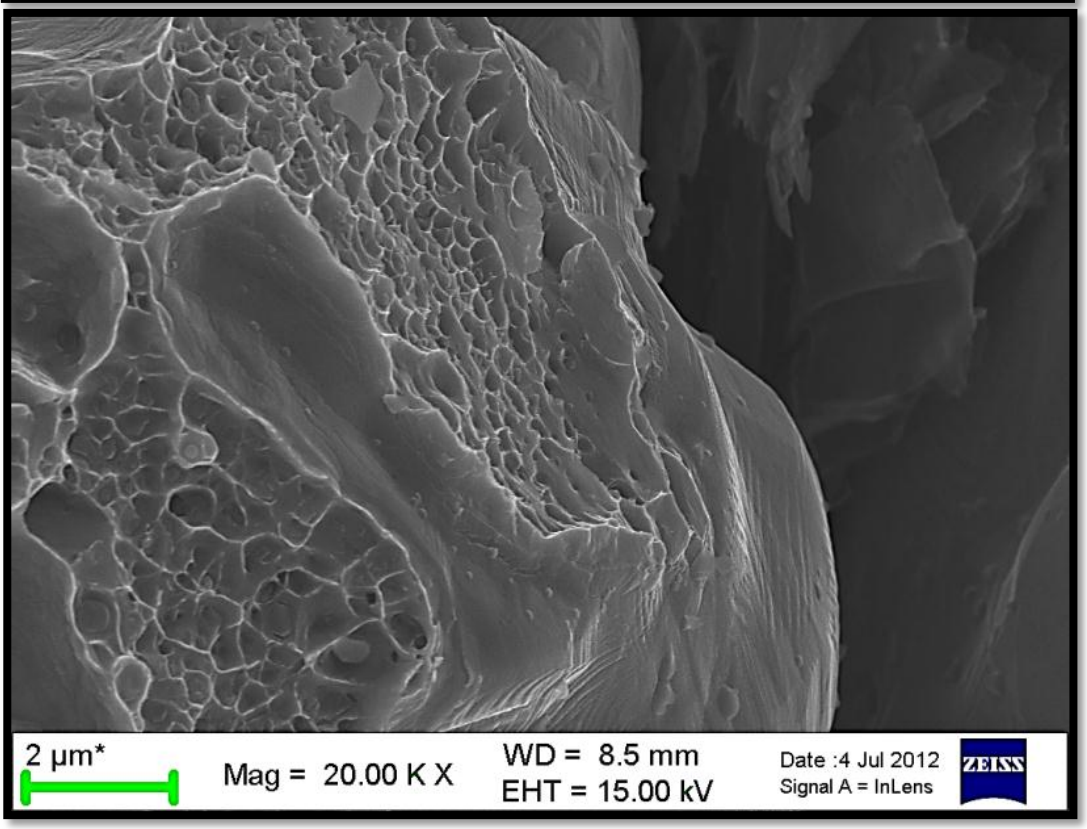

SEM-N_2/10%H_2-1120˚C-F10

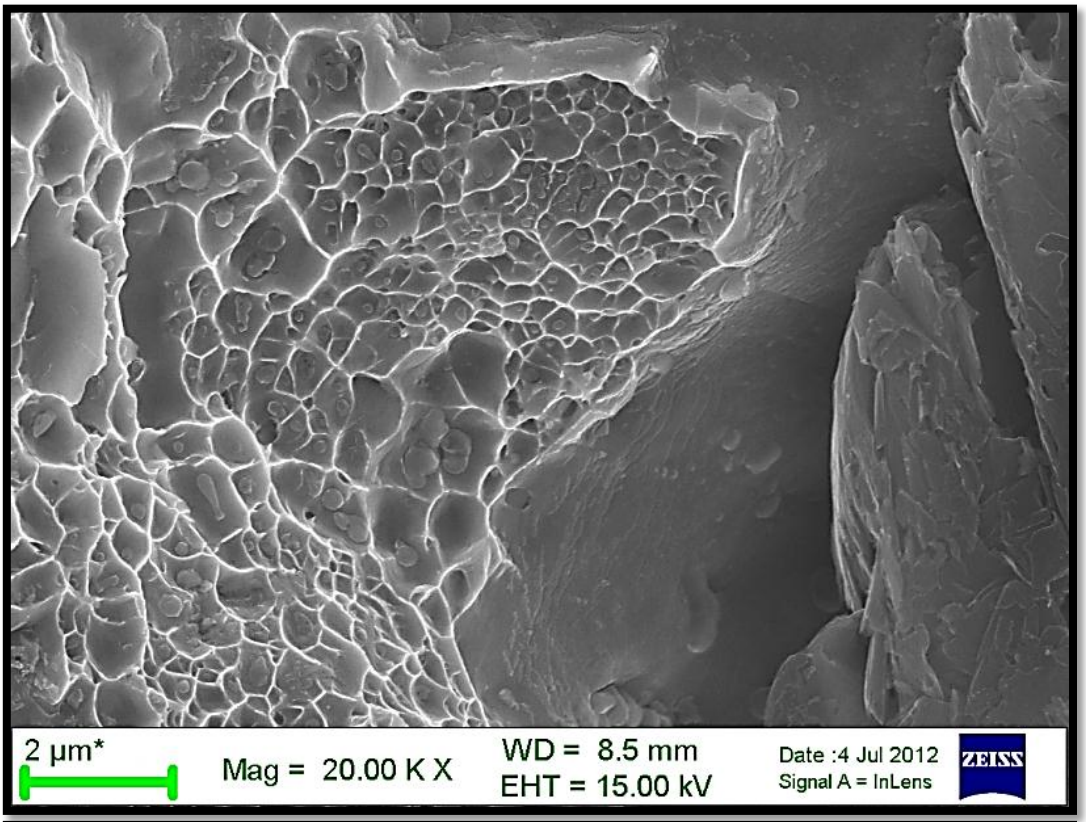

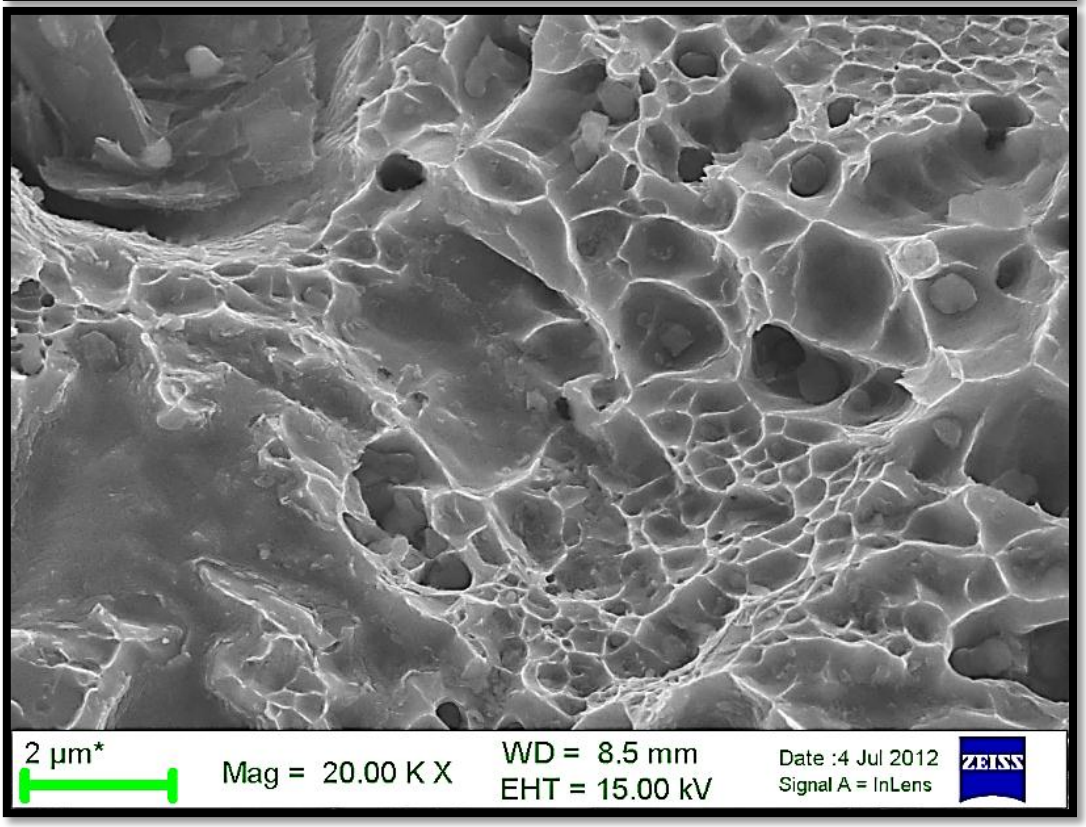

SEM-N_2/10%H_2 -1120˚C-KS4

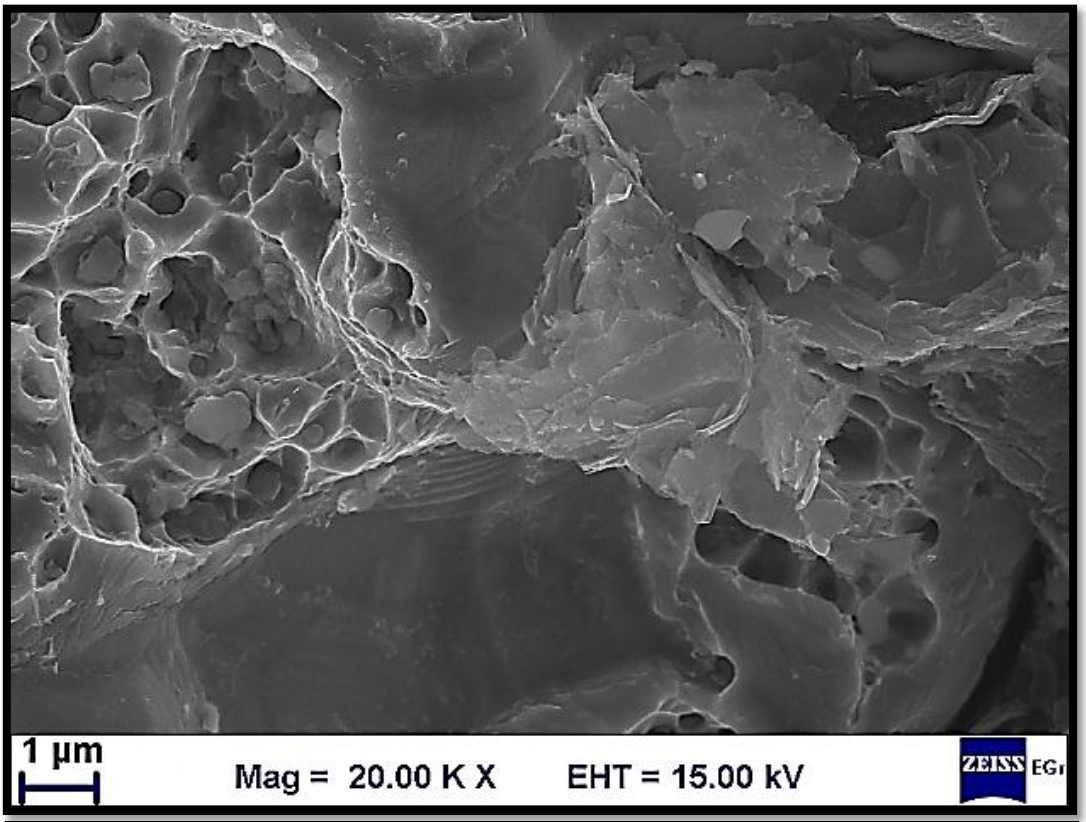

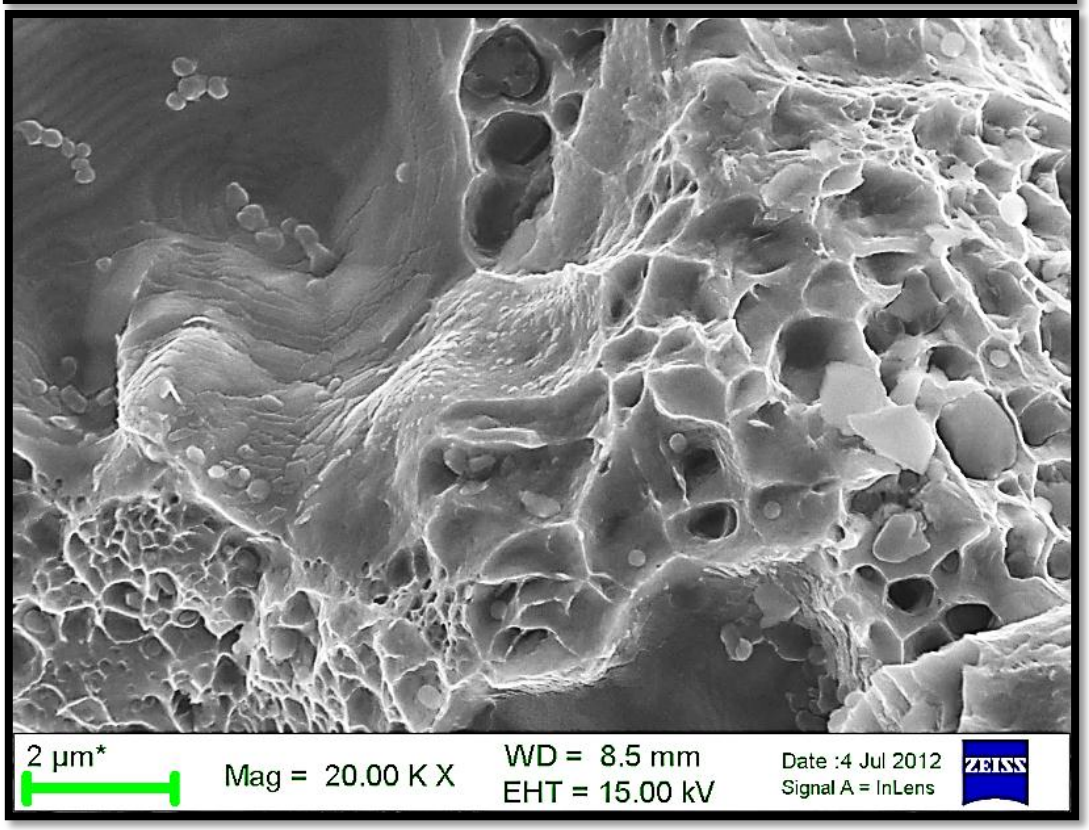

SEM-Ar/10%H_2 -1120˚C-DIL-ENSACO 250

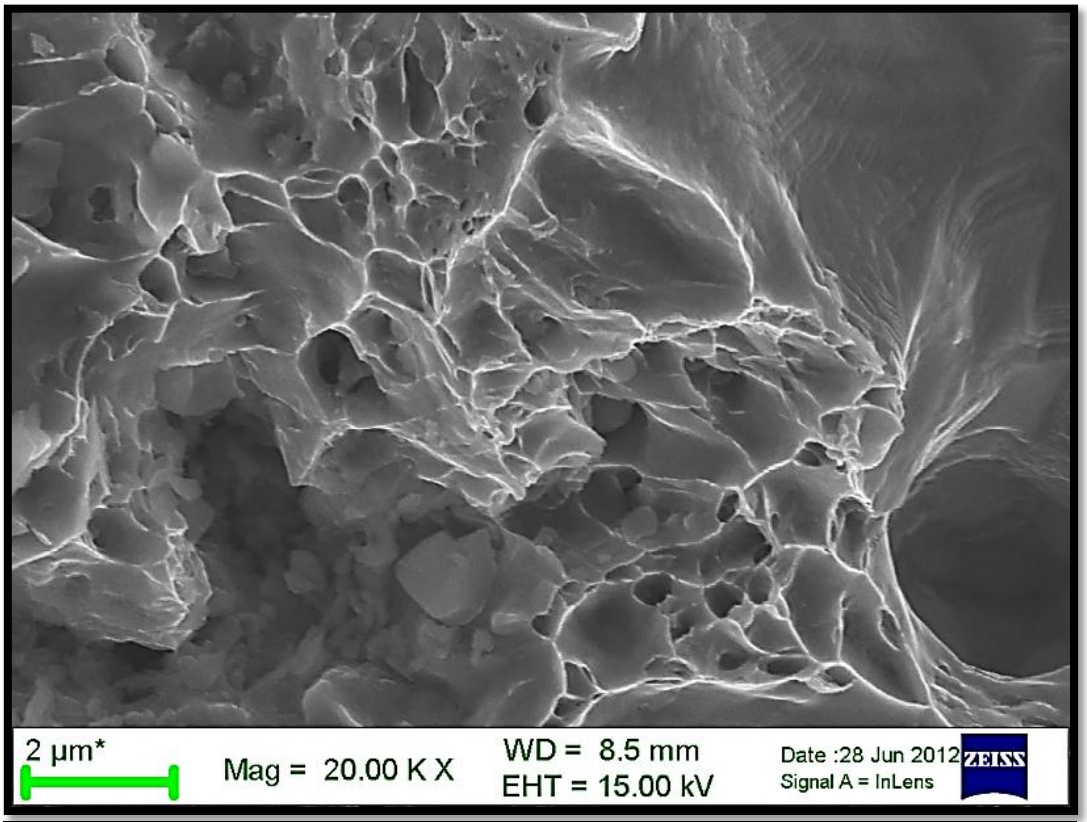

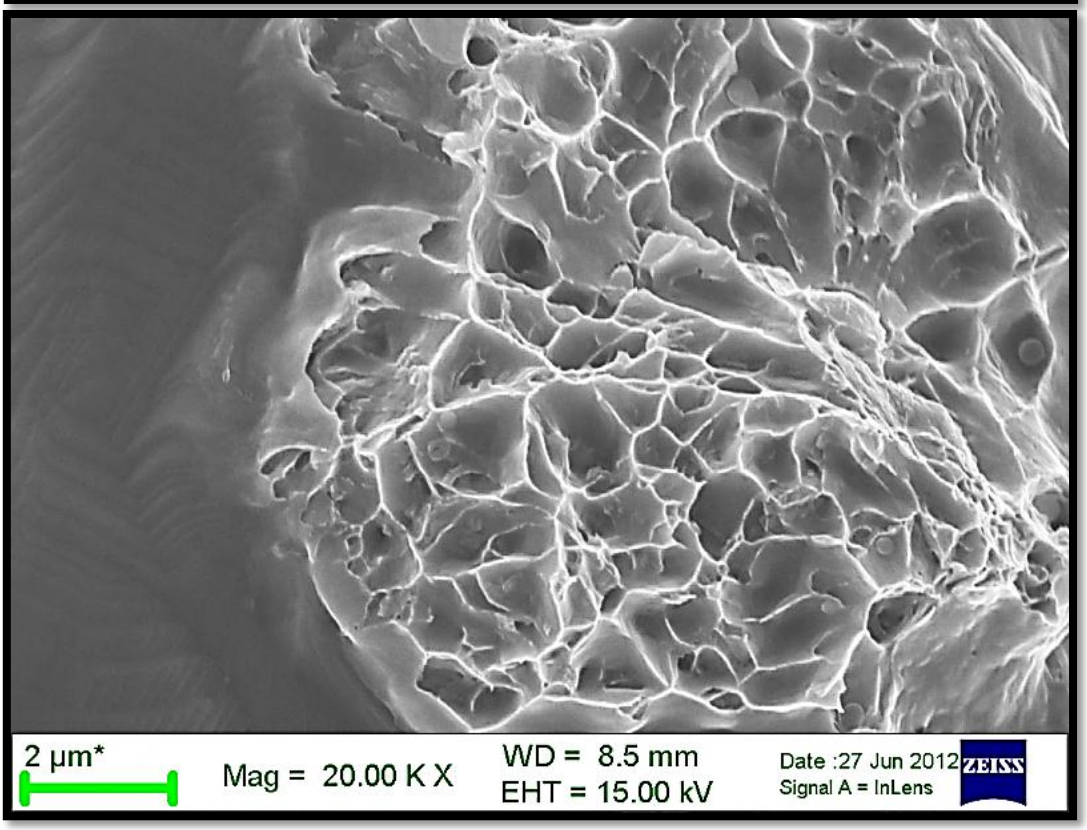

SEM-Ar/10%H_2-1120˚C-DIL-ENSACO 250

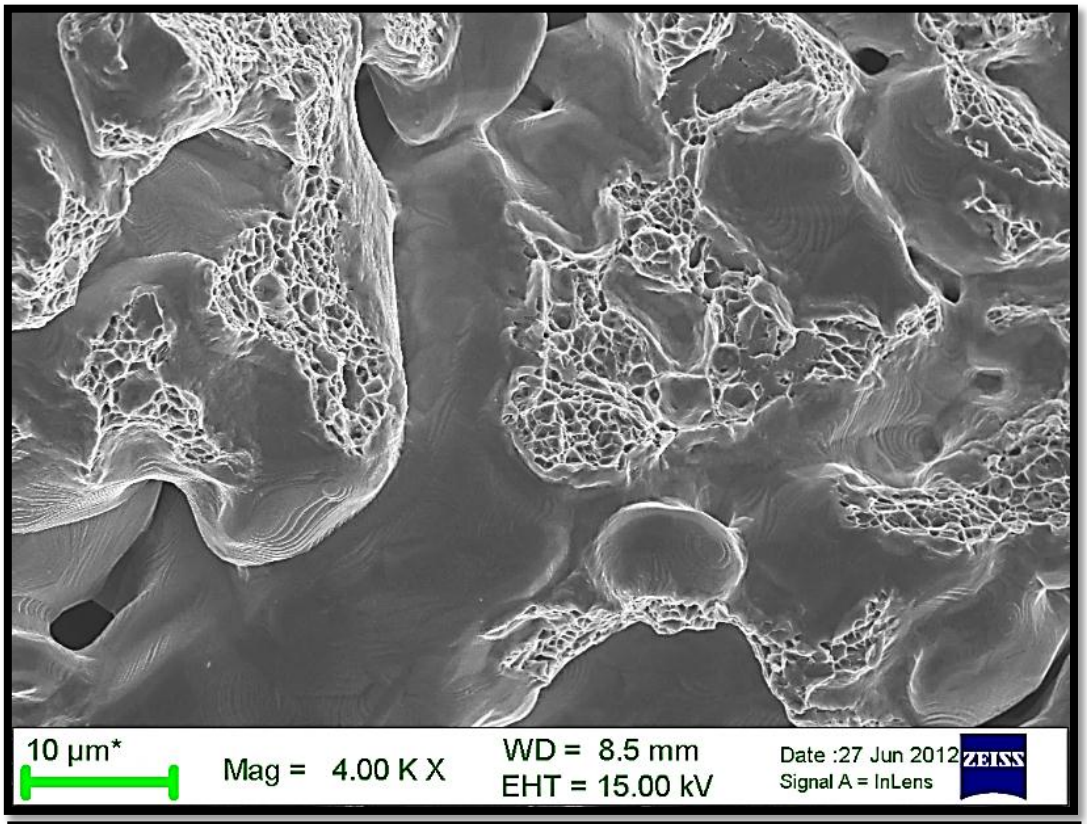

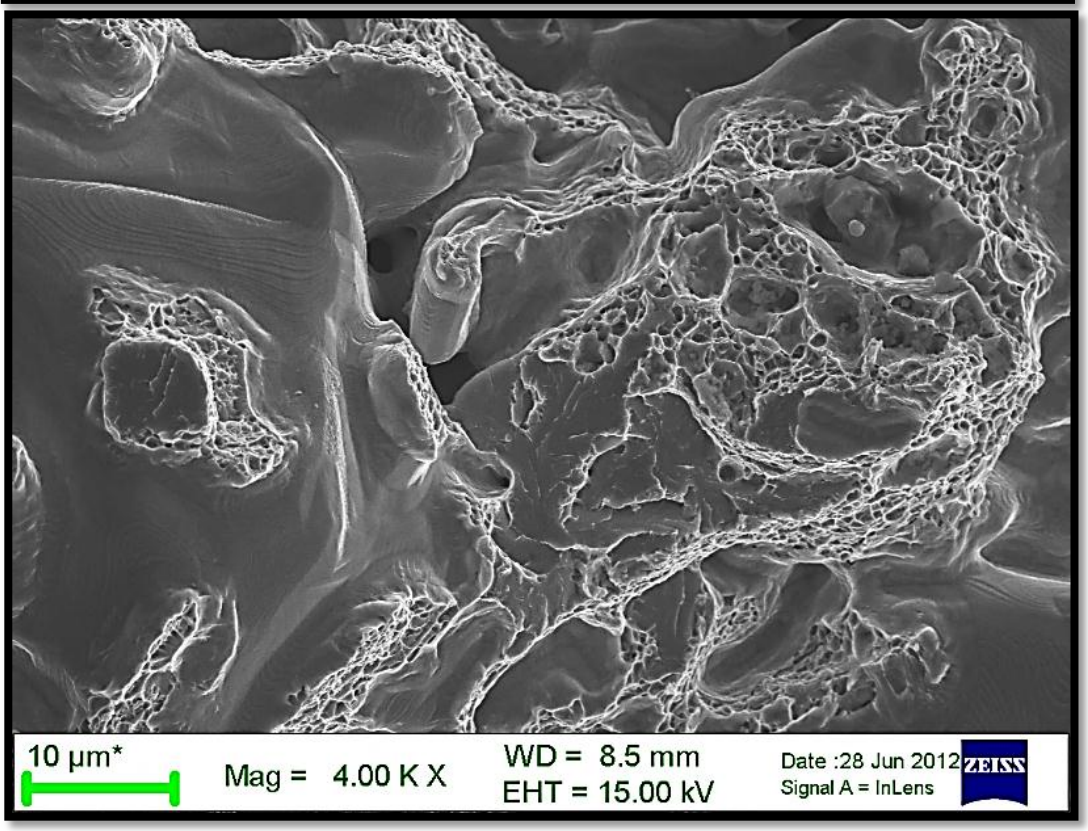

SEM-N_2/10%H_2-1120˚C-30min-PG25

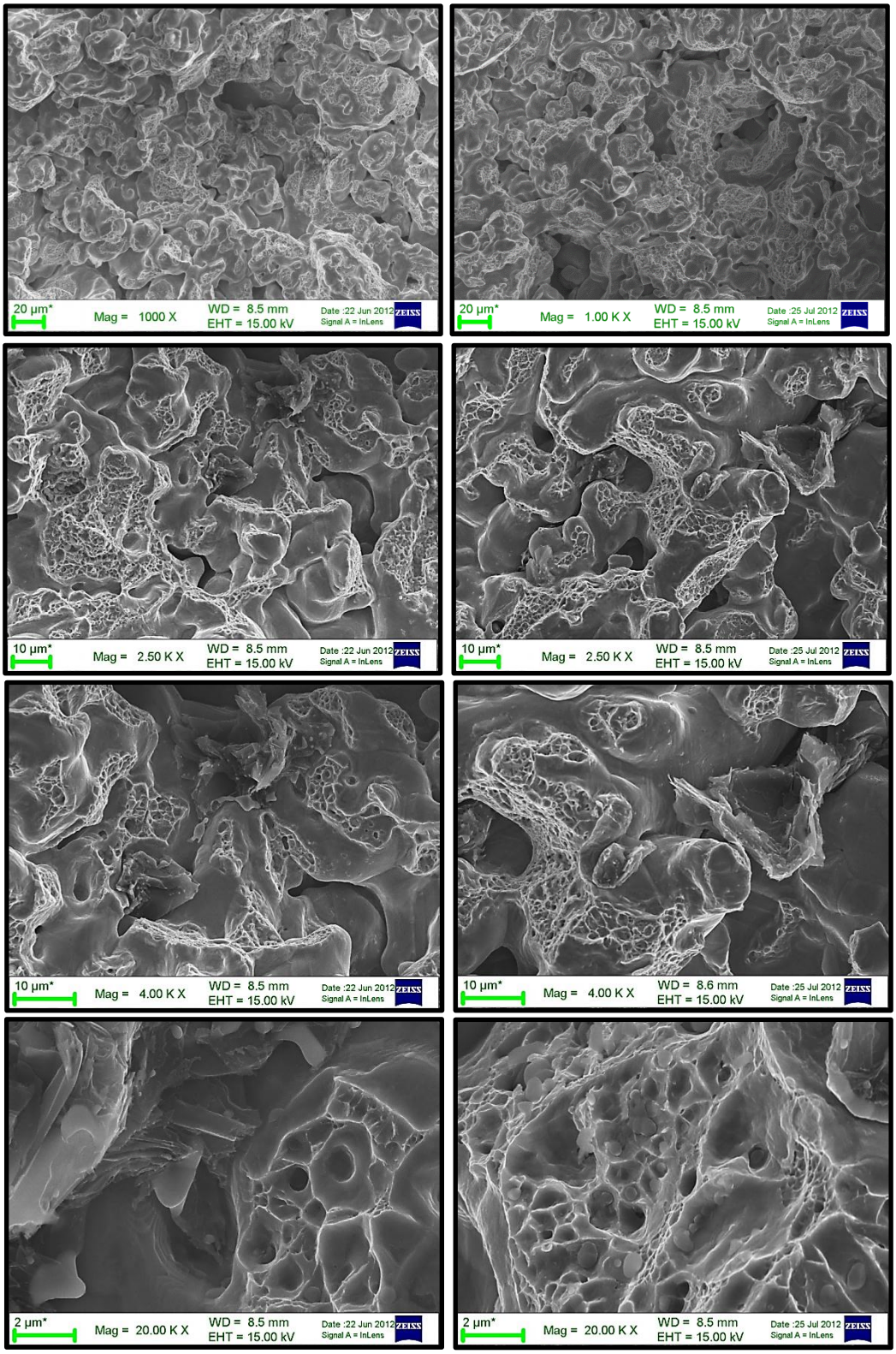

SEM-N_2/10%H_2-1120˚C-30min-PG10

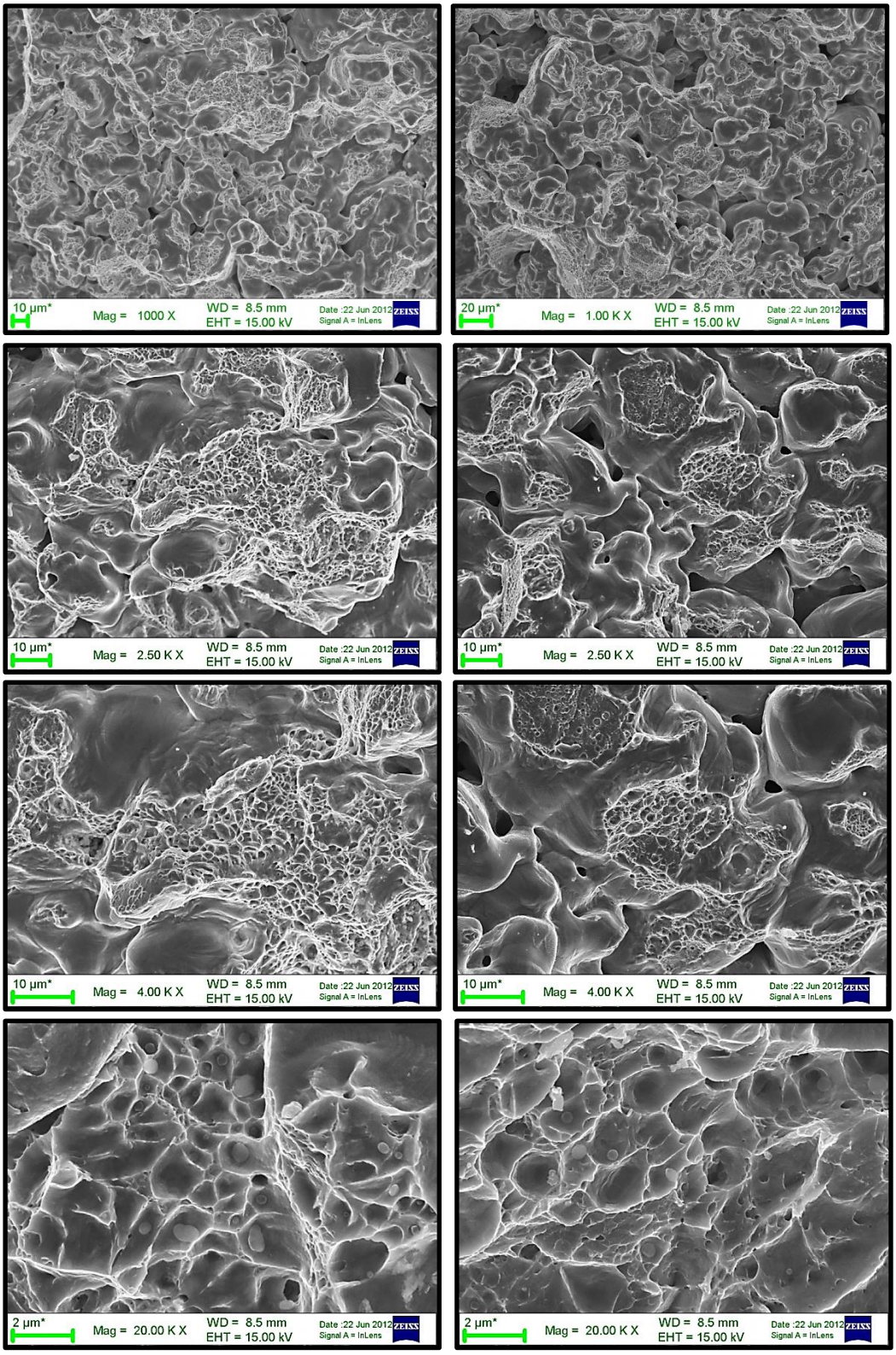

SEM-N_2/10%H_2-1120˚C-30min-F25

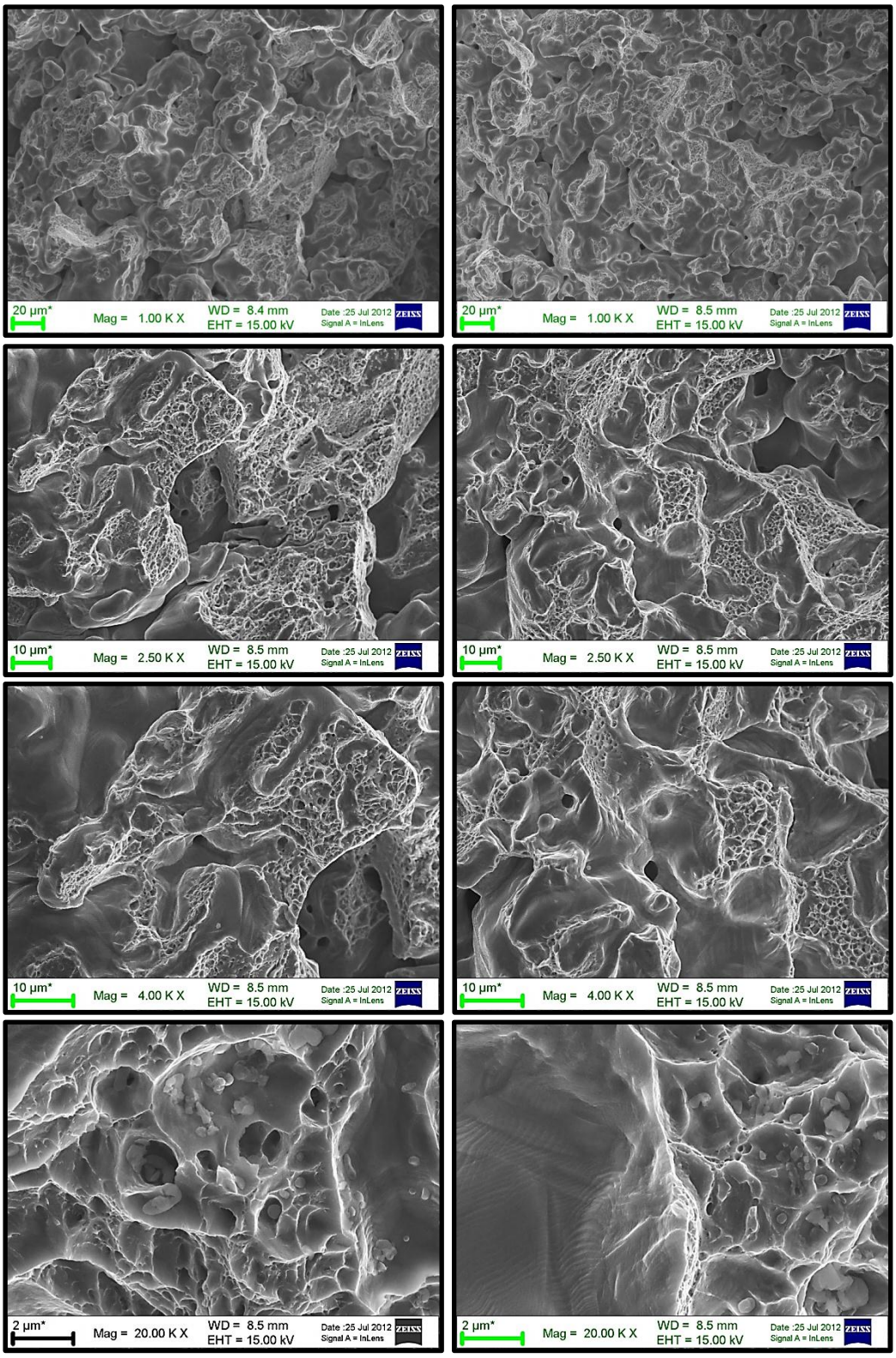

SEM-N_2/10%H_2-1120˚C-30min-F10

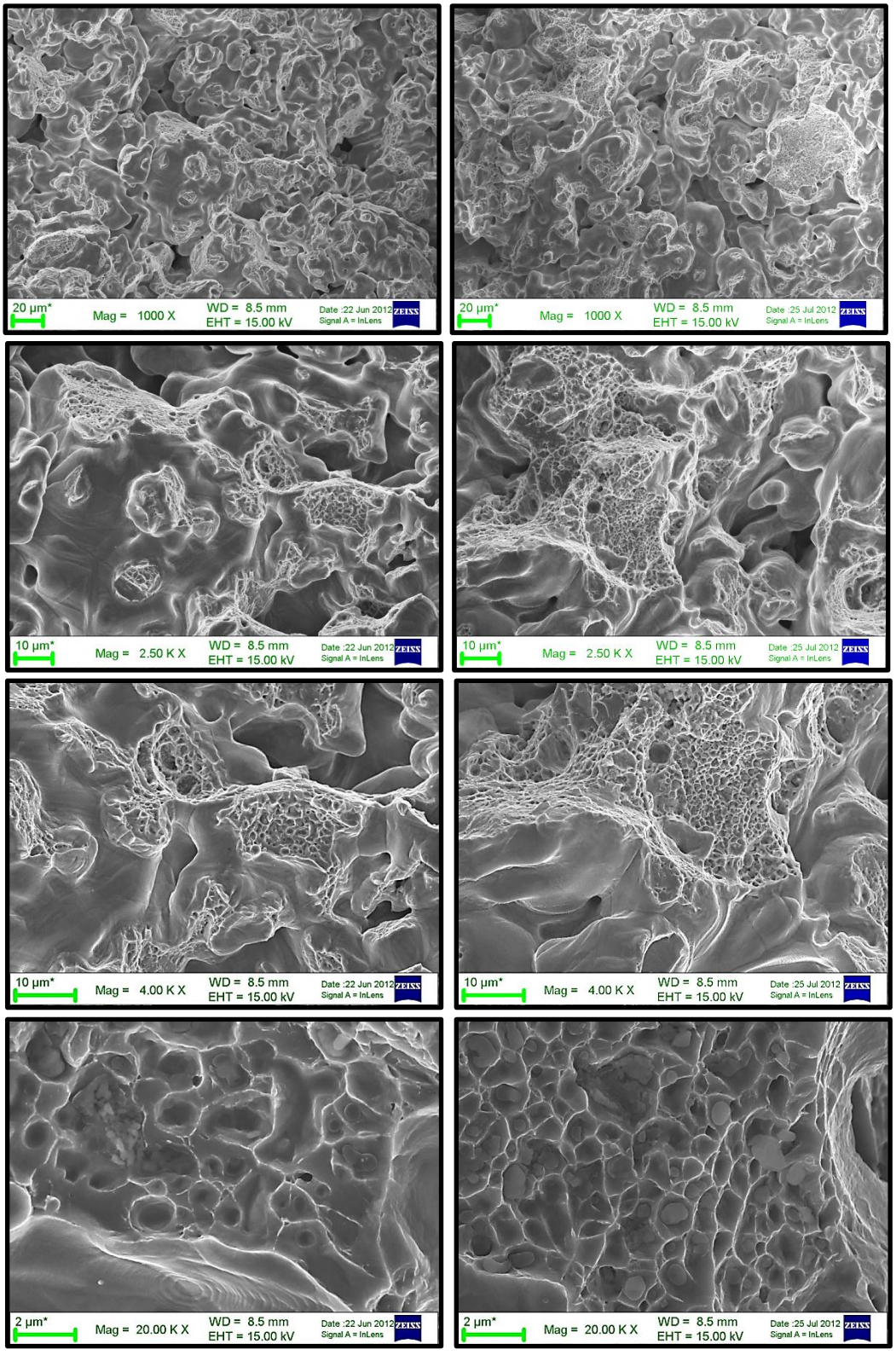

SEM-N_2/10%H_2-1120˚C-30min-KS4

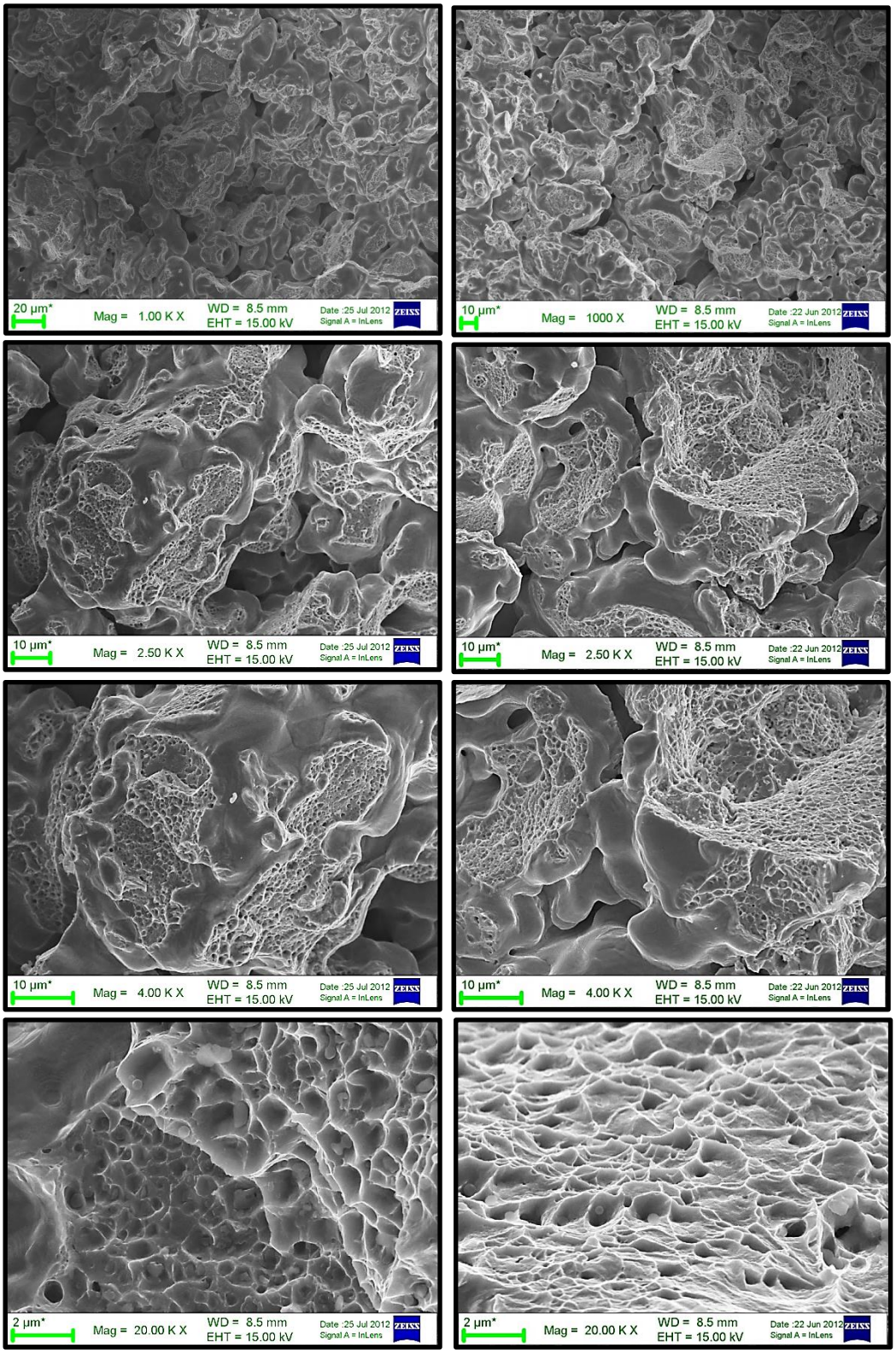

SEM-Ar/10%H_2 -1120˚C-30min-DIL-ENSACO 250

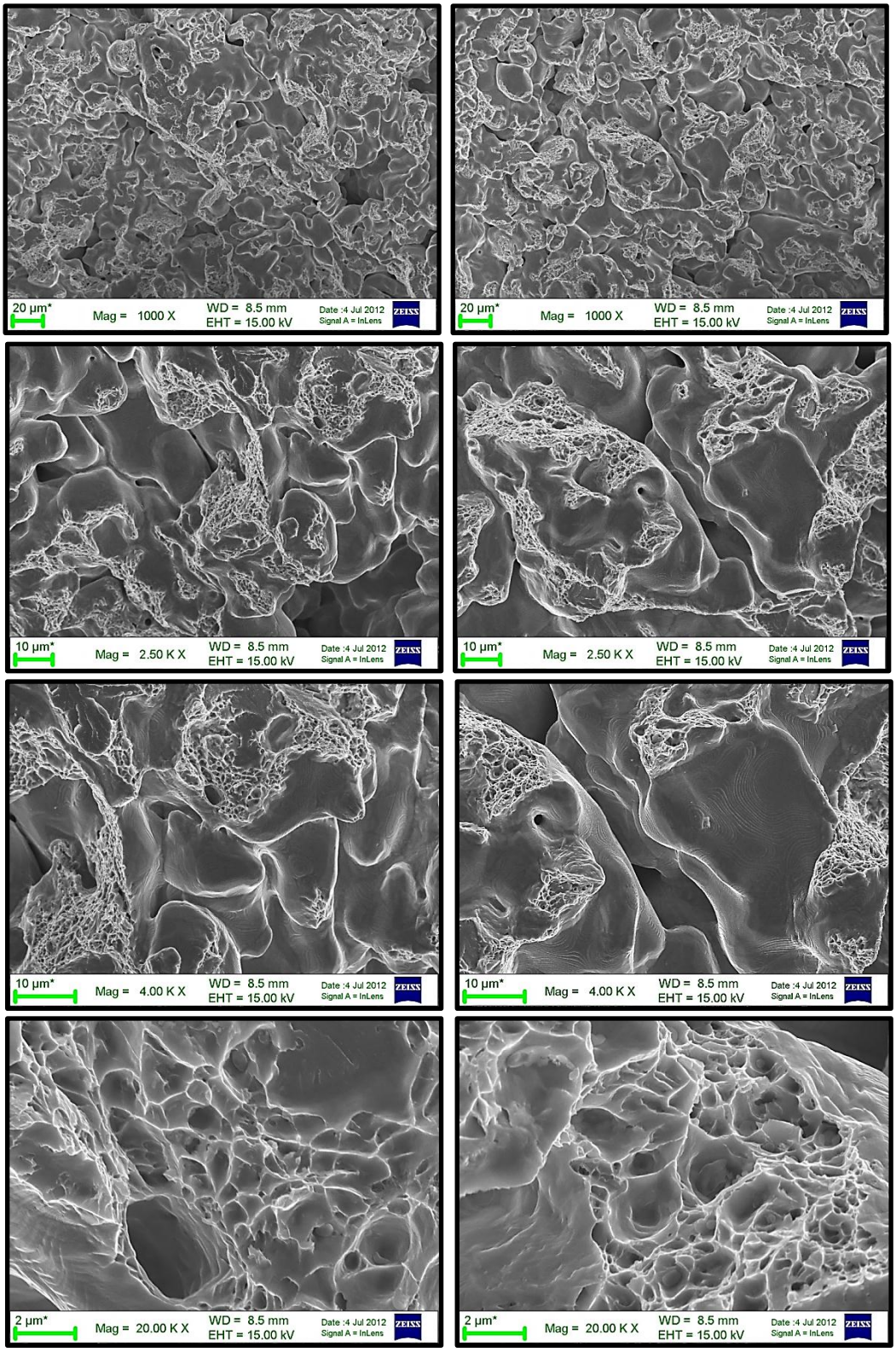

Chemical analysis